Doctoral Thesis

Study on Wireless Transmission from In-body to On-body and On-body to Off-body for Healthcare Purpose in an Aging Society

(高齢化社会におけるヘルスケアを目的としたインボディからオンボディ／オンボディからオフボディへの無線伝送に関する研究)

March 2022

Md. Ismail Haque

Dedication

To my beloved father,
To my dearest mother,
To my grandparents,
To my all respected teachers in primary school,
To my all respected teachers in high school,
To my respected teachers in undergraduate university,
To my respected teachers in graduate university,
To my respected teachers in postgraduate university,
To the spirit of my dear and pious brothers and sisters,
To all members of my family,
Those people's love is always the source of my motivation.

Contents

List of Figures

List of Tables

Chapter 1

Introduction

1.1 Background

Old age or elderly consists of ages closely a surpassing the average lifespan of individual increasing number of old people in the world. People worldwide are living longer. Nowadays most people can expect to live into their sixties and beyond. Most of the countries in the world is experiencing evolution in both the size and the proportion of older persons in the population. By 2030, 1 in 3 people in Japan and 1 in 6 people in the world will be aged 60 years or over. By 2050, the world's population of people aged 60 years and older will double (around 1.6 billion). The number of persons aged 80 years or older is projected to triple between 2020 and 2050 to reach 426 million. Between 2015 and 2050, the proportion of the world's population over 60 years will nearly double from 12% to 22%. By 2050, the number of people aged 60 years and older will be more than children younger than 5 years. The tread of population ageing is much rapidly than in the past as shown in Fig.1.1.

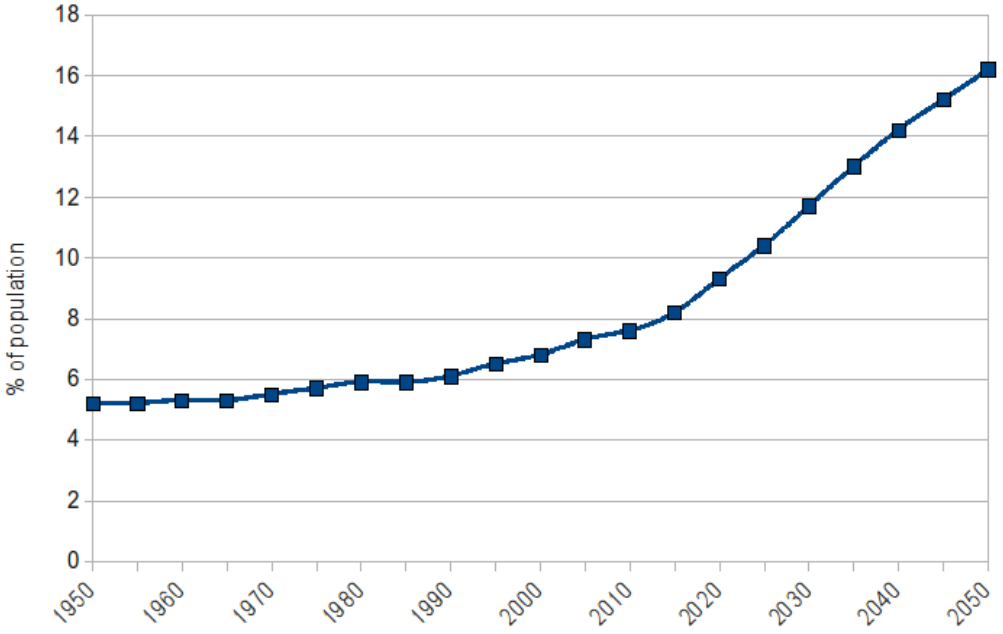

Fig. 1.1. Percentage of the world population over 65, 1950-2050 [1]

They are suffering many issues such osteoporosis, sudden falls, dizzy falls, difficulty sleeping, malnutrition, swallowing issues, hearing loss and memory loss etc. All countries face major challenges to ensure that their health and social systems are ready to make the most of this demographic shift. While this shift in distribution of a country's population towards older ages – known as population ageing – started in high-income countries, it is now low- and middle-income countries that are experiencing the greatest change. By 2050, two-thirds of the world's population over 60 years will live in low- and middle-income countries. Some researchers were mentioned some applications like medical diagnosis and treatment [2]- [4], physiological monitoring [5]- [9] and energy harvesting to make independent technology [10]– [17]. Therefore, a study of wireless body area network and the invention of self-power wireless network regarding body area communication are the most essential to overcome the challenges that elder people has ever made. As a result, wireless communication technology is the innovative progress of small electronic devices and, wireless body area networks (WBAN) have proven to be as extremely versatile investigative attention in medical services and healthcare applications. In this research, for dealing the issues of elderly, WBANs are classified into two types according to the locations of the transmitter and receiver devices on or in or off the body; one is On-body to In-body Network (OB2IBN) and On-body to OFF-body Network (OB2OBN). Wearable OB2IBN is basically based on in-body communication by which we can transmit medical data or image from the internal portion to external portion of human body such as capsule endoscopes and wireless cardiac pacemaker, whereas OB2OBN is based on on-body and off-body communication by which we can properly identify a person's location in daily life such as shoe-mounted BLE sensor. Possible frequency bands for WBAN possess 10-60 MHz human body communication (HBC) band, 400 MHz band, 2.4 GHz band and Ultra-Wide Band (UWB) etc. according to IEEE802.15.6.

1.2 Two issues for elderly

1.2.1 Patient monitoring and healthcare facilities

Nowadays, aging population is leading to an inclusive-scale demand for more progressive and well-organized medical and healthcare treatment using wireless communication techniques. For example, the demand for wireless health-state monitoring

for both in hospital and at-home patients is increasing dramatically. This is because wireless patient monitoring can effectively reduce the inconvenience of wire links, and save time and resources when people are monitored remotely at home. Body area communication provides a wide range of possibilities in supporting such medical and healthcare services [2], [18]- [19]. It may cover three areas: medical check-up; physical rehabilitation; and physiological monitoring. As a typical usage model, the body area communication device is a transceiver together with a health information sensor or a set of health information sensors. For medical check-up, such devices can collect electroencephalogram (EEG) data for monitoring brain electrical activity, electrocardiogram (ECG) data for monitoring heart activity, breathing data for monitoring respiration, as well as blood pressure, heart rate and body temperature. For physical rehabilitation, tilt sensors for monitoring accidental falls, foot sensors for monitoring steps, movement sensors for monitoring activities, breathing sensors for monitoring respiration, as well as blood pressure sensors, heart rate sensors and body temperature sensors are all possible candidates. Fig. 1.2 shows the concept the body area communication for healthcare. The sensor data are collected at an on-body server as shown by the circle in the center of the body, and then sent to a hospital or medical center. The wireless link to the on-body server needs a body area communication technique, while the data transmission to a hospital or medical center can employ cellular systems or local area networks (LANs). This usage mode reduces the work load of the medical staff and results in increased efficiency of patient or at-home elderly people management. Moreover, capsule endoscopy is a process used to record internal images of the gastrointestinal zone for usage in medical diagnosis. Innovative developments are also able to take surgeries and release medication at specific locations of the entire gastrointestinal tract [20]- [21]. The capsule is similar in shape to a standard pharmacological capsule, although a little larger, and contains a small image sensor and an array of LEDs powered by a battery. After a patient swallows the capsule, it passes along the gastrointestinal tract taking a number of images per second which are transmitted wirelessly to an array of receivers connected to a portable recording device carried by the patient. The primary use of capsule endoscopy is to examine areas of the small intestine that cannot be seen by other types of endoscopy such as colonoscopy or

esophagogastroduodenoscopy (EGD). Another example of body area communications for medical diagnosis is the wireless cardiac pacemaker, as one of application examples of in-to-on-body communication. A wireless cardiac pacemaker is an electronic device which helps people with irregular heart beat problems. The main purpose of a pacemaker is to conserve an adequate heart rate, either because the heart's natural pacemaker is not fast enough, or because there is a block in the heart's electrical conduction system. Current pacemakers are externally programmable and consent a cardiologist, particularly a cardiac electrophysiologist to select the ideal pacing modes for individual patients. Modern devices are demand pacemakers, in which the stimulation of the heart is based on the dynamic demand of the circulatory system. An artificial pacemaker is a medical device that generates electrical impulses delivered by electrodes to cause the heart muscle chambers to contract and therefore pump blood; by doing so this device replaces and/or regulates the function of the electrical conduction system of the heart. The pacemaker also collects sympathetic nerve signals using sensors and sends them to a control unit. Then, the control unit calculates the correct heart beat rate and instructs the pacemaker. Finally, the pacemaker helps to adjust the heart beat to the correct beating rhythm.

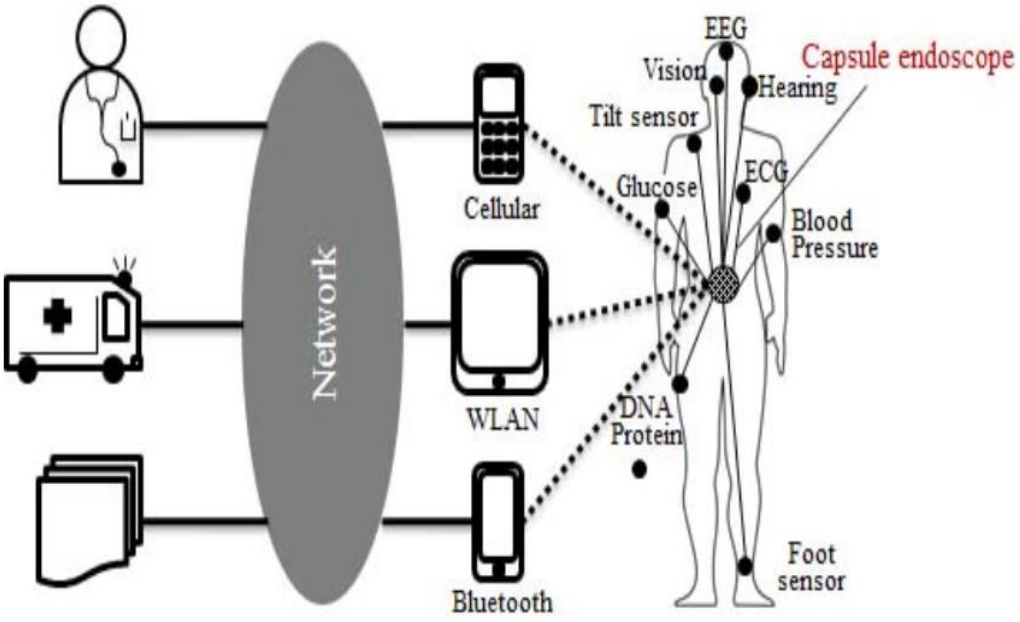

Fig. 1.2. Body area communication for healthcare [22]

1.2.2 Wandering behavior

Wandering by elderly persons at acute hospitals and nursing homes poses a significant problem to providing patient care as such incidents can lead to injury and even accidental morbidity or patient missing. These problems are particularly serious given aging populations around the world. This behavior is one of most serious symptoms of dementia. Dementia is a neuro-degenerative disease that decreases independence. Dementia affects the lives of ~ 50 million people worldwide [23], which is estimated to increase to 131.5 million in 2050. According to the Alzheimer's report from 2016, around 0.46 million Bengali, 4.6 million Japanese, 1.5 million German and 5.5 million Americans suffer from Alzheimer's dementia resulting in medical expense of $659 billion. Family members spend 18.2 billion hours per year amounting to $230.1 billion [24]. Dementia is sometimes revealed through 'wandering', which is a pervasive behavioral symptom in dementia patients [25]. It is defined as "a syndrome of dementia-related locomotion behavior having a frequent, repetitive, temporally disordered, and/or spatially-disoriented nature that is manifested in lapping, random, and/or pacing patterns, some of which are associated with eloping, eloping attempts, or getting lost unless accompanied" [26]. It may be triggered by various factors such as frustration, the intent for socialization or work, boredom or escaping tendencies [25]; however, it is quite unforeseeable and therefore requires supervision for detection, identification, and arbitration. Unattended aimless roaming of a patient may lead to agitation, fatigue, vertigo and in extreme cases physical harm due to falling or colliding with objects in the vicinity [24]. Moreover, wandering has been identified as one of the main reasons for nursing home placement or institutionalization [27], as it has proven to be too arduous for caregivers to manage in home environments. Technological intervention, for identification, detection, and mediation of wandering behavior, would share the load of human labor and may also improve the privacy and independence of the patient. For example, an automatic wandering detection BLE module can be integrated with an intervention module (i.e., for generating alert signals) to build a real-time system to produce prompt warnings [28]. This would help in reducing immediate health hazards associated with the aimless movement. Additionally, wandering behavior is correlated with the cognitive state of a

dementia patient. Automatically generated records of wandering frequency and patterns would aid in keeping track of patients' cognitive health. As mentioned before, wandering behavior requires a considerable amount of caregiver vigilance; an automated technological solution has the potential to lower caregiver burden as well as medical cost. A comprehensive survey or review on technological interventions for wandering management would contribute to research efforts in computation and cognitive health sectors and create a platform for future studies. In this thesis, we developed a novel method to address the problem of wandering patients using shoe mounted sensor worn. Our approach does not require charging frequently to make an independent monitoring system.

1.3 On-body to Off-body (OB2OB) wireless transmission

OB2OB wireless transmission is a central point in the development of body-centric wireless communications (BCWCs). In common healthcare monitoring scenarios, it is very important for the antenna to radiate over the body surface directionally and directive towards off the body units to get the best on-body and off-body radio channel performances i.e., minimizing the link loss to ensure power efficiency. Body-centric wireless devices need to offer low power consumption to extend the battery life of the body worn devices and need to provide power efficient and reliable on-body and off-body communications. Fig. 1.3 shows the concept of different transmission channels where D represents the On-body to OFF-body communication network.

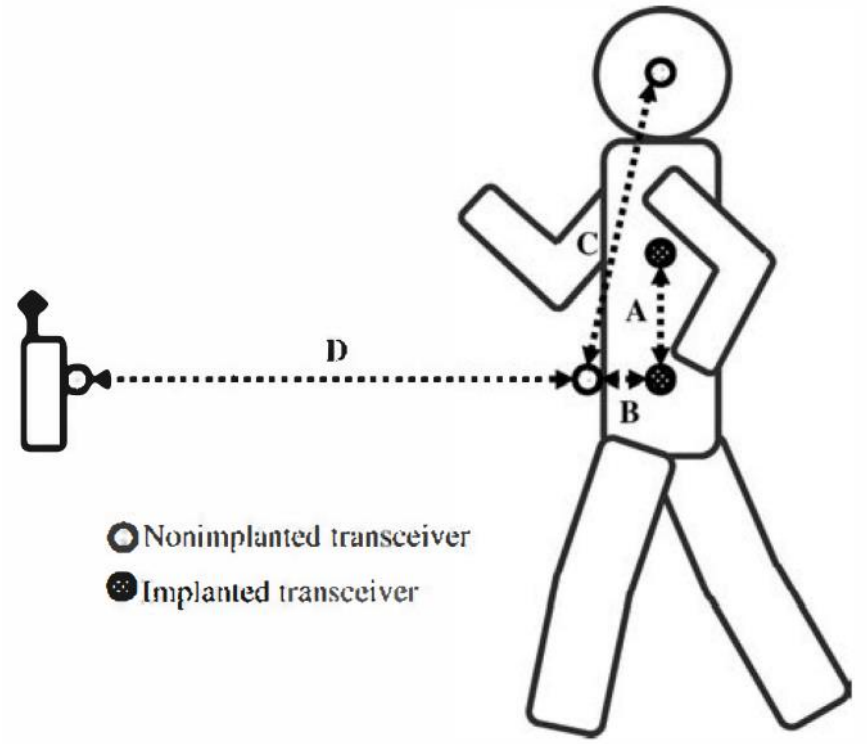

Fig. 1.3. On-body to off-body transmission [36]

Recently there have been growing interest and research development both in academia and industry in designing narrowband body worn antennas [29]- [35]. Hall et al. [29] - [30] have undertaken extensive studies on narrowband antennas (2.45 GHz) for on-body communication. In [31] a dual band button antenna for WLAN (2.45 GHz, 5.2 GHz) applications was presented by Batchelor. The antenna shows same radiation characteristics at both frequency bands. Alomainy et al. [32]- [34] presented various wearable antennas in the 2.4 GHz (ISM band) for on-body communications. Furthermore, in [35], Scanlon et al. presented a set of higher mode microstrip patch antennas operating at 2.45 GHz for over the body surface communications. Antenna radiation pattern influences the on/off-body radio channels performance. Antenna with omnidirectional radiation pattern over the body surface improves the path gain for the on-body links while antenna with directive off-body radiation pattern improves the path gain for off-body channels. However, a little research has been performed in designing of shoe-mounted antenna for power efficient on-body and off-body communications to meet the requirements of BLE beacon. In this paper, a BLE band and diverse radiation pattern is proposed for efficient and reliable cooperative on-body and off-body communications.

The antenna performance parameters of the proposed BLE band and diverse radiation pattern antenna are investigated by both simulation and experiment.

1.4 On-body to In-body (OB2IB) wireless transmission

Body area communications can also be used in medical diagnoses and treatment. In this scenario, an in-body device should consist of a sensor, a transceiver, and an operation unit. The sensor data are sent to an on- or off-body control unit by the wireless transceiver. The control unit makes a medical measurement and sends the corresponding command for medical treatment to the operation unit. The operation unit then carries out medical treatment based on the received command. One example of this scenario is an example of body area communications for medical diagnosis is the capsule endoscope. The ingestible capsule consists of a camera and a transceiver. It takes pictures during its course through the digestive tract after being swallowed and transmits the pictures or video data in real time from the in-body transceiver to On-body/off-body medical instruments. Fig. 1.4 shows the concept of this scenario, which can effectively promote the noninvasive diagnosis. In addition, automatic insulin injection for diabetes patients is also a possible application of body area communications. Using the data from a glucose sensor under the skin, an injection control unit linked by the body area communication technique can decide the correct amount of insulin to be injected. Then, an insulin pump carries out the injection according to the instruction from the control unit.

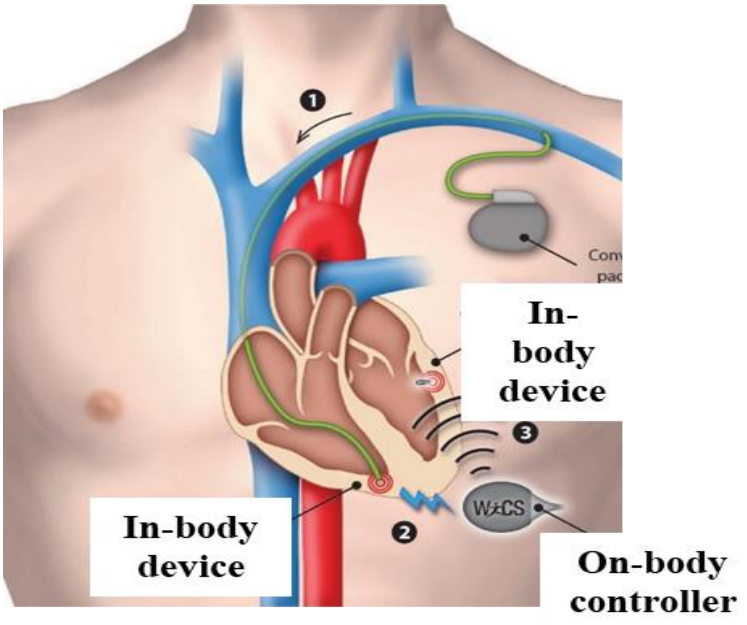

Fig. 1.4. On-body to In-body transmission

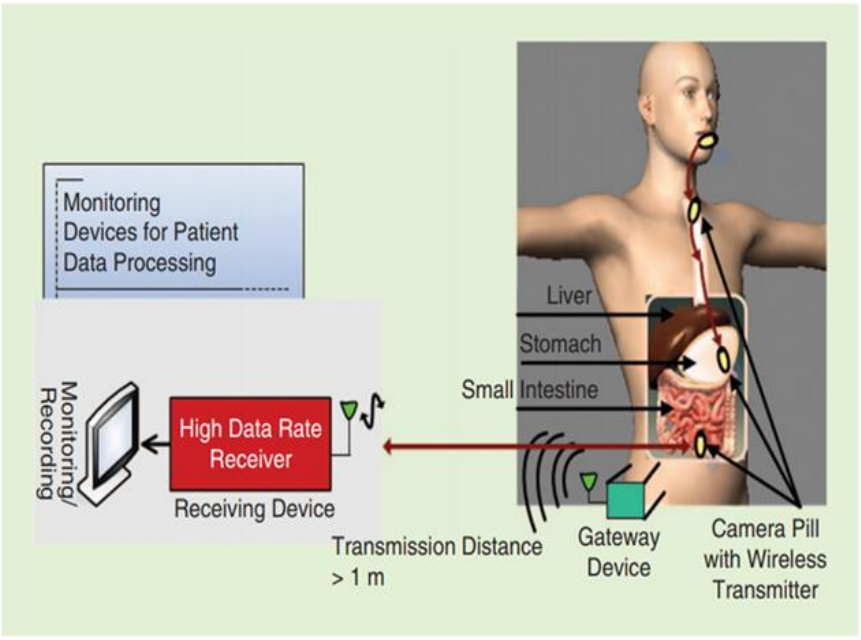

Fig. 1.5. Dosing robot of OB2IB communication

Fig. 1.5 shows the concept of this scenario of wireless control between on-body controller and in-body dosing robot. This scene indicates capsule endoscopy phenomena which also includes diagnosis for polyps, ulcers and tumors of small intestine, and diagnosis etc. The images captured by the miniature camera during a session are transferred wirelessly to an external receiver worn by the patient, using any one of a band of appropriate frequencies.

The collected images are then transferred to a computer for display, review, and diagnosis. A transmitted radio-frequency signal can be used to precisely evaluate and investigate the location of the capsule and to track it in real time inside the body and gastrointestinal tract.

1.5 Related previous studies

There are very limited previous studies from our group related with contents of this thesis. As the world fertility rate is falling, studies in [92] have presented that adults with small families have a longer lifespan compared to larger ones, so in the future, the elderly population is expected to be higher than that of the youth. In this view, where there is limited attention to elders, alternative health care support applications must meet user expectations in terms of portability, sensitivity, accuracy, durability, integrity, security, and interoperability [92, 93]. Further to that, technology advances in health care services expect fully deployment of the wireless body area networks to do more than it can do today for remote health and mobility monitoring and communication over the wireless interface. In [94], the authors discussed the WBAN sensors measure biological parameters such as blood pressure, temperature, sugar, electroencephalograph (EEG) and other body vital signs while actuators respond to the instruction based on the sensor measurement after computation. For instance, in diabetic illness, the actuator regulates blood sugar by controlling the insulin level. WBAN sensors can be deployed in or on the body using invasive and noninvasive techniques as body implants, surface contacts, or as wearable devices. The coverage distance of the WBAN devices in transmitting and detecting signals is limited to within the body. The assistance of other technologies like WiFi, WAN, ZigBee, and other wireless communication technologies, WBAN can forward information to the remote health care units for further decision support. Fig.1.6 illustrates a WBAN and beyond WBAN architecture consist of three functional sections, namely; intra-BAN, inter-BAN, and the health care unit [90].

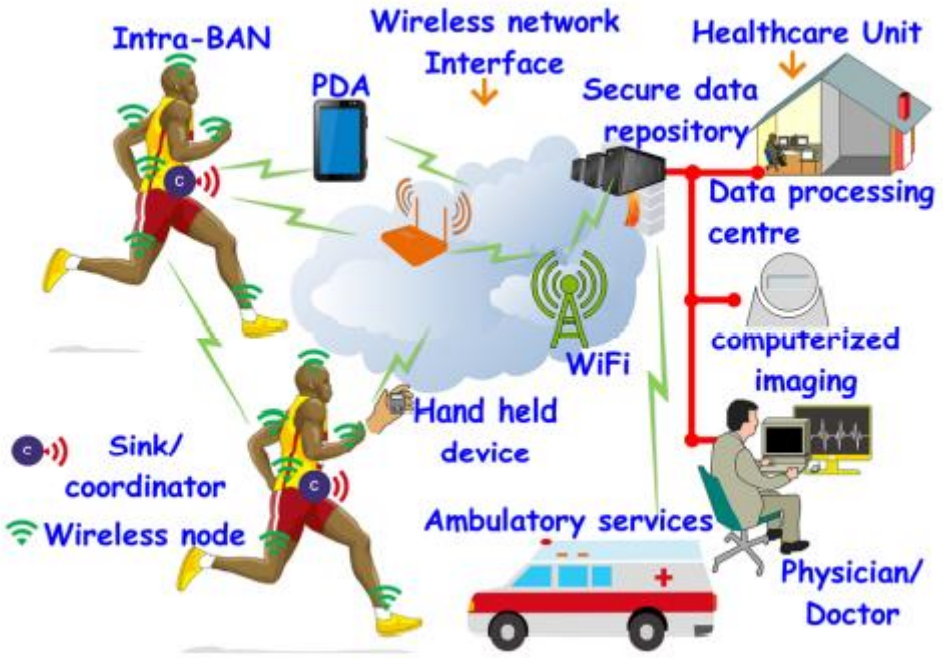

Fig. 1.6. WBAN and beyond WBAN architecture [90]

They discussed WBAN performance improvement issues, which recapitulates key challenging areas on the basis signaled through signal processing, security, network routing and reliability. In addition, they also included essential considerations on the path loss, anomalies, and network faults since shortly the healthcare system avails to the big data processing. This idea is quite attractive but prospects for health care services should have specific study as an increasing demand from In-body to On-body and On-body to Off-body with advances in technology and innovation. We have investigated channel characteristics and link budget analysis for 10-60 MHz band implant communication which will be described more details in chapter 2. We have also designed and evaluated directional antenna for shoe-mounted sensor for position identification of elderly wanderer, and conducted experimental measurement of energy harvesting by piezo material for powering shoe-mounted sensor which will be described in chapter 3 and 4. The overall investigation indicates that our work better and more convenient than the others so far. A healthcare monitoring system consists of the parts in Fig.1.7, and our study focus on the unestablished parts: in-body to on-body healthcare information transmission and on-body to off-body location information transmission to meet the

purpose of healthcare in an aging society. Bringing in new technologies and applying this idea to meet the purpose of healthcare are also novelties of our work.

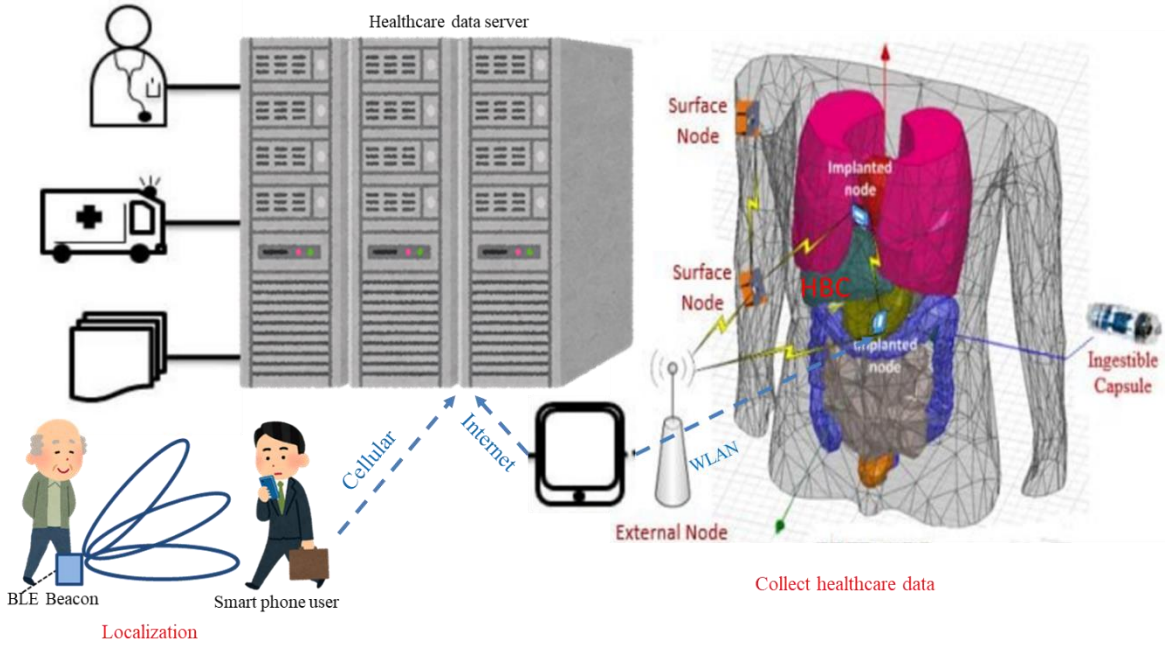

Fig. 1.7. Wireless transmission for healthcare purpose

1.6 Contents of this thesis

OB2IB i.e. Capsule endoscope mainly uses 400 MHz medical implant communication service (MICS) band for image transmission [89]. But in the 400 MHz MICS band, the transmission bandwidth is strictly limited to 300 kHz. On the other hand, ultra wide band (UWB) low-band communication enables high-speed transmission as compared with the MICS band, whereas the UWB low-band possesses large attenuation due to the UWB signal propagates through a human body [89]. So, the UWB low-band degrades the reliability of implant communication. The industrial, scientific and medical (ISM) can solve these problems but a drawback of this band is the lack of any protection against interference from other communication services in the same band. By investigating the above situations, the application of HBC (10- 60 MHz) band offers a great possibility for this wireless link to fulfill the above requirements. Fig. 1.6 shows a semi-infinite large plane medium of homogeneous human muscle tissue with a normal plane wave incidence

to it. The corresponding path loss was calculated theoretically at two typical depth of 5 and 10 cm. Compared to the 400-MHz band and UWB band, the path loss at the 10–60-MHz band is much smaller, which can thus provide a significant improvement on the communication distance in the human body. This result suggests that the implant communication is more appropriate at lower frequencies from the point of view of path loss. In addition, the 10–60-MHz band falls in the extremely weak radio band in Japan. According to a Japanese radio law, as long as the radiated electric field intensity is lower than 500 μV/m at a distance of 3 m, it is legally available for use [43]. This requirement is actually easy to satisfy because of the implant transceiver's small size, low transmit power, and usage in lossy media.

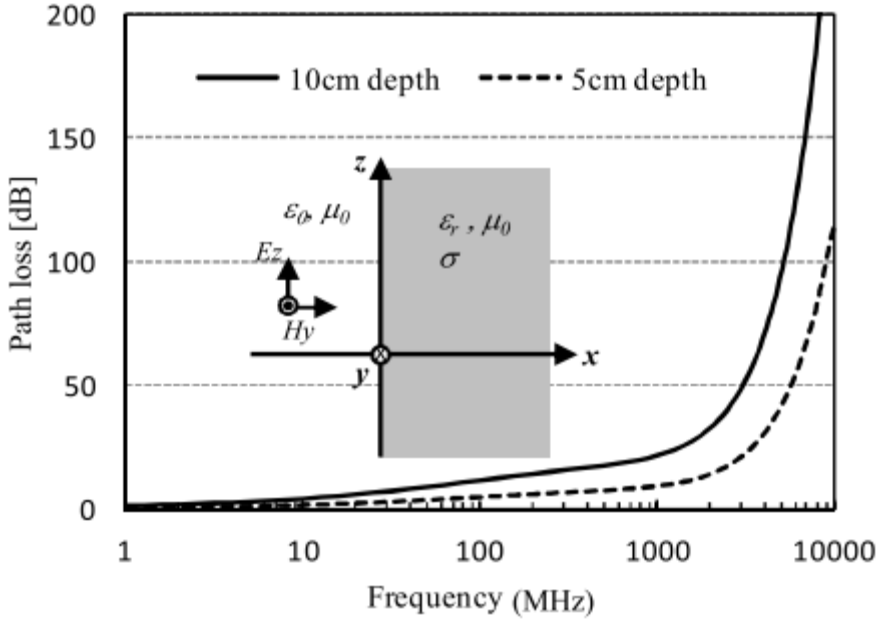

Fig. 1.8. Frequency dependence of path loss for muscle tissue [43]

OB2OB network consists of the transducers for signal detection, a power source, and the transceiver circuitry for wireless linkages. WBAN uses battery-powered wireless biological sensors to measure and transmit vital information over the wireless media to remote health units [90]. Due to the reduced size of the biological sensors, WBAN devices cannot be replaced easily. Similarly, the durability of the WBAN battery depends on its size. Therefore, a miniaturized battery size threatens WBAN operational lifetime. Apart from power constraints, WBANs face hindrance and other media impediments due to the harshness of the working environment for identifying location or interfering frequencies in the on-body to off-body transmission when operated near other devices within the same

radio frequency spectrum such as ZigBee and WiFi coexistence in the ISM band (2.4 GHz). Therefore, 2.4 GHz BLE band has been investigated and evaluated for on-body to off-body transmission.

In this study, a core idea runs through all our works: wireless body area communication specialized for issues for the elderly. We propose antenna designs that employ wireless transmissions, perform simulations, and performance analysis to show their effectiveness in OB2OB and OB2IB communications. We make a comparison with the most popular conventional antenna, i. e., Dipole antenna and Loop antenna under a conventionally recognized condition and analyze their superiority or inferiority quantitatively. We consider about both dipole and loop antenna, point out the difference of them for 10-60 MHz band implant communication, and provide the feasibility implant communication due to actual needs. To detect the position identification of elderly wanderer, we proposed a novel method to accomplish this job using a shoe-mounted sensor. The sensor is made with an originally designed directional antenna in the BLE beacon. According to the demand of elderly wanderer position identification, we designed patch arrays antenna to investigate the position identification rate if a wanderer is within from a smart phone user or a utility pole, which denotes the usefulness of the proposed monitoring system of elderly wanderers.

Chapter 1 is the introduction to this thesis.

Chapter 2 discusses the idea of driving the channel characteristics at 10-60 MHz band and link budget analysis, and provide a novel design of transceiver. Computer simulations between two different antennas and experimental evaluations were performed to make a comparison among them. With computer simulation and experimental results, we quantitatively show how our approach performs in improving the communication performance.

Chapter 3 is about a robust technology i.e. a monitoring system using BLE beacon to detect wanderer location identification which is one the promising parts of our research. The monitoring system can provide an elderly person with a BLE beacon for early detection of wandering elderly. The signal from the BLE module is received by a base station installed in a building or a power pole, or by a smartphone owned by a person who happens to pass by. Then the position of the elderly person can be detected from the received signal and accumulated in a server, because the position of the base station is known in advance and the position of the person holding the smartphone is known from the smart phone signal. This enables early detection during loitering. Directive antenna design and simulation evaluations were also performed at first. After that, we make manufacturing the one to check the performance, and do experimental evaluations on it

to evaluate its validation.

Chapter 4 proposes an energy harvesting technique to make an independent system to our monitoring method. Pressure produced voltage measurement was performed to explain the mechanism. Implementation of our approach was also conducted by placing NKN and BCTZ piezo materials. Experiments are performed to verify its effectiveness.

Chapter 5 is a summary of the thesis.

Chapter 2
Characterization of 10-60 MHz Band On-body to In-body Transmission

2.1 Overview

The objective of this chapter is to clarify the basic channel characteristics of 10-60 MHz HBC band from a theoretical approach. By using a typical electric dipole and a magnetic dipole (current loop), the path loss and group delay are calculated using the finite difference time domain (FDTD) method and an anatomical human body model. Then the path loss model is derived, and the electric and magnetic field distributions are analyzed to clarify the propagation mechanism. To support the analysis results, an experimental measurement results present for validation using a biological-equivalent liquid phantom. Here, we will show link budget analysis for giving guidelines for transceiver design.

Wireless communication technology is making great progress with innovative advances in small electronic devices, and wireless implant communication has proven to be promising for medical services and health care applications. It links nodes in and on the human body to send in-body diagnostic information to the outside or control in-body nodes from the outside for diagnosis and drug administration [36], [37]. Typical examples of implant communication are capsule endoscope [38] and wireless cardiac pacemakers [39]. For this purpose, the in-body to on-body wireless channel requires high reliability and high transmission speeds.

Implant communication mainly uses 400 MHz medical implant communication service (MICS) [38]. But in the 400 MHz MICS band, the transmission bandwidth is strictly limited to 300 kHz so that it is difficult to realize high transmission speeds and large transmission capacity. Some attempts were performed in the 2.4 GHz industrial, scientific, and medical (ISM) band [39] and ultra-wide band (UWB) [40]- [42], that might provide higher transmission speed. However, the human body is a lossy dielectric medium, and

its dielectric properties are frequency dependent. As discussed in [36], the penetration depth decreases significantly as the frequency increases. At an in-body to on-body communication distance of 10 cm for muscle tissue, the penetration depth is nearly 2.2 cm at 2.4 GHz and 0.9 cm at 5 GHz. Such a characteristic makes it almost impossible for implant communication deep inside the human body. So, the UWB can only allow communication with nodes at depths not exceeding 5 cm [41]. The 2.4 GHz ISM band signal can propagate to deeper locations compared to UWB, but a drawback of this band is its high possibility of interference from other communication services in the same band. Based on the above considerations, the authors' group proposed to employ the 10-60 MHz human body communication (HBC) band for the wireless implant communication to meet its requirements. Compared to the 2.4 GHz ISM band and 3.1-10.6 GHz UWB, the penetration depth at 10 MHz is nearly 22 cm. The large penetration depth or small path loss provides more possibilities for high-reliability communication, and the 50 MHz bandwidth provides data rates of more than 20 Mbps. The authors' group has developed a transceiver for the implant communication using the 10 - 60 MHz HBC band, and demonstrated its feasibility with living swine [43]-[45]. The experiment has achieved a high data rate of 10 Mbps up to 26 cm depth in the living swine body. The developed implant transceiver has the best results reported so far in the literature in terms of data rate and transmission depth. However, the propagation characteristics in this frequency band have not been theoretically analyzed to an adequate level. The propagation characteristics in the human body are very complicated. There are absorption phenomena in the human body because of the lossy dielectric properties of body tissues and scattering due to the heterogeneous nature of body tissues. That is why the transmitted signal is largely attenuated. Moreover, shadowing arises due to diffractions in the different organs of the body, and creeping waves exist along the body surface. Consequently, a received signal may end up being the superimposition of several attenuated, delayed, and distorted replicas of a transmitted signal. So, an implant communication channel undergoes severe signal decay and shadowing during the transmission inside the body, and channel modeling needs to incorporate the path loss and group delay characteristics.

2.2 Analysis Method and Channel Characteristics

The implant channel characteristics are not easy to measure with a living body. A usual method to derive them is to employ the FDTD simulation and an anatomical human body model. Since the in-body to on-body channel is a near-field situation in the 10-60 MHz HBC band, the channel characteristics are antenna dependent. This makes it difficult to remove the transmitting and receiving antenna gains so that the calculated path loss includes them. So, it is desirable to use a representative antenna to analyze the channel characteristics. In this study, an electric dipole and a current loop are used as two representative implant antennas. Here, we used anatomical human body model as an investigative simulation tool. The simulation environments of human body with a small dipole antenna and loop antenna on its surface to receive the capsule endoscope data are illustrated in Fig. 2.1 and Fig. 2.2 respectively.

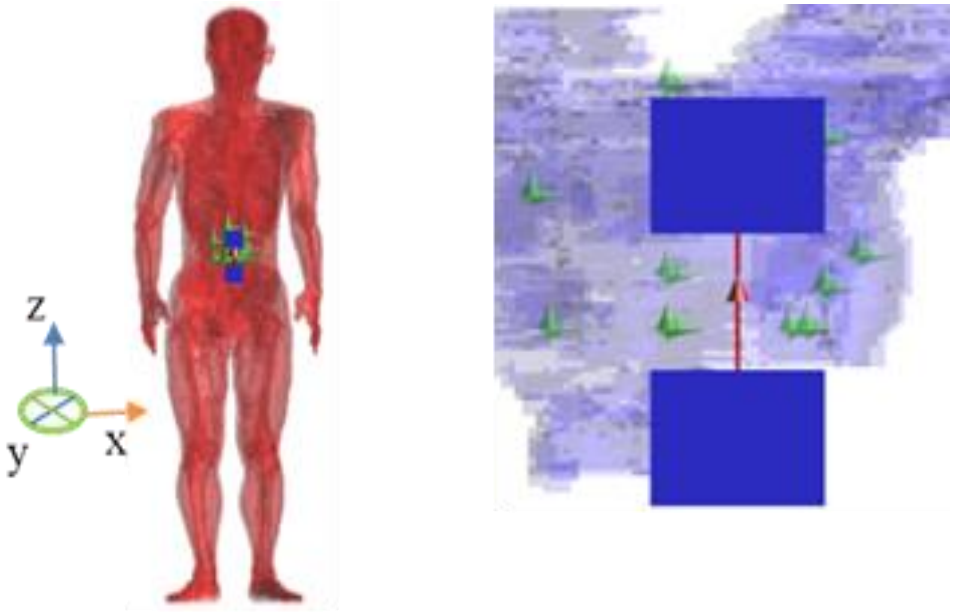

a) Overall view

b) Enlargement of small intestine area to show transmitting antenna position

Fig. 2.1. FDTD simulation environment with dipole antenna

The human body model is constituted of detailed anatomical structure which has more than 50 types of tissue and 2-mm spatial resolution [46]. The database on the dielectric properties of biological tissue is mainly based on Gabriel's measurement data [47]. The

dielectric properties were used for the anatomical human body model in the frequency range from 10 to 60 MHz for path loss and group delay analysis. In an implant communication system, either the transmitting antenna or the receiving antenna is inside the body and the other one is on the body. The implant antenna was installed at 15 locations in the human torso in x, y or z directions, whereas the on-body antenna was supposed to have the same orientation as those. When the implant antenna was a 10-mm long electric dipole, the on-body antenna was a 150-mm long electric dipole, whereas when the implant antenna was a 10-mm diameter current loop, the on-body antenna was a 150-mm diameter current loop. The thickness of the antenna elements was 2 mm.

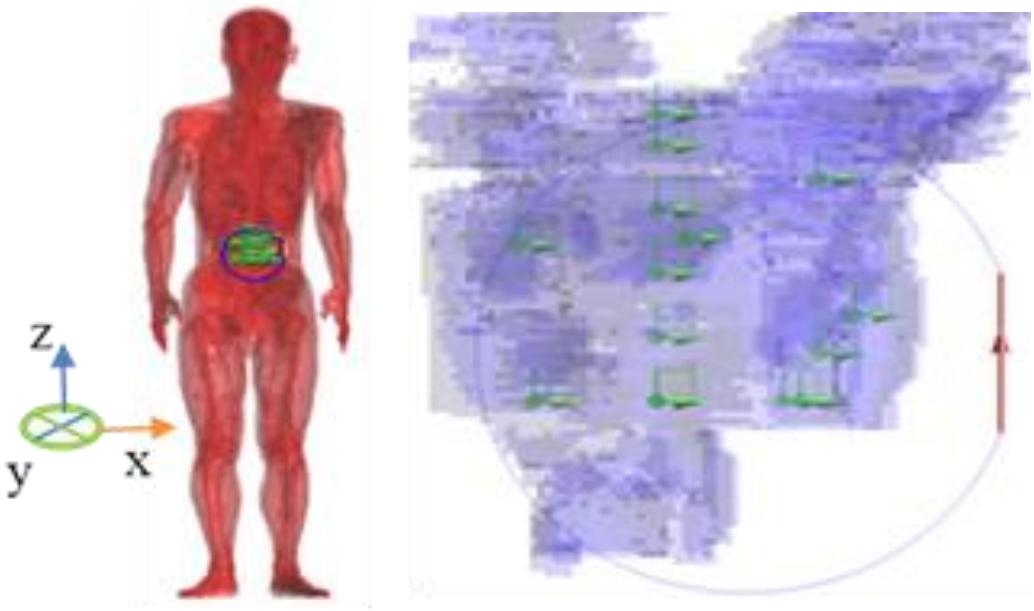

a) Overall view b) Enlargement of small intestine area to show transmitting antenna position

Fig. 2.2. FDTD simulation environment with loop antenna

The 45 edge sensors for dipole antenna and 45 current sensors for loop antenna were placed inside the body at the polarization directions x, y and z based on practical moving rotations of capsule endoscope. As a result, at in-body location, we obtained 45 data for extracting the propagation channel characteristics. For path loss analysis, the simulation setting was harmonic simulation, and it was performed by finite difference time domain (FDTD) method incorporated with the anatomical human body model; considering different relative permittivity and electrical conductivity at 10 to 60 MHz respectively.
And for group delay analysis, the simulation setting was broadband simulation and we considered pulse transmitting signal. Fig. 2.3 shows the *Tx* and *Rx* view for loop antenna.

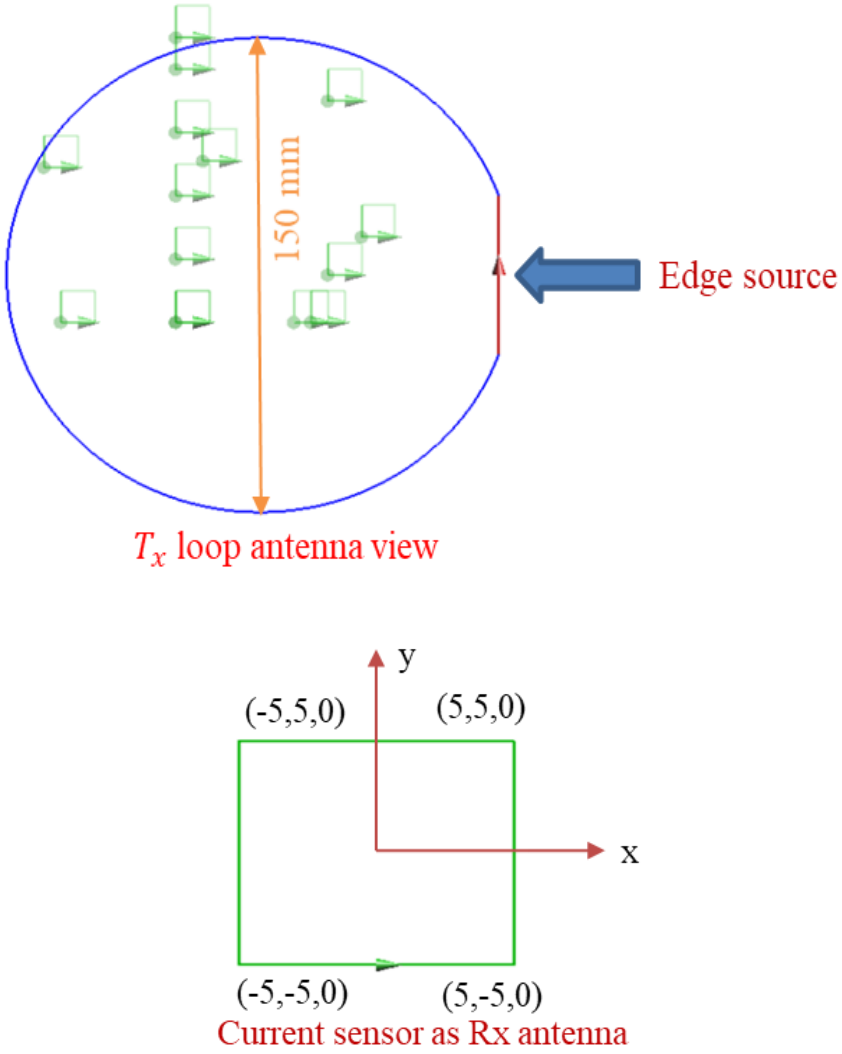

Fig. 2.3. Overall size of loop antenna

Fig. 2.4 and Fig. 2.5 shows the time waveform and frequency spectrum of the transmitted pulse signal for the dipole antenna respectively. Fig. 2.6 and Fig. 2.7 shows the time waveform and frequency spectrum of the transmitted signal in case of the loop antenna respectively.

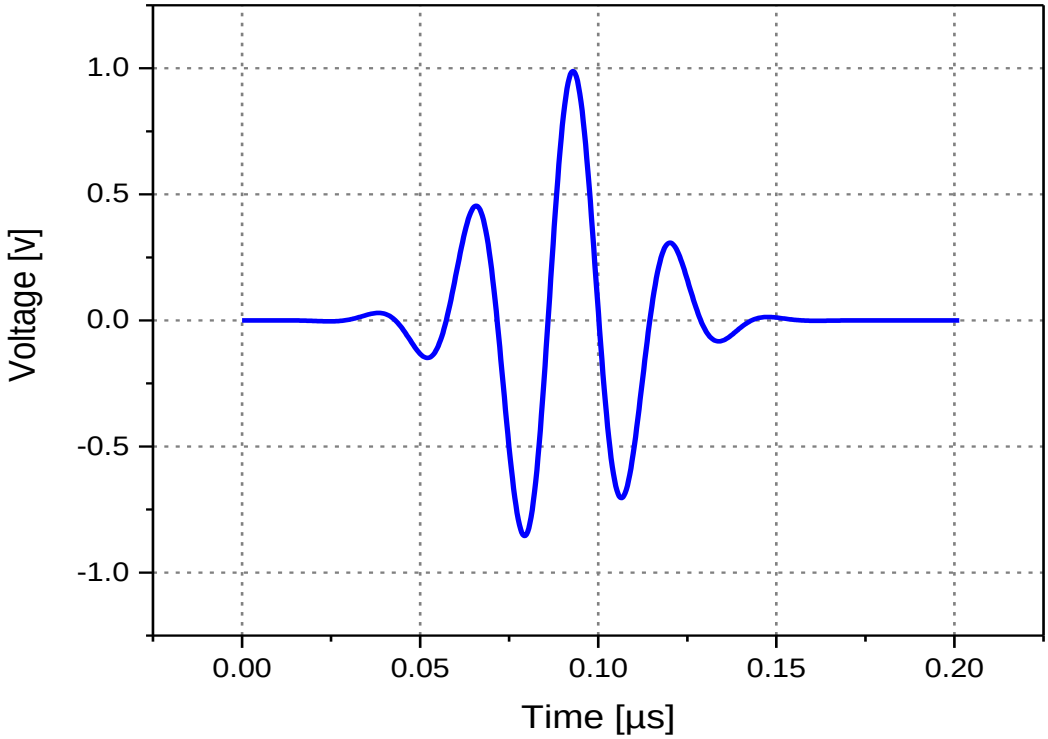

Fig. 2.4. Time waveform of transmitted signal for dipole antenna

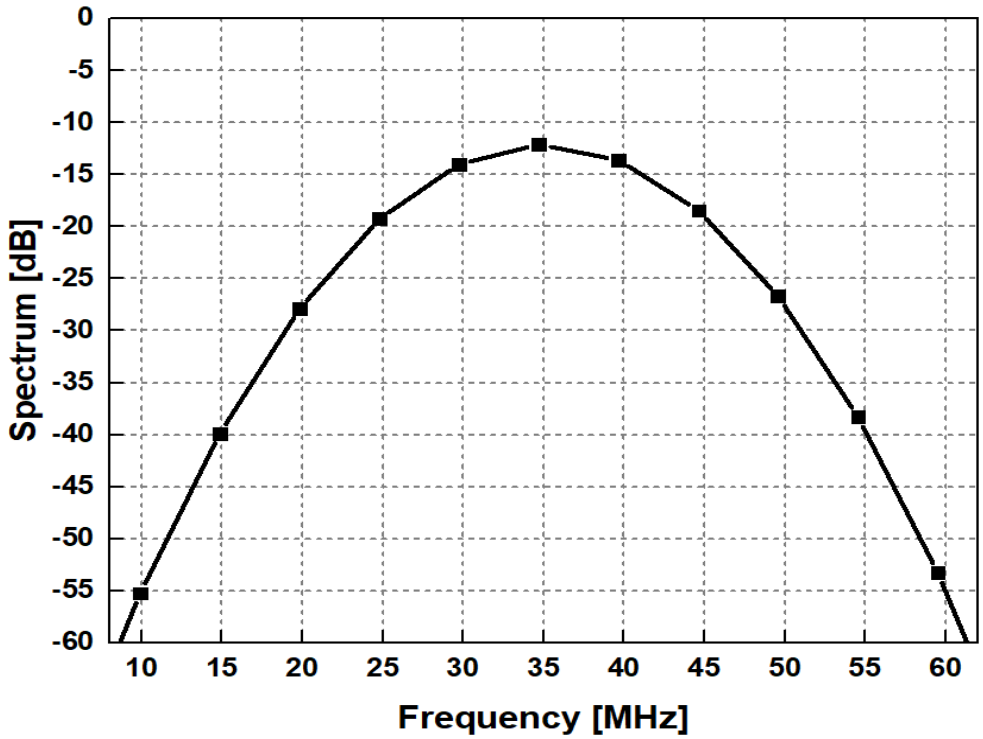

Fig. 2.5. Frequency spectrum of transmitted signal for dipole antenna

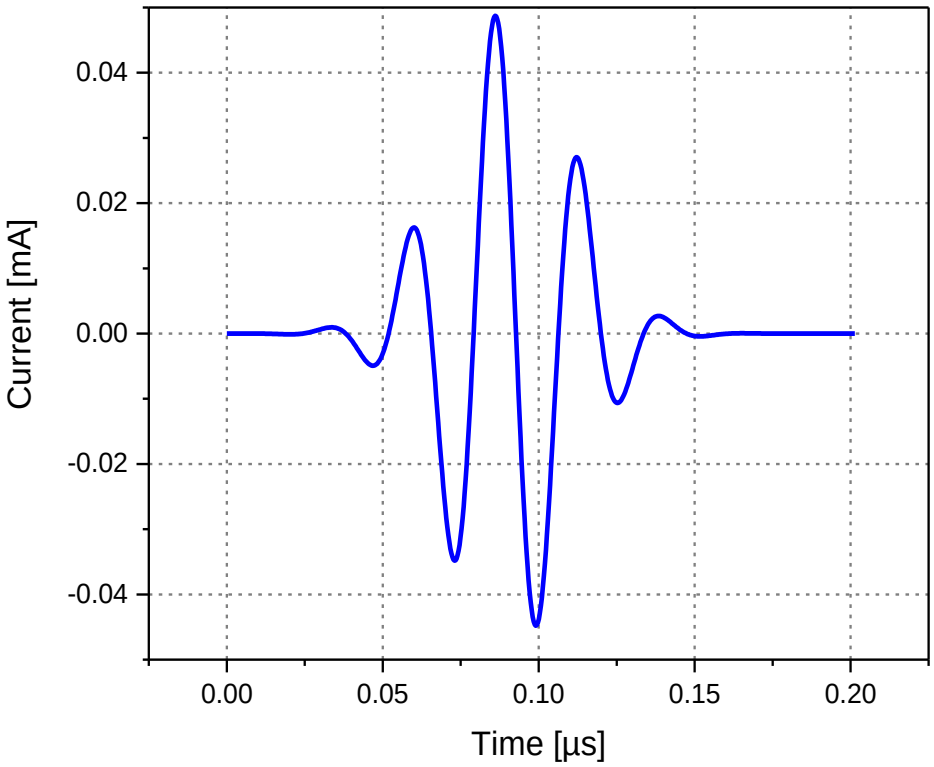

Fig. 2.6. Time waveform of transmitted signal for loop antenna

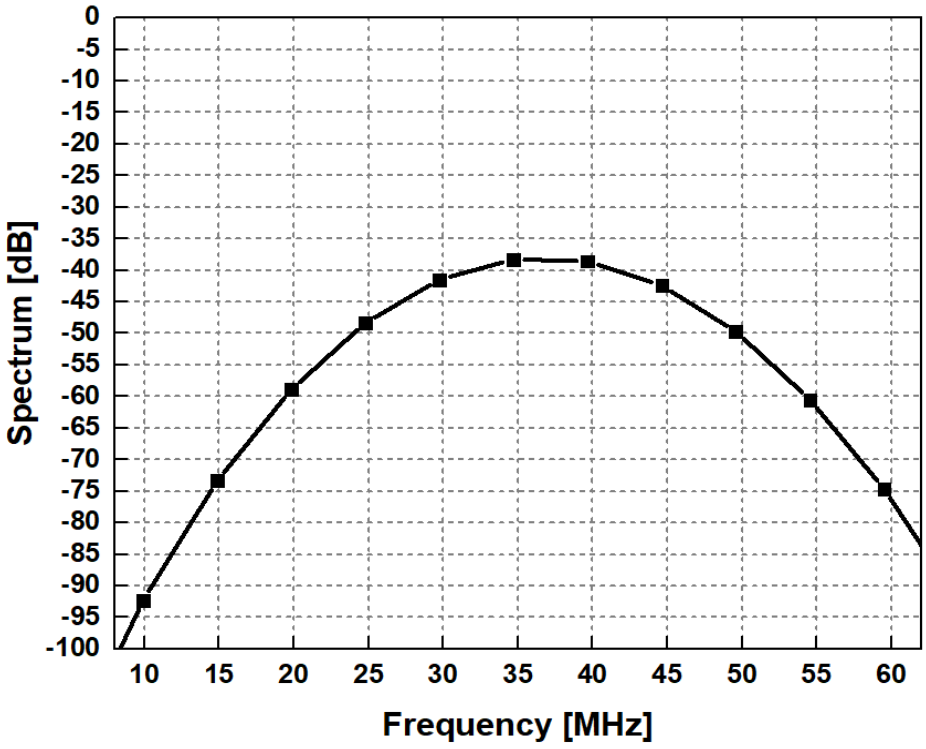

Fig. 2.7. Frequency spectrum of transmitted signal for loop antenna

2.2.1 Path loss analysis

In each case of dipole and loop antennas, the implant antenna was excited using a harmonic voltage source, and the received voltages and powers were calculated at the on-body antenna using the FDTD method. From the FDTD- calculated transmitted power P_t and received power P_r at different frequencies from 10 to 60 MHz, the path loss at a distance d between the transmitting antenna and the receiving antenna is obtained as

$$PL_{dB}(d)=10log_{10}\left[\frac{P_t}{P_r}\right] \quad (2.1)$$

The calculated path loss contains the effects of the transmitting and receiving antennas due to the difficulty in removing them in such a near-field communication situation. Fig. 2.8 shows the calculated path loss at 10–60 MHz when both the transmitting and receiving antennas are dipoles, and Fig. 2.9 shows the calculated path loss at 10–60 MHz when both the transmitting and receiving antennas are loops. Assuming an empirical power decay law function, the path loss in *dB* at some distance *d*, including shadowing, can be approximated by the following equation

$$PL_{dB}(d)=PL_{dB,d0}+10nlog_{10}\left[\frac{d}{d_0}\right]+S_{dB} \quad (2.2)$$

where $PL_{0,dB}$ is the path loss at a reference distance d_0, and n is the path loss exponent which depends on the environment where the radio frequency signal is propagating through. For example, it is well known that $n = 2$ in free space. But in the implant channel, the path loss exponent can be much larger than free space. In addition, S_{dB} is called shadowing or random scatter around the mean path loss and represents deviation in *dB* caused by different tissues/organs (e.g., bone, muscle, skin etc.) surrounding the transmitter. As reported in[40]for simulation using an anatomical human body model and[41]for measurement using a swine, the difference in tissue types and thickness between the transmitter and receiver will significantly affect the path loss. A high water-content tissue such as muscle has a larger path loss, whereas a low water-content tissue such as fat and bone has a smaller path loss. The in-body path loss is therefore dependent on not only the distance but also the types and thickness of tissue between the transmitter and receiver.

This characteristic caused the deviation from the mean path loss. The mean path losses for dipoles and loops were respectively derived by fitting the path losses in Figs. 2.8 and 2.9 using Eq. (2.2). The shadowing S_{dB} was obtained by taking the difference between the FDTD-calculated

path loss and the mean path loss, where σ_{dB} is defined as the standard deviation of the shadowing S in unit of dB. It reflects how concentrated the path loss is around its mean value as well as the degree of the shadowing strength. To focus the discussion on the exponent n and shadowing S, the vertical axises in Figs. 2.8 and 2.9 are set to PL_{dB} -$PL_{0,dB}$.

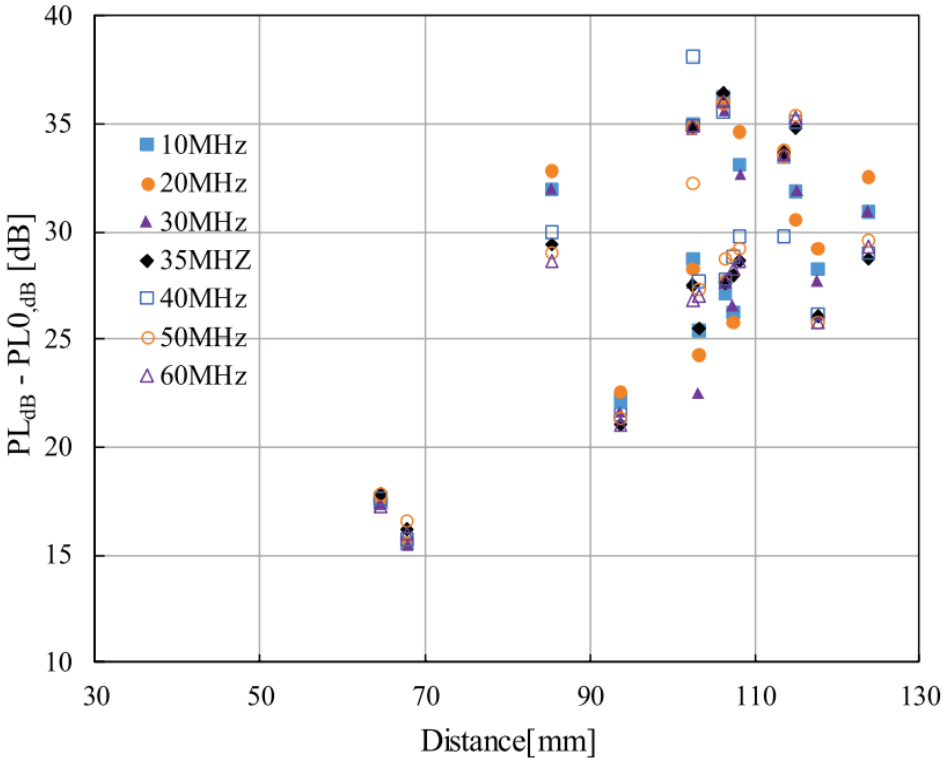

Fig. 2.8. $PL_{d\ B} - PL_{0,\ d\ B}$ versus distance for dipole antenna

Table 2.1 shows the fitted parameters for individual path loss model from 10 to 60 MHz when the transmitting and receiving antennas are both dipoles or both loops, respectively. It turns out that the loop antennas give a smaller exponent n and standard deviation σ at all frequencies from 10 to 60 MHz, and the frequency dependence is insignificant. The path loss averaged over 10–60 MHz band was then calculated and shown in Fig. 2.10. The parameters fitted using Eq. (2.2) are shown in Table 2.2. The path loss exponent n was found to be 5.6 when the transmitting and receiving antennas were dipoles, and 3.9 when the transmitting and receiving antennas were loops. Moreover, the standard deviation σ of shadowing was 4.0 dB for dipoles and 3.1 dB for loops. Therefore, the loop antennas exhibit the smaller path loss exponent n and standard deviation σ.

In addition, the shadowing data were also processed to observe cumulative distribution function (CDF). Fig. 2.11 shows the CDF versus shadowing for dipole and loop antennas. The classical second-order Akaike information criterion (AIC) test[48]was performed to find the statistical distribution of shadowing term. The candidate distributions were considered as normal, log-normal, Rayleigh, Rice and Weibull distributions. The parameters of the specific distributions were estimated using the maximum likelihood estimation technique. From the observation of Table 2.3, the statistical distribution of the shadowing *S* was found to be well approximated by log-normal distribution in both dipole and loop antenna cases (normal distribution when the shadowing is in dB as shown in Fig. 2.11), because it has the largest log likelihood. The standard derivation not exceeding 4 dB suggests a weak shadowing effect around the human body in the 10–60 MHz band, which is our desirable phenomena.

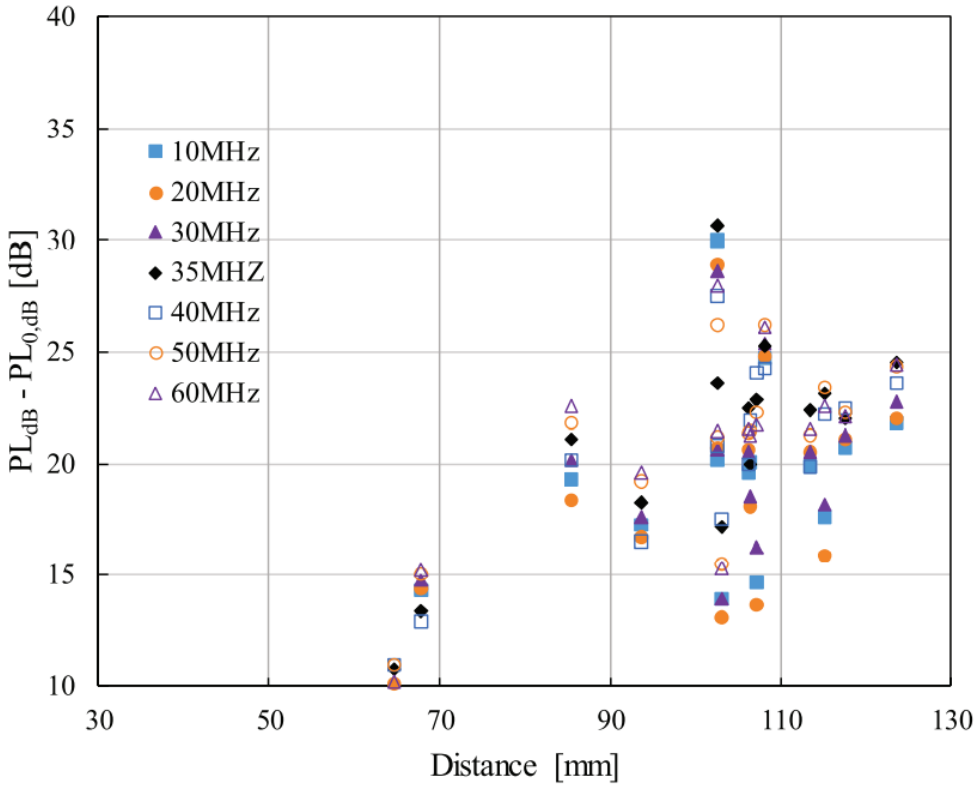

Fig. 2.9. $PL_{d\,B} - PL_{0,\,d\,B}$ versus distance for loop antenna

Table 2.1. Fitted path loss parameters

f [MHz]	n	σ [dB]	n	σ [dB]
	Dipole		Loop	
10	5.5	4.1	3.3	4.0
20	5.6	4.3	3.2	4.1
30	5.4	4.3	3.3	3.7
40	5.4	4.1	4.2	3.2
50	5.4	4.0	3.9	2.7
60	5.5	4.0	3.9	3.1

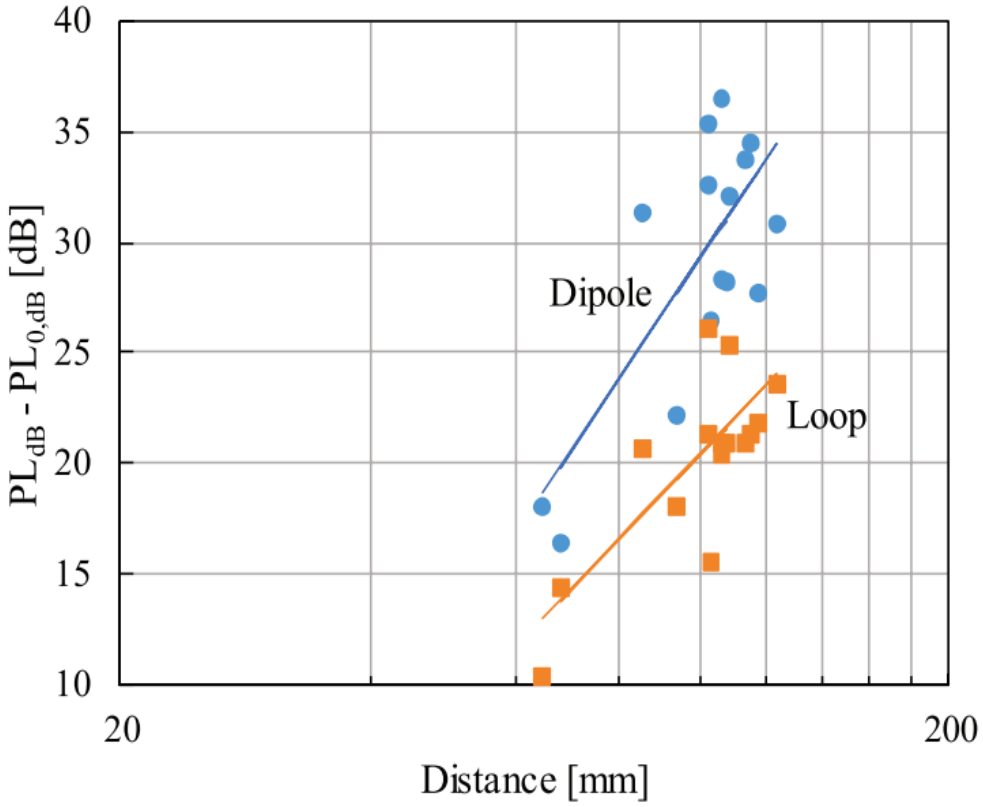

Fig. 2.10. Band-averaged $PL_{dB} - PL_{0,dB}$ versus distance

Table 2.2. Fitted band-averaged path loss parameters

Antenna	n	σ [dB]
Dipole	5.6	4.0
Loop	3.9	3.1

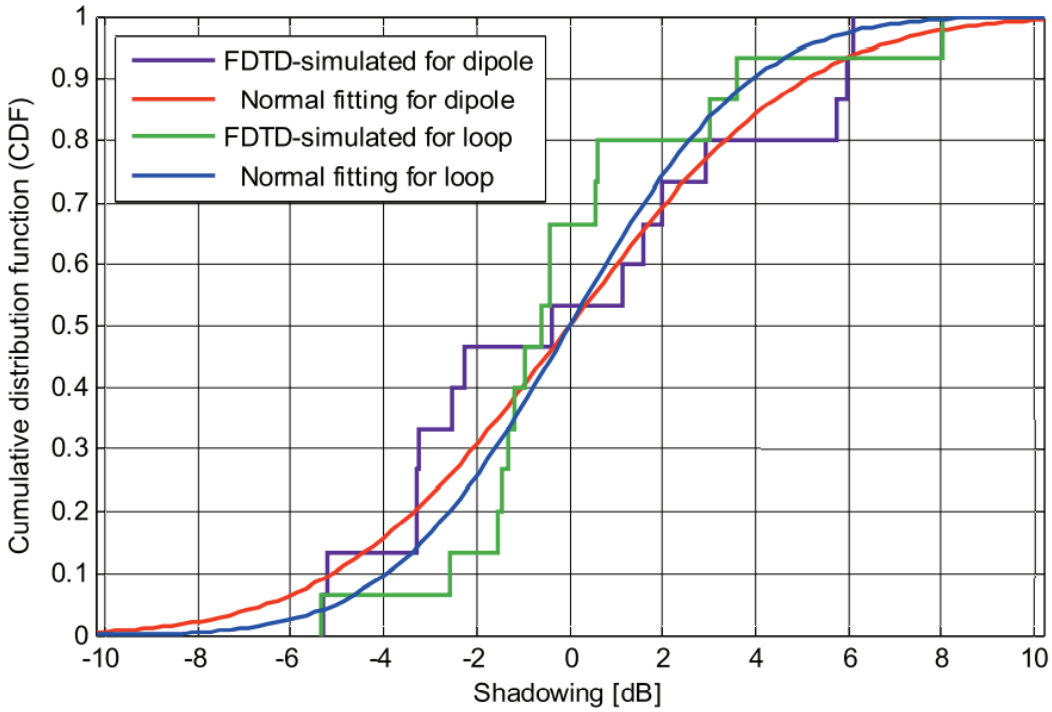

Fig. 2.11. CDF of shadowing for dipole and loop antenna

Table 2.3. Log likelihoods of statistical distribution fitting

Dtstribution	Dipole	Loop
Normal	−25.5	−26.6
Log-normal	−19.5	−15.6
Rayleigh	−25.2	−24.8
Rice	−25.2	−24.8
Weibull	−20.5	−18.9

2.2.2 Group delay Investigation

Group delay is a measure of how the phase response of the channel deviates from the ideal linear response. It is defined as the derivative (or slope) of the phase response. A channel with a linear phase response usually has a constant (or flat) group delay. In this study, from the ratio of FDTD-calculated received voltage and transmitted voltage, the transfer function *H* (f*)* was obtained, and then the group delay was calculated by

$$T_g = -\frac{d\varphi}{d\omega} \quad (2.3)$$

where φ is the phase in radian of the transfer function H (f), and ω is angular frequency. Figure 2.12 shows the group delay variation with respect to the group delay at the central frequency of 35 MHz as a function of frequency at a communication distance of 10 cm. The variation between 10 and 60 MHz is between 0.90 ns and 0.38 ns for dipole antennas and between 0.77 ns and 0.18 ns for loop antennas. The group delay at the central frequency is around 1 ns. Considering a data rate of 20 Mbps for implant communication, the group delay variation is in the order of smaller than 1 ns, which is only 1/50 of one-bit period, so the channel is almost a linear phase response. Moreover, the loop antennas provide a smaller variation of group delay, and therefore a flatter channel.

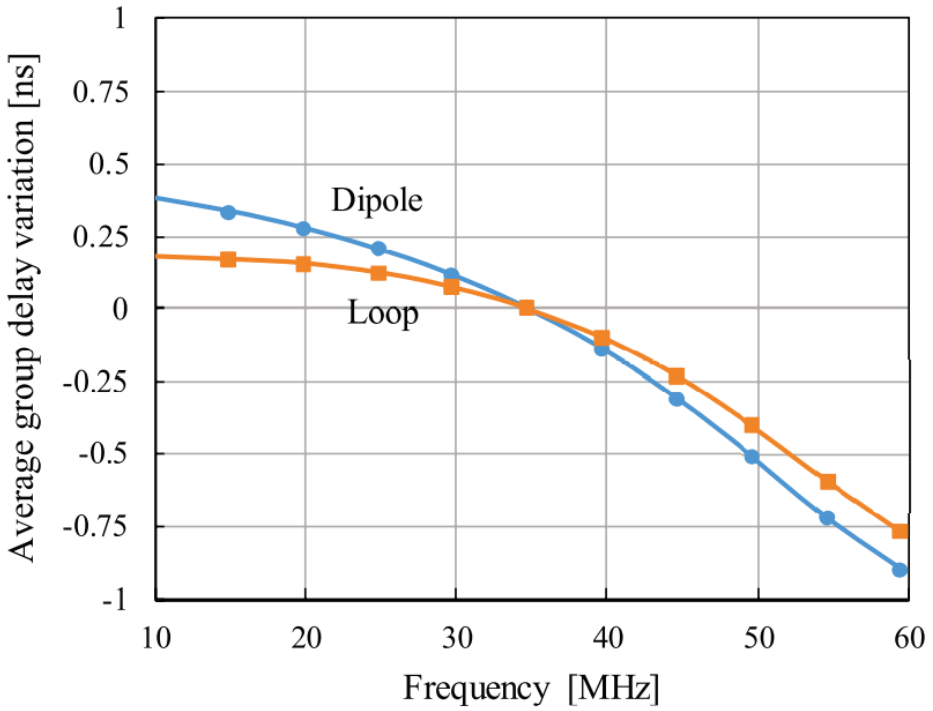

Fig. 2.12. Group delay variation with respect to the group delay at the central frequency of 35 MHz

2.2.3 Field Distribution

From the analysis results of path loss and group delay, the loop-type transmitting and receiving antennas exhibit more advantages than dipole-type antennas. To clarify the mechanism, the electric field and magnetic field distributions were analyzed in the human body. Figure 2.13 shows the electric field distribution for an on-body dipole antenna

excitation and the magnetic field distribution for an on-body loop antenna excitation in the vertical plane at 60 MHz. Figure 2.14 shows the electric field distribution and the magnetic field distribution inside the human body. It is observed that the electric field strength around the on-body transmitting dipole antenna is relatively strong, but gradually decays as the distance increases. The Permeability, μ properties of air and Human body are same, and permeability property affects the intensity of magnetic field. On other hand, the relative permittivity, ε_r and electrical conductivity, σ_s of human body are larger than air, and these properties affect the intensity of Electric field. In comparison with the electric field distribution, the magnetic field strength around the on-body transmitting loop antenna is also relatively strong, and decays much slowly compare to the electric field as the distance increases. This result suggests that the magnetic field component is more effective to propagate into the human body in the 10–60 MHz HBC band[49], and also supports the above path loss and group delay results. So a magnetic antenna is more effective for the implant communication in this frequency band.

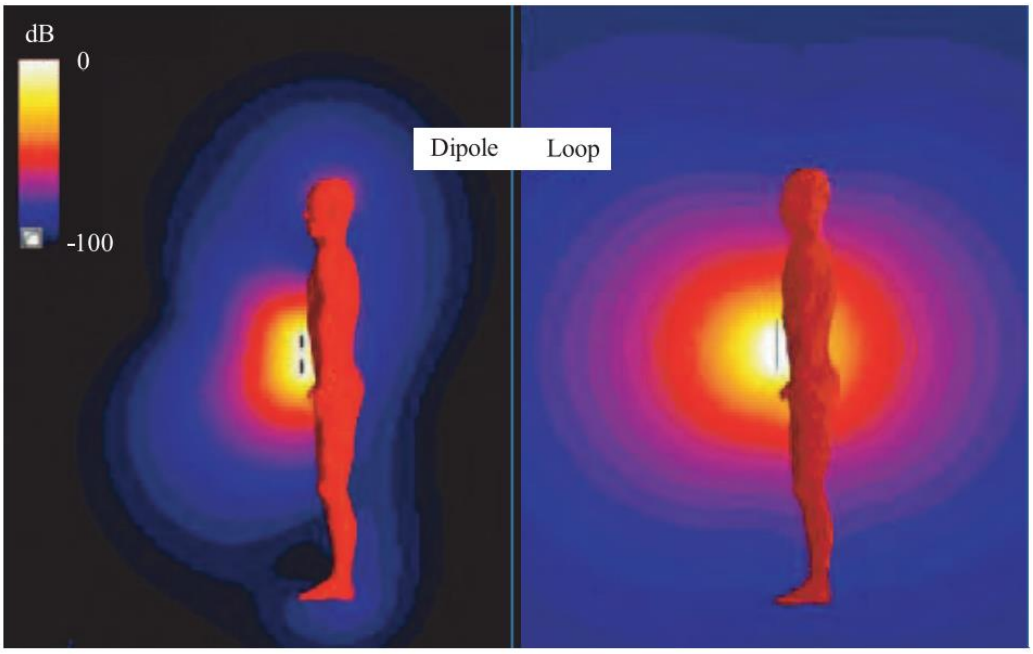

Fig. 2.13. (a) Electric field distribution for an on-body dipole antenna excitation. (b)Magnetic field distribution for an on-body loop antenna excitation. For both distributions the maximum field strength is normalized to 0 dB

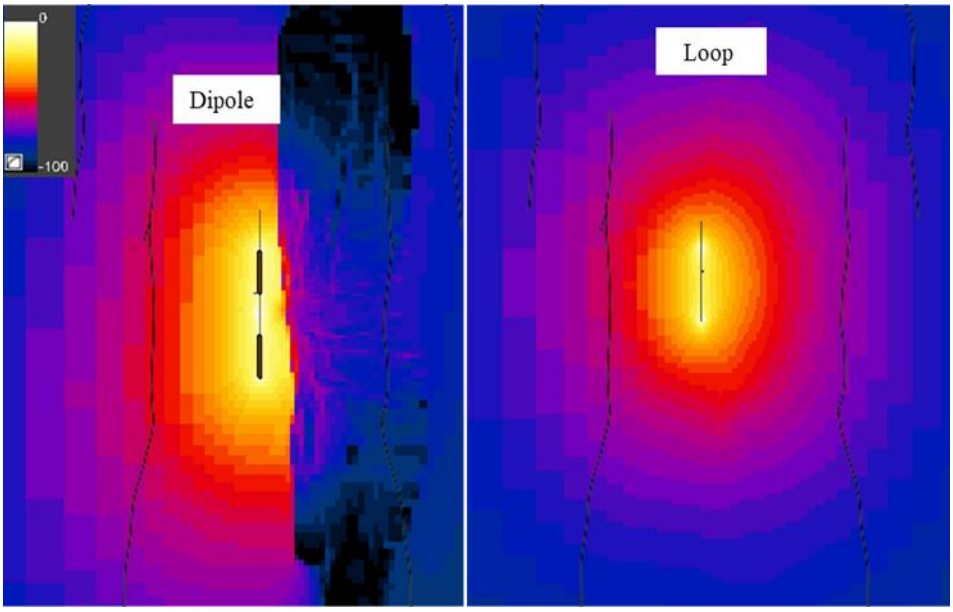

(a) **(b)**

Fig. 2.14. (a) Electric field distribution inside the human body for dipole antenna excitation. (b)Magnetic field distribution inside the human body for loop antenna excitation. For both distributions the maximum field strength is normalized to 0 dB

2.3 Path Loss Measurement

From the findings in the previous sections, the magnetic field components are easier to be transmitted, and therefore a helical invert-F antenna was developed for both in-body transmitter and on-body receiver[43]. Since we are considering the case of near filed communication, it is difficult to remove the antenna characteristics from the calculated path loss. Therefore, in the numerical simulation, we used two representative antennas of dipole and loop. The derived path loss should be more general. In actual use, however, a simple dipole or loop will not give good communication performance. We therefore designed the more efficient helical invert-F antenna and used it for communication experiment. As shown in Fig. 2.15[43], the helical invert-F antenna has a hollow cylindrical shape with a diameter of 16 mm and a length of 26 mm, and consists of three layers. In the inner layer, a copper foil forms a hollow cylinder with a diameter of 14.6 mm, and this plays the role of antenna ground. The middle layer is a flexible magnetic sheet with both high permeability and high permittivity so that a double wave- length

shortening effect can be expected by fabricating the helical element on it. The outer layer is the helical element formed of a copper foil with a width of 4 mm and a pitch of 6 mm in order to act mainly as a magnetic antenna. But an inverted-F structure is introduced so that the feeding source between the helical element and the ground is set at the upside of the cylinder and a short pin between the helical element and the ground is set at the top of the cylinder. This results in a helical-dipole structure, which is no longer a simple magnetic antenna. A helical antenna can be considered as a combination of many small loops and small dipoles. Therefore, the loop structure ensures that the magnetic field component is excited and detected.

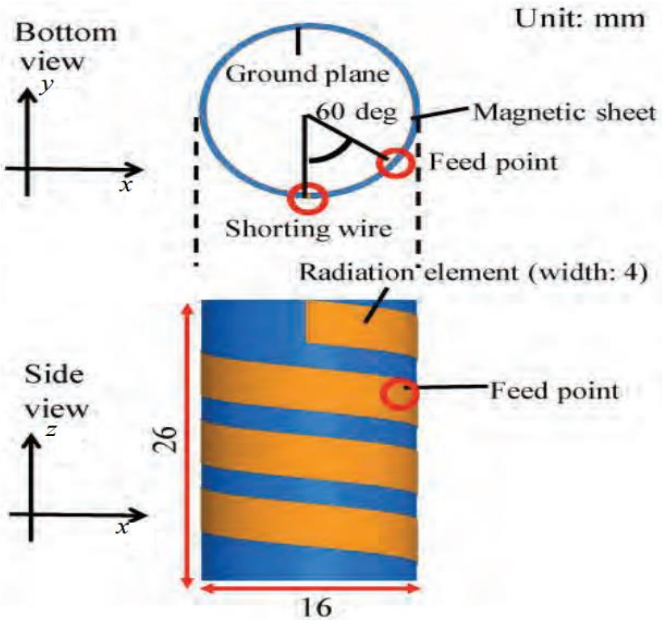

Fig. 2.15. Structure of helical invert-F antenna

In addition, with this structure, it is possible to increase the antenna length by increasing the number of helical turns, which is advantageous in realizing miniaturization of the antenna at tens of MHz. Fig. 2.16 shows the setup of path loss measurement using the helical invert-F antenna in a biological equivalent liquid phantom in place of the human body. The biological-equivalent liquid phantom was 28 cm × 16 cm × 22 cm, made of deionized water, sugar, sodium chloride, and so on, and its dielectric properties were adjusted to have relative permittivity of 56.05 and conductivity of 0.52 S/m at 50 MHz, nearly 2/3 times the muscle's values at 50 MHz. Although the homogeneous liquid phantom is difficult to express scattering and shadowing from various organs in the human body, it is useful to experimental validate the mean path loss.

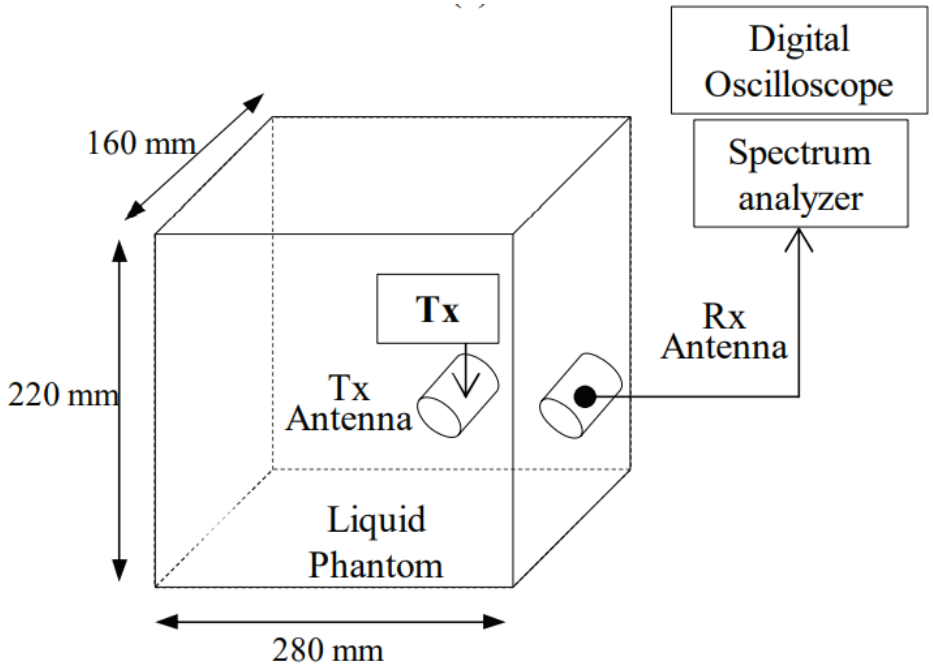

Fig. 2.16. Measurement setup of path loss using the helical invert-F antennas in a liquid phantom

Before the path loss measurement using the above setup, we first measured S_{11} using a network analyzer when inserting the antenna into the liquid phantom as shown in Fig. 2.17. The result shows an absolute -10 dB bandwidth of 8.4 MHz (relative bandwidth of 16%) from 50 to 58.4 MHz. Possible body area communication bands include the tens of MHz as described in the IEEE 802.15.6 standard and other literature [36], [45]. Here we selected 10-60 MHz with 50 MHz bandwidth to increase the data rate to at least 20 Mbps for high speed transmission. This frequency band is the weak radio band in Japan, so it is convenient to use without a license. To transmit signals in the 10-60 MHz band efficiently, it is, of course, desirable that the antenna also have a sufficient bandwidth from 10 to 60 MHz. However, this means that the relative bandwidth of the antenna is 1.4 (the ratio of the bandwidth of 50 MHz to the central frequency of 35 MHz). Antennas with such a large relative bandwidth are usually difficult to realize. Although the antenna in Fig. 2.15 achieved only -10 dB bandwidth of 8.4 MHz from 50 to 58.4 MHz under the limited antenna dimension conditions, it does not mean that other frequency components with S_{11} below -10 dB were completely removed. Some of them still radiated from the antenna (as shown later in Fig. 2.19).

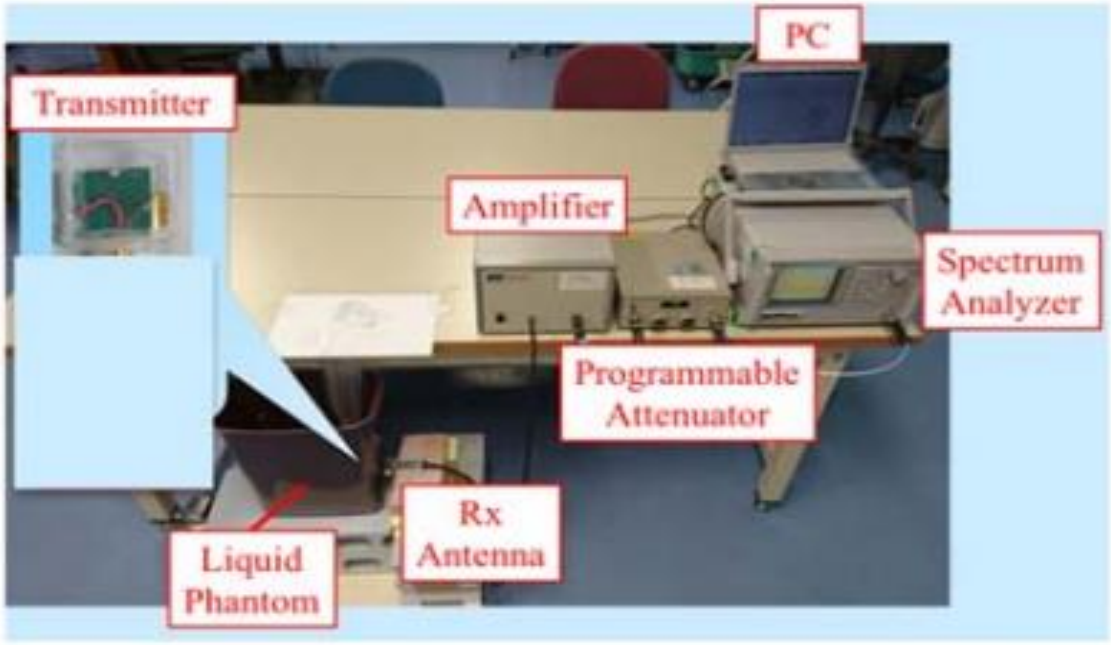

Fig. 2.17. Experimental setup for S_{11} measurement

In the in-body to on-body path loss measurement, we therefore used a 10-60 MHz impulse radio transmitter together with the helical invert-F antenna and inserted them into the liquid phantom. Although the implant antenna was inserted into the liquid phantom, it did not directly touch the liquid. There was a thin dielectric layer (low relative permittivity) between the antenna and the liquid, which made no significant difference in the antenna input impedance when the antenna was inserted in the liquid or air. In addition, the implant antenna was directly connected to the transmitter. There was no cable between them. The receiving antenna was the same type of antenna, but the dimensions of the elements were slightly different. It was set on the phantom surface and connected to a spectrum analyzer or digital oscilloscope using a ferrite-covered coaxial cable. This avoided direct coupling between cables and achieved good isolation. Fig. 2.18 shows the measured band-averaged path loss as a function of distance. The band used for averaging ran from 10 to 60 MHz. The transmitting and receiving antennas were arranged in parallel. Also shown in the figure is the curve fitted using Eq. (2.2). The obtained parameters are shown in Table 2.4. As can be seen, the power decay law fits well the measured path loss. The obtained path loss exponent n is 5.0, which falls in the range of 3.9 for loop and 5.4 for dipole in Table 2.2. Given that the antenna is actually a helical-dipole structure, the result is consistent with the theoretical approach in previous section, which provides

useful knowledge on channel characteristics and antenna design.

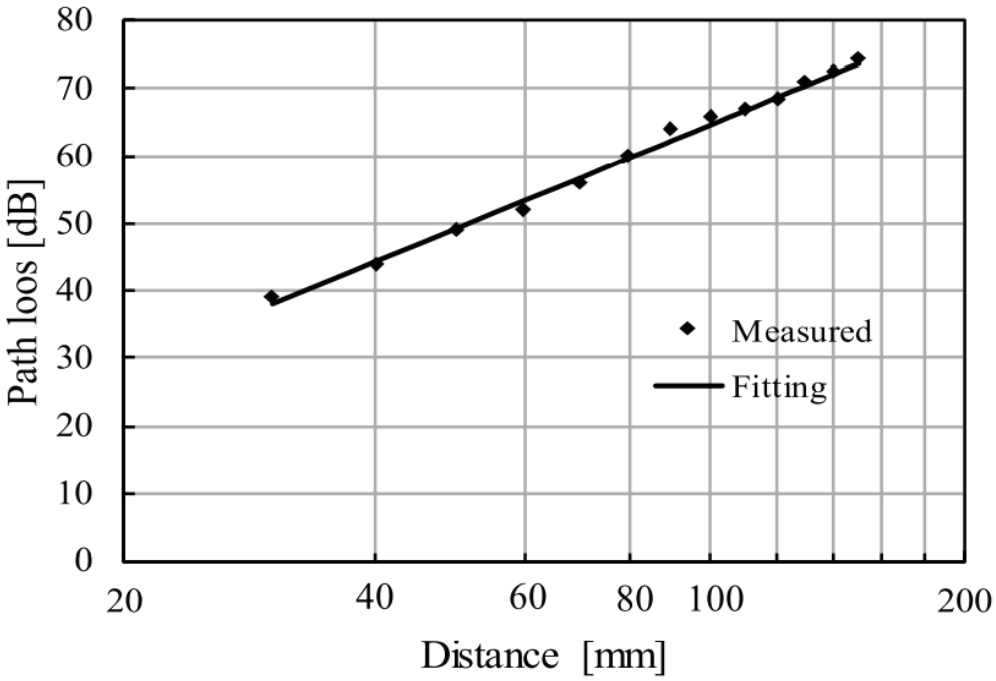

Fig. 2.18. Measured and fitted band-averaged path loss

Table 2.4. Fitted parameters for measured band-averaged path loss

n	PL_0 [dB]	d_0 [mm]
5.0	37.9	30

2.4 Link Budget Analysis

Based on the measured path loss in the 10-60 MHz band, a link budget analysis to clarify achievable communication performance was conducted. As shown in [43], an IR scheme with binary pulse position modulation (PPM) was adopted in the transmitter where the information bits are sent as position information of a pulse. For K bits to be transmitted, the PPM signal s(t) can be expressed

$$s(t) = \sum_{k=0}^{K} p(t - b_k \frac{T}{2} - kT) \tag{2.4}$$

where p(t) is the pulse to be transmitted, $b_k \in (0, 1)$ is the kth transmitted bit, and T is the bit duration. Since the helical invert-F antennas used in this study had insufficient bandwidth, waveform distortion was caused in the received signals.

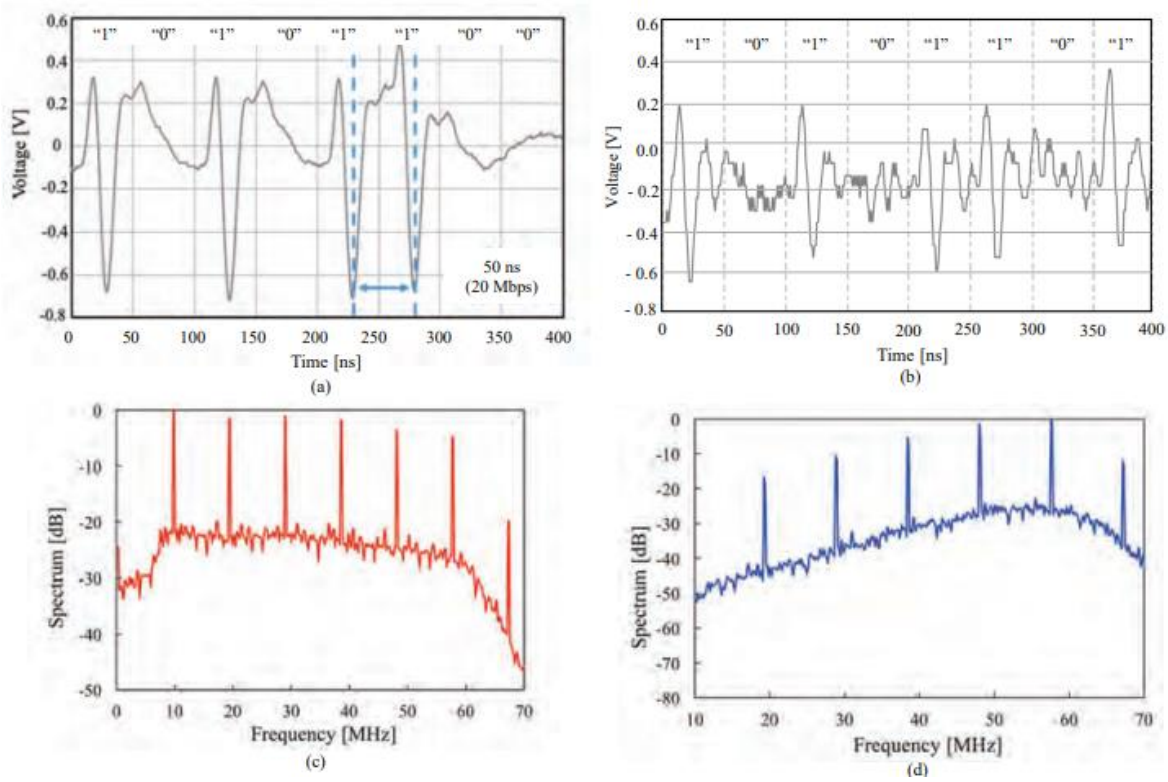

Fig. 2.19. (a) Transmitted and (b) received time waveform using the IR-PPM transceiver with helical invert-F antennas (the signal in (b) is not the received signal in (a) itself because the timing is not synchronized). (c) Normalized frequency spectrum of the transmitted signal. (d) Normalized frequency spectrum of the received signal.

This limited the use of correlation detection and communication speeds. To reduce the effect of bandwidth limitation by the antennas, we set proper time intervals between the transmitted pulses and adopted energy detection at the receiver. A waveform equalization algorithm can also be used to suppress the waveform distortion [43], [53]. Fig. 2.19 shows the transmitted and received signal waveforms and frequency spectra measured at an implant communication distance of 10 cm using the helical invert-F antennas. As can be seen in Fig. 2.19(a), the time duration of one-bit signal was 50 ns, or 20 Mbps. Comparing the transmitted and received frequency spectra, the distortion in frequency components indeed exists. However, comparing the waveform shapes of "1" in Figs. 2.19(a) and 2.19(b), the distortion of the received signal waveform is limited after the signal has propagated 10 cm in the biological-equivalent liquid phantom. This result supports the findings that the group delay is almost flat in the HBC band. It also suggests that the

received signal may be distinguishable bit by bit, in other words, the -10 dB bandwidth of 8.4 MHz may enable an implant communication at 20 Mbps.

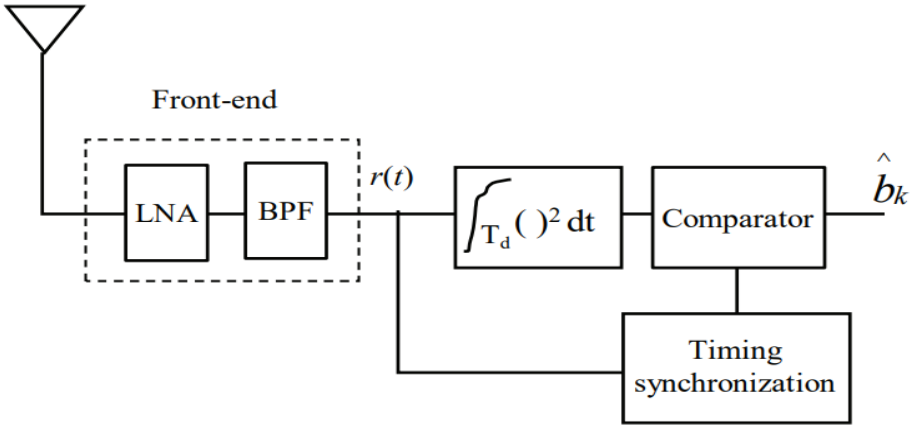

Fig. 2.20. IR-PPM receiver structure with energy detection

Fig. 2.20 shows a typical receiver structure of energy detection. After the front-end such as low-noise amplifier and band-pass filter, the energy U_k^0 and U_k^1 are calculated by integrating the squared *r(t)* from kT to $kT + T_d$ and $(k + 1/2)T$ to $(k + 1/2)T + T_d$, respectively, where T_d is the energy detection duration. By comparing U_k^0 and U_k^1, the received bit b_k can be determined as

$$\hat{b_k} = \begin{cases} 0 & \text{if } U_k^0 > U_k^1 \\ 1 & \text{otherwise} \end{cases}$$

The receiver *r(t)* contains a wide band noise *n(t)*. According to [49], a wide band signal can be approximated as M narrow band signals when M is sufficiently large, so that $2M \approx 2BT_d$ where B is the frequency bandwidth of signal and T_d is the energy detection duration. Since each approximated narrow band noise is a zero mean independent Gaussian distribution with variance of $N_0/2$, the detected energy U_k^0 or U_k^1 will be a sum of $2M$ independent variables with a chi-square distribution, whose probability distribution can be approximated as a Gaussian distribution according to the central limit theorem. If we take the energy detection duration T_d as the reciprocal of the frequency bandwidth, i.e. $1/B$, then M becomes 1. Under this assumption, the bit error rate (BER) P_e can be approximated as [50]

$$P_e = \frac{1}{2} e^{-E_b/2N_0} \tag{2.5}$$

where E_b/N_0 is the energy per bit to noise power spectral density ratio

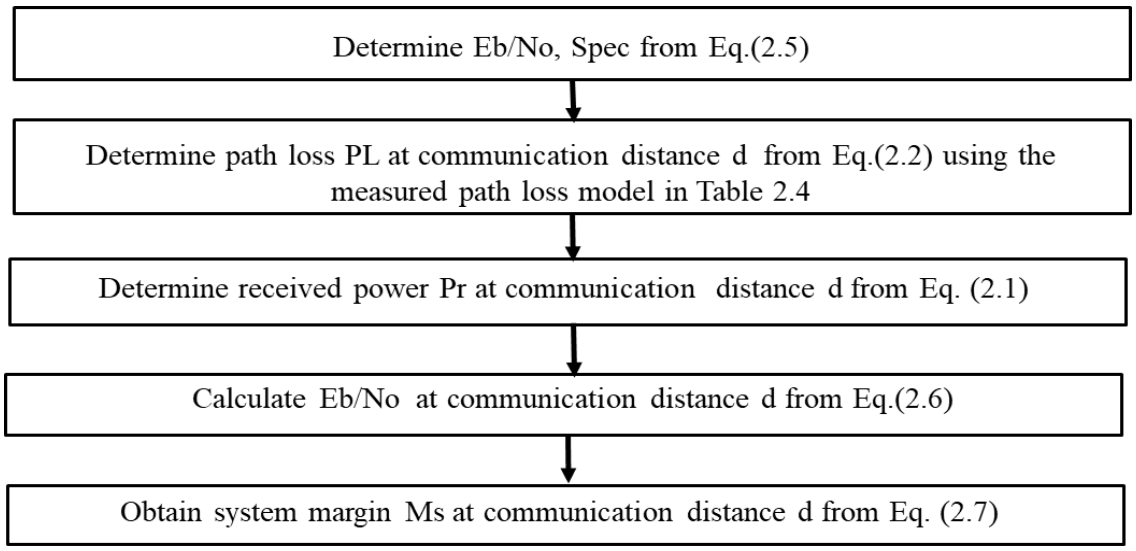

Fig. 2.21. Flowchart to obtain system margin. Required parameter values are listed in Table 2.5

An acceptable BER level in the physical layer is usually 10^{-2} because at this level an error-free communication can be achieved by introducing a forward error correction technique. The link budget was therefore performed by choosing BER = 10^{-2} as an index. From Eq. (2.5), an E_b/N_0 of 8.9 dB is required to achieve this BER level, which is named as E_b/N_0, *Spec*. In addition, from Table 2.2, the standard deviation σ_{dB} of shadowing is 4.0 dB for dipole antenna and 3.1 dB for loop antenna. To cover a range of σ_{dB}, at least another 4 dB is required. Fig. 2.21 shows the flowchart to obtain system margin. By denoting f_b as the data rate and B as the bandwidth, E_b/N_0 can be related to the power Pr received at the receiver as

$$E_b/N_{0,dB} = P_{r,dBm} - 10\log_{10}\frac{f_b}{B} - N_{dBm} \tag{2.6}$$

where $N = k\,T\,BN_F$ is the noise power, k is the Boltzmann constant, T is the environment temperature, N_F is the noise figure of the front-end of receiver, and $P_{r,dBm}(d) = P_{t,dBm} - P\,L_{dB}(d)$. Under the specifications listed in Table 2.5 for the link budget analysis, the system margin Ms can be obtained as

$$M_{s,dB} = E_b/N_{0,dB} - E_b/N_{0,dB,Spce} \tag{2.7}$$

where $E_b/N_{0,dB}$ is calculated using Eq. (2.6) with the path loss modeled in Table 2.4, and the transmitting power of -5 dBm is based on our transmitter design in [43]. The electric field strength radiated from this transmitter was pre-measured in an anechoic chamber and found to be less than 30 dBμV/m at a distance of 3 m from the transmitter, which complies with Japan's weak radio regulations (54 dBμV/m) [52].

Table 2.5. Specifications for link budget analysis

Modulation	IR-PPM
Transmitting power $P_{t,dBm}$	-5 dBm
Data rate f_b	1.25, 10, 20 Mbps
Bandwidth B	8.4 MHz
Demodulation	Energy detection
Dnergy detection duration T_d	1/8.4 μS
In-body environment temperature T	310 K
Front-end noise figure $N_{F,dB}$	6 dB

Fig. 2.22 shows the system margin versus implant communication distance for 1.25 Mbps, 10 Mbps and 20 Mbps with 8.4 MHz bandwidth, the realized -10 dB bandwidth by the helical invert-F antenna. As can be seen, the system margins to secure a BER of 10^{-2} at an implant communication distance of 15 cm are 19.9 dB for 1.25 Mbps, 10.9 dB for 10 Mbps, and 7.9 dB for 20 Mbps, respectively. The system margins were obtained from the measured path loss in Fig. 2.18, which corresponds to a mean path loss. If the shadowing due to diffractions from various organs and tissues was considered based on Table 2.2, at least another 4 dB should be subtracted from the above values, so that the system margins are 15.9 dB for 1.25 Mbps, 6.9 dB for 10 Mbps, and 3.9 dB for 20 Mbps, respectively.

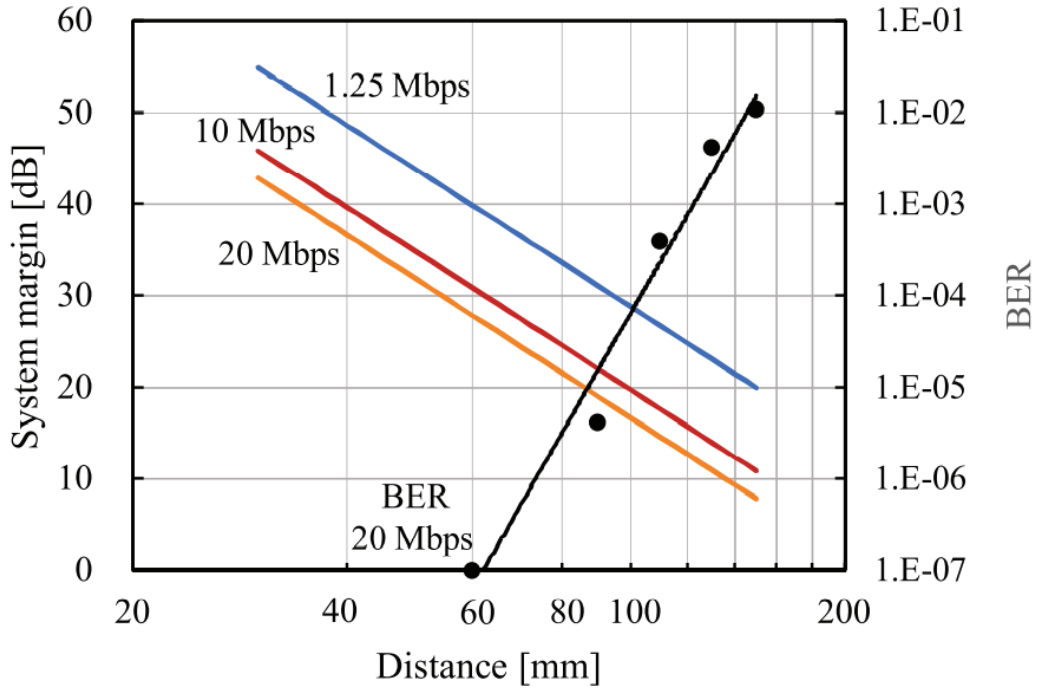

Fig. 2.22. System margin and measured BER versus implant communication distance

These results show that the 10-60 MHz band has sufficient potential to provide high-speed implant communication at 20 Mbps deep into the human body. To further verify this finding, the BER was measured using our developed IR-PPM transceiver at 20 Mbps with the helical invert-F antennas in the liquid phantom. The measured BER was also shown in Fig. 2.22. It can be seen that the BER does not exceed but nearly 10^{-2} at an implant communication distance of 15 cm, which is consistent with the analysis result where the system margin at the implant communication distance of 15 cm is only 3.9 dB at 20 Mbps.

2.5 Conclusion and Discussion

For high-speed and high-reliability implant communication, the channel characteristics of 10-60 MHz band have been analyzed for an electric dipole and a current loop using the FDTD simulation together with an anatomical human body model. The results for path loss and group delay have been obtained. When the transmitting and receiving antennas are both dipoles, the path loss exponent and the standard deviations of shadowing are found to be 5.6 and 4.0 dB, respectively. When the transmitting and receiving antennas are both loops, the path loss exponent and the standard deviations of shadowing are found to be 3.9 and 3.1 dB, respectively. The group delay variation has been found to be around 1 ns, and the phase responses of channel for both dipole and loop are nearly flat with frequency. The electric and magnetic field distributions have revealed that the magnetic field components dominate in-body signal transmission in this frequency band. Based on the analysis results of the implant channel, link budget has been analyzed. An experiment with our developed IR-PPM transceiver has been performed to validate the path loss model and BER performance in a biological equivalent liquid phantom. The experimentally derived path loss exponent lies between the theoretically derived electric dipole path loss exponent and the current loop path loss exponent, and the BER measurement shows the feasibility of 20 Mbps implant communication up to a body depth of at least 15 cm. Improving the implant antenna S11 performance to achieve wider bandwidth will be one of the challenges in the future.

Chapter 3

Shoe-mounted Sensing for Position Identification of Elderly Wanderer Inverter

3.1 Overview

There were about 727 million people who have age 65 or over in the world in 2020. The number of elderly people is increasing day by day and it is projected to more than double by 2050 [54], [55]. This suggests that an aged society is coming. Elderly people are affected by many diseases such as degenerative neurological disorders, vascular disorders, Alzheimer diseases and so on [56]– [61]. Dementia is one of the most alarming diseases for elderly people in the current era. It is a broad term which describes a loss of thinking ability, memory, and other mental abilities. Symptoms of dementia are disability, disorientation, and the most serious one is wandering behavior [62]. According to the nursing care work field survey 2018, the shortage of employees at nursing care facilities is very high at 69.2% [63]. As a result, elderly people with dementia may not be able to see even within the nursing care facilities or they may go out alone. Therefore, it is difficult to discover them and about 10,000 elderly people with dementia are lost each year only in Japan, and many people are also suffering from the same problem in other countries over the world.

As a solution to identify the wanderer's position, global navigation satellite system (GNSS) terminals are typically used. However, they require charging every few days. In contrast, Bluetooth low energy (BLE) beacons can operate on button batteries for over a year, and the BLE signals can be easily received from smart phone users within dozens of meters [64], [65]. A monitoring system using BLE beacons at 2.4 GHz band has been previously proposed in [66], [67]. The monitoring system provides an elderly person with a BLE beacon as a sensor for wanderer position identification. As shown in Fig. 3.1, the signal from the BLE beacon worn by the elderly person is received by a smart phone

owned by a person who happens to pass by. By installing a software on the smart phone in advance, the smart phone can send its position signal to a server after receiving the BLE signal, and then the position of the elderly person can be identified based on the smart phone's position and informed to his/her family. Another option to receive the BLE beacon signals is to set a receiver at utility poles. Such a monitoring system enables wanderer position identification. In addition, this monitoring system is kind to the elderly people. It almost does not require the elderly people to charge the BLE beacon. Only smart phone users need to charge every day. To wear the BLE beacon as a position sensor, one option is to wear it on the chest. Another option is to mount it on the shoes. The latter has an advantage to prevent forgetting to carry. There is also a possibility of energy harvesting, which uses a piezoelectric element mounted to the shoe sole to convert pressure into voltage and power the BLE beacon [68]- [75].

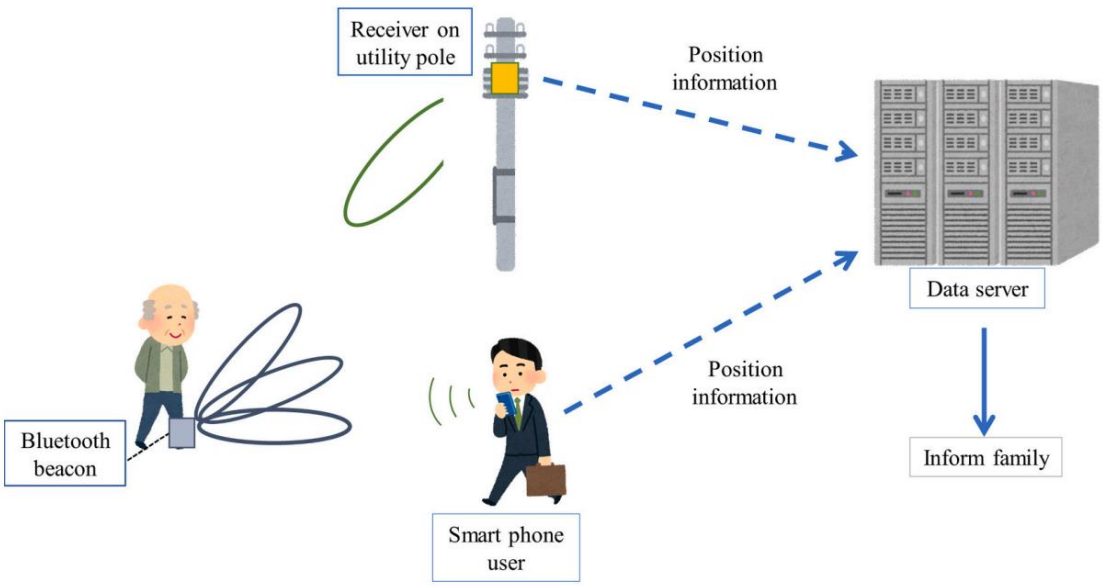

Fig. 3.1. Schematic diagram of elderly wanderer position identification system using BLE as a position sensor

In this study, we assume to mount the BLE beacon on the shoes. An example of a position estimation system that currently uses beacons is the runner's chip used at marathons [76]. The runner's chip uses radio-frequency identification (RFID). It is distributed to the participants of the competition and worn on the shoes. It can record the

time from the start point to the goal via each passing point individually on the server and measure the accurate time. However, RFID has a short communication distance compared to BLE, and the latter is more suitable for identifying the position of the wanderers. Since a smart phone is usually at chest or waist height, the BLE beacon mounted on the shoes should have an antenna pattern with an up tilt. This requires designing a directional antenna with the main beam pointing diagonally forward and upward and a narrowed beam width for more accurate position identification. It should be also capable of sweeping to correspond to different heights. Moreover, by increasing the radiation efficiency and narrow the beam width of the antenna, it is possible to expand the identification distance and improve the accuracy of the identification direction.

The objective of this chapter is to develop a directional array antenna for BLE beacon mounted on the shoes for the elderly wanderer monitoring system. A patch array antenna is designed to be mounted on shoes. The antenna performances are analyzed using the finite element method. To support the analysis results, measurement results are presented for validation using a biological tissue-equivalent gel phantom and actual human foot wearing shoes. A patch array antenna with dielectric lens is also designed for receiving BLE beacon signals by mounting it on utility poles. Finally, a verification experiment in urban environment is also shown to demonstrate the usefulness of BLE beacons as position sensors with the designed directional antenna.

3.2 Shoe-mounted Transmitting Antenna Design

3.2.1 Design Structure

The antenna for BLE beacon is assumed as a patch array antenna with four elements for acting as a directional antenna on the shoe of the wandering person. Fig. 3.2(a) shows a simplified model of foot with shoe and leg. The database on the dielectric properties of biological tissue is based on Gabriel's measurement data [47]. The dielectric properties in the database were used for the human body model at 2.4 GHz. The relative permittivity ε_r and conductivity σ were set to 36.33 and 1.23 S/m respectively that indicate nearly 2/3 times of the muscle's values. The antenna has a planar or curve patch structure as shown in Fig. 3.2(b) and 3.2(c) respectively. The curved structure should be more suitable for

easy and practical mounting on the shoe, although its manufacture is not easy. The relative permittivity ε_r and conductivity σ_s of the shoe were set to 4.0 and 0.0 S/m respectively that indicate rubber material.

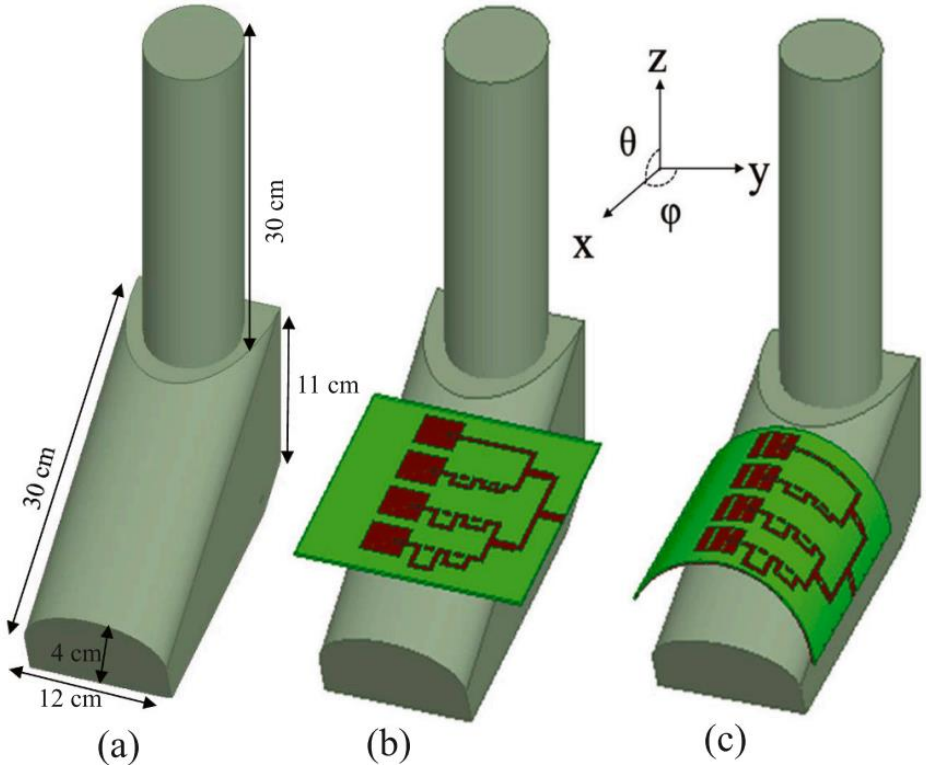

Fig. 3.2. (a) Simplified foot, shoe and leg model. (b) Planar antenna mounted on the foot with shoe. (c) Curve antenna mounted on the foot with shoe

Fig. 3.3 shows the schematic diagram and structure of the designed phase-controlled patch array antenna. Since the antenna is mounted on the foot with shoe, it is easily affected by the human foot and leg. The patch antenna structure with a ground plane can prevent impedance mismatch due to the foot. The antenna is built on a 1.6 mm thick FR4 board ($\varepsilon_r = 4.4$). The antenna elements are arrayed to improve directivity and control the main beam direction. When the antenna elements are fed in the way of Fig. 3.3, the combined directivity $E(\theta)$ is approximately expressed as [78]

$$E(\theta) = G(\theta) \sum_{n=0}^{N-1} a_n e^{j\varphi_n} e^{jk_0 n\, d\sin\theta} \tag{3.1}$$

where $G(\theta)$ is the directivity of a single antenna, an is excitation amplitude, φ_n is excitation phase, N is the number of elements, d is the spacing between two adjacent elements, and k_0 is the wave number in free space.

For feeding signal to each antenna element, the feeding line is bent in a meandering shape as a delay line according to Fig. 3.3, and the feeding line is switched by two switches S_1 and S_2 to control the phase to each element.

When the delay length is Δl, the phase difference $\Delta\varphi$ is

$$\Delta\varphi = 2\pi\frac{\Delta l}{\lambda} \tag{3.2}$$

where λ is the wavelength when the signal propagates along the micro strip lines. To direct the main beam in the desired direction, the excitation phase φ_n to each antenna element should be adjusted. The delay length Δl of the feed line is $\Delta l_1 = 3$ mm and $\Delta l_2 = 6$ mm.

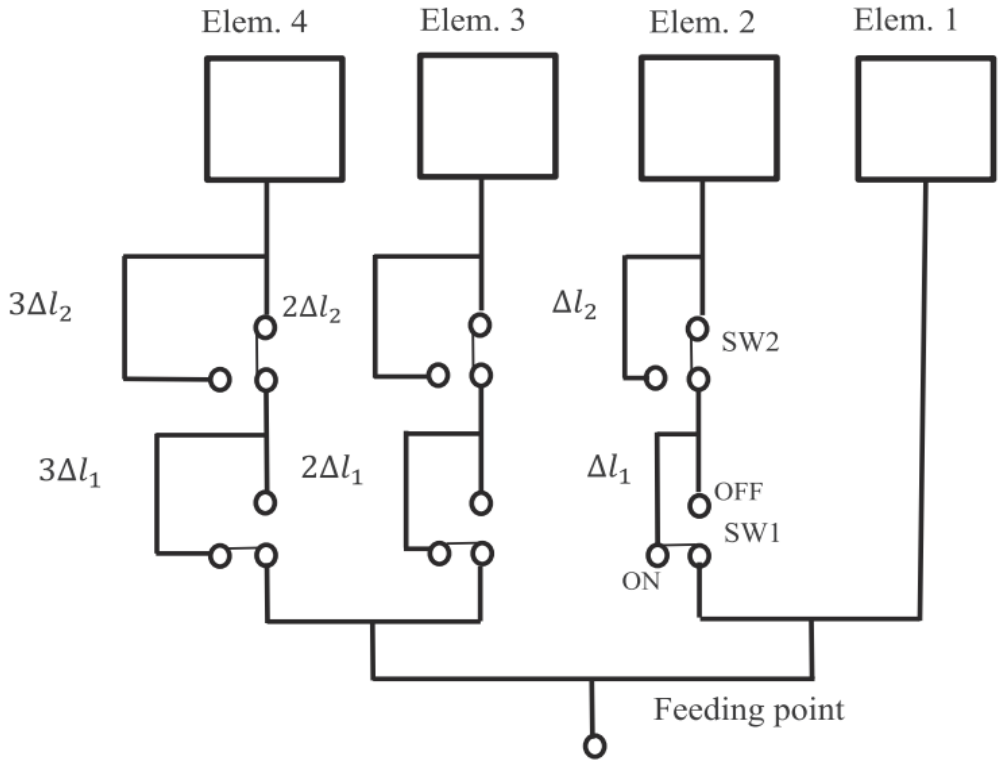

Fig. 3.3. Schematic diagram of feeding circuit

The excitation phase is adjusted by controlling the two switches S_1 and S_2 to produce required delay lengths in the feeding circuit of the array. Depending upon the combination of the two switches, we are able to make four feeding antenna structures that are shown in Fig. 3.4. Based on these structures, four types of excitation phases are adjusted by combining ON and OFF of the two switches.

Table 3.1. Excitation phase and state of switches in each feeding route

Route	S_1	S_2	Elem. 1	Elem. 2	Elem. 3	Elem. 4
1	OFF	OFF	0°	0°	0°	0°
2	ON	OFF	0°	31°	62°	93°
3	OFF	ON	0°	62°	124°	186°
4	ON	ON	0°	93°	186°	278°

Table 3.1 shows the excitation phase φ_n to each antenna element and the state of the switches in each structure for different feeding routes. Impedance matching is performed by loading a λ/4 transformer on the branches. The schematic diagram of the feeding circuit shown in Fig. 3.3 is for Route 2 in Fig. 3.4 (b) previously reported at a conference [77].

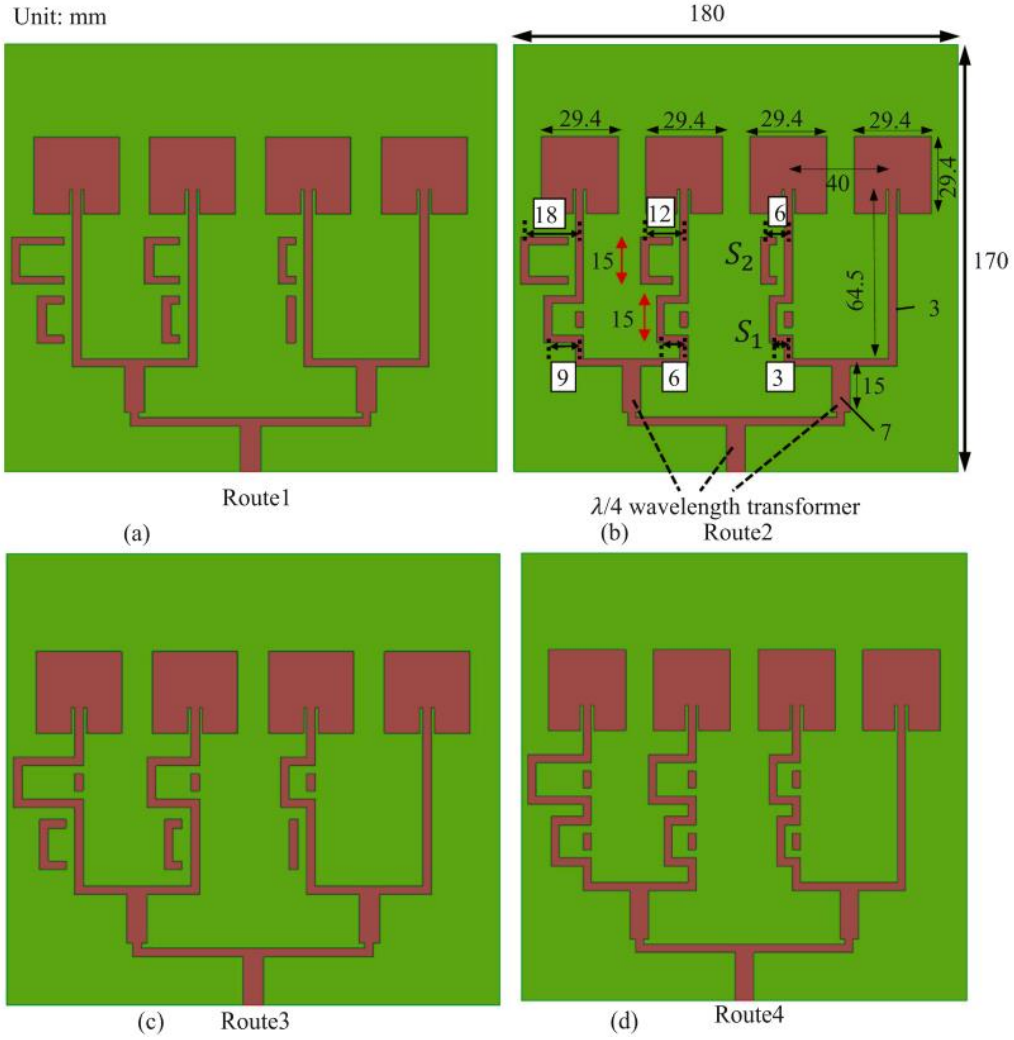

Fig. 3.4. Antenna structures of four different feeding routes

3.2.2 Simulation Results

To evaluate the array antenna performance, first, a simulation was performed to confirm the influence of the ground (earth's surface). Fig. 3.5 shows a simplified model of foot with ground plane.

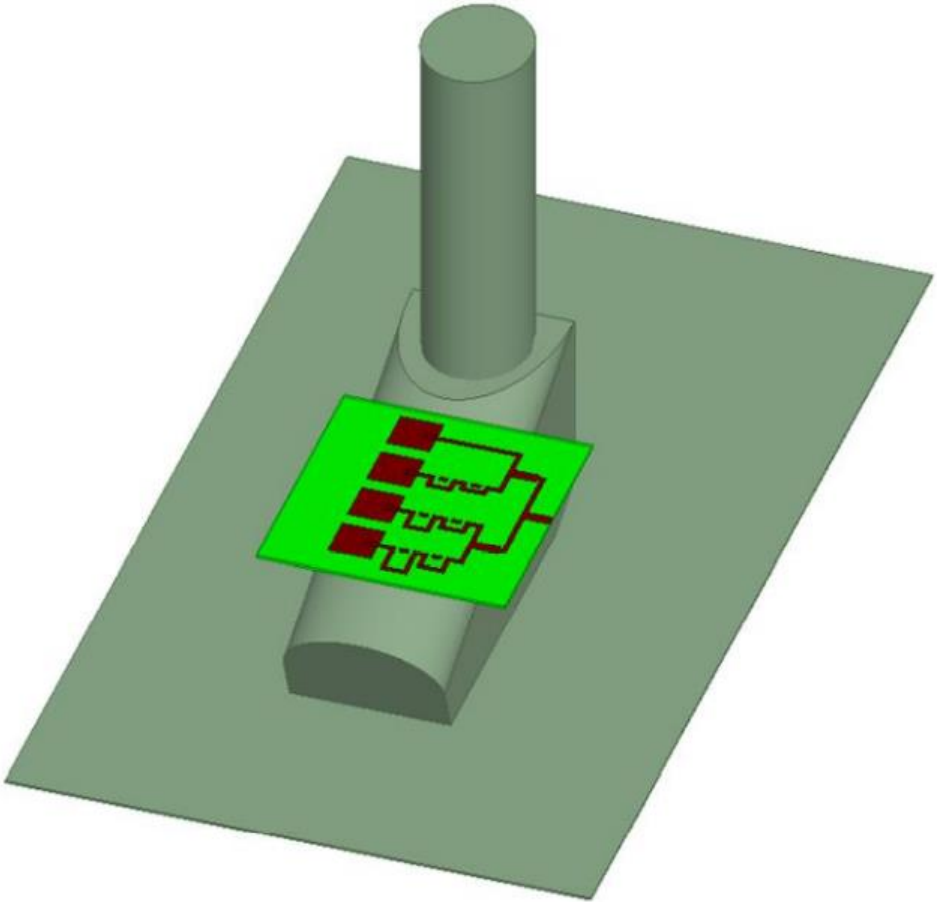

Fig. 3.5. Simulation model with ground plane

Fig. 3.6 shows the comparison of reflection coefficient S_{11} between ground and without ground plane for the route 4 when the planar antennas are mounted on the foot with shoe. The simulated S_{11} results show that there is little difference between with and without the ground. This is because the array antenna has a patch structure with a ground plane on the back. This prevented the ground (earth's surface) from affecting the performance of the antenna. Therefore, we ignored the influence of the ground (earth's surface) in future simulations. Fig. 3.7 shows the simulation results of reflection coefficient S_{11} for the four different feeding routes when the planar antennas are mounted on the foot with shoe.

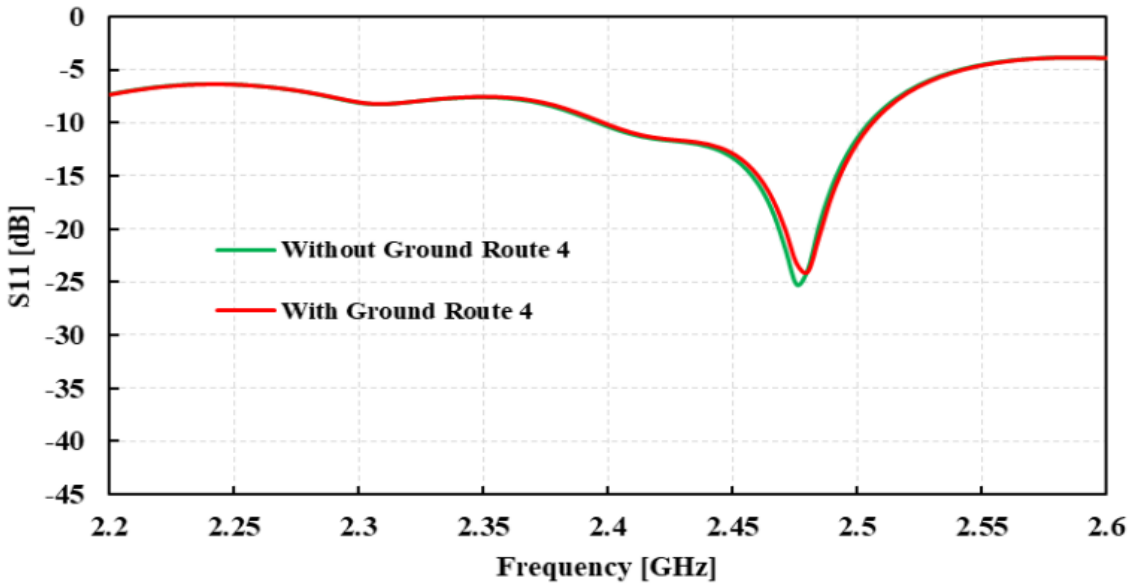

Fig. 3.6. Comparison of S_{11} performances between the ground and without ground plane for Route 4

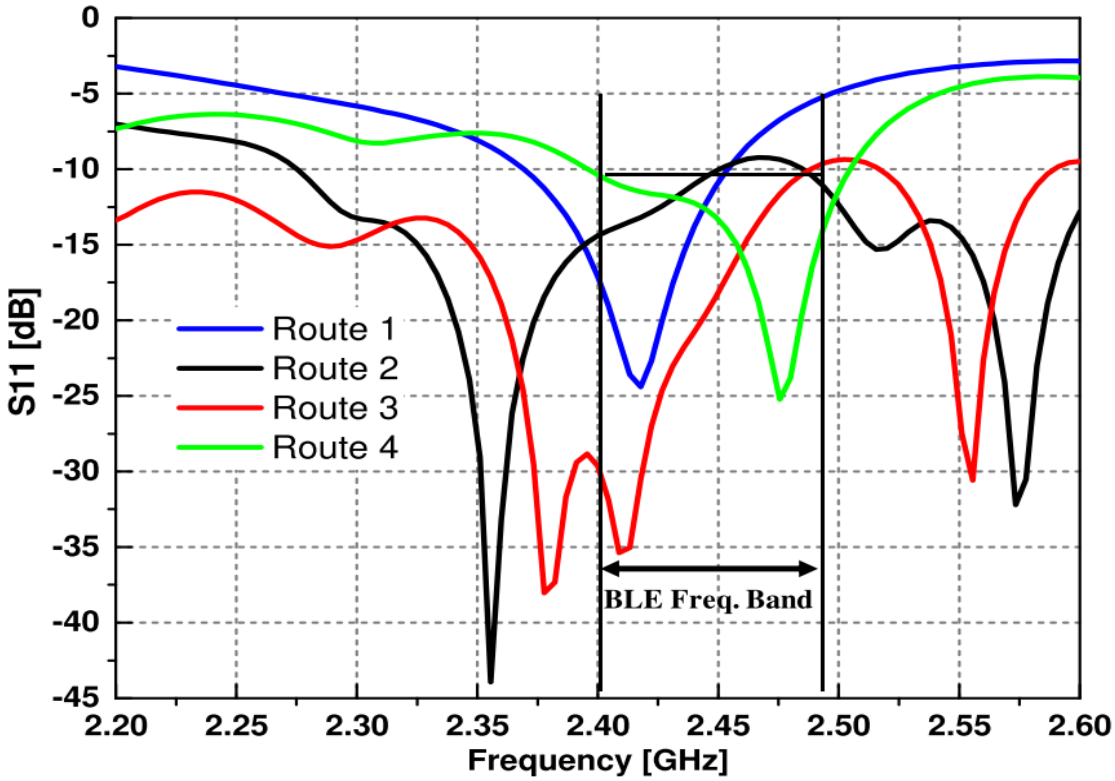

Fig. 3.7. S_{11} performances of the planar patch array antennas mounted on the foot with shoe

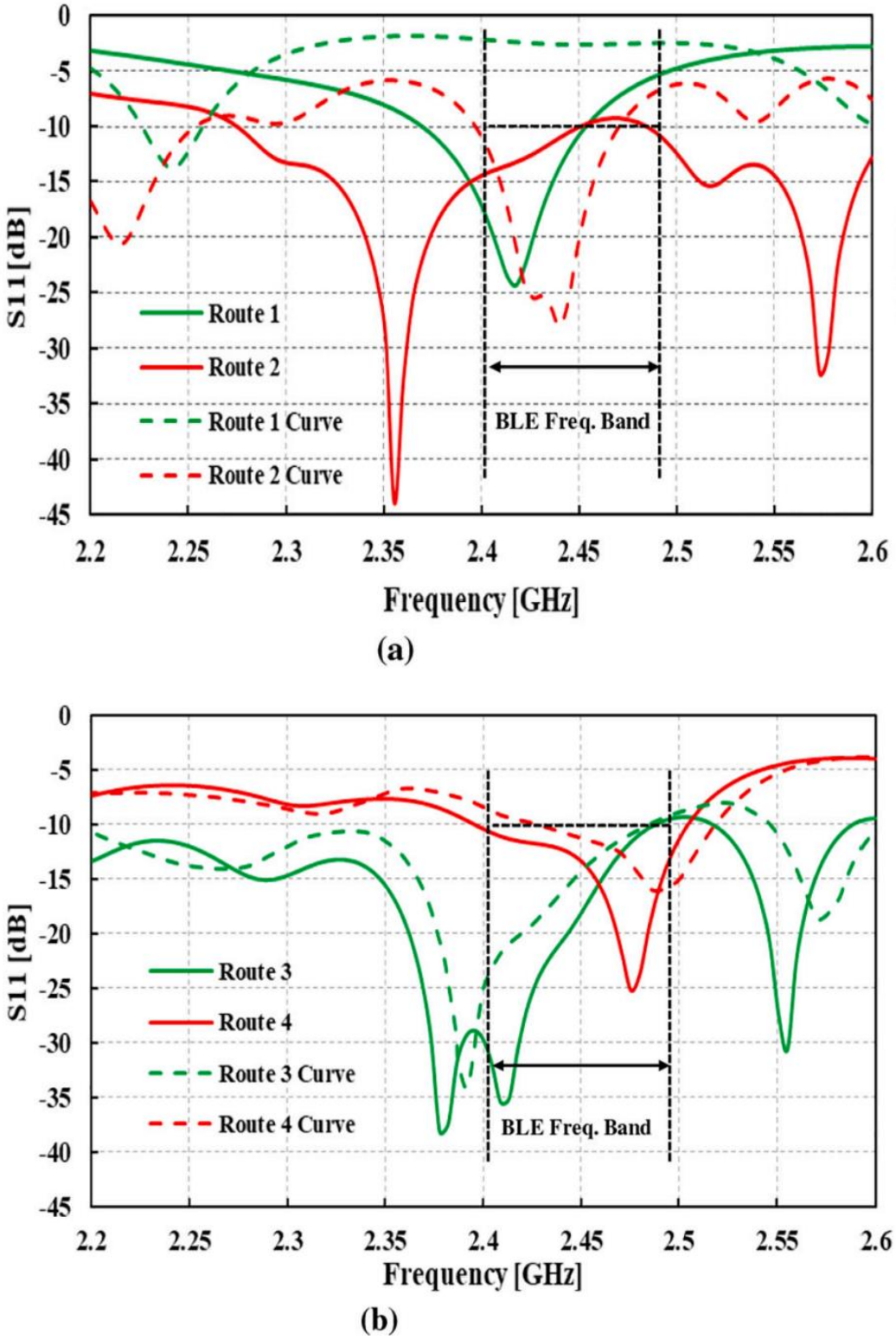

Fig. 3.8. Comparison of S_{11} performances between the planar and curved patch array antennas for (a) Route 1 and Route 2. (b) Route 3 and Route 4

BLE uses the frequency band from 2.402 to 2.480 GHz in a frequency hopping method. As can be seen, for the planar structure, S_{11} is basically less than -10 dB within this frequency band, except for that Route 1 is slightly not satisfied. Fig. 3.8 compares the difference between the planar structure and curved structure where 3.8(a) for Route 1 and 2; 3.8(b) for Route 3 and 4. S_{11} of the curved structure exhibits similar performance to the planar structure, but with some differences due to the effect of curvature.

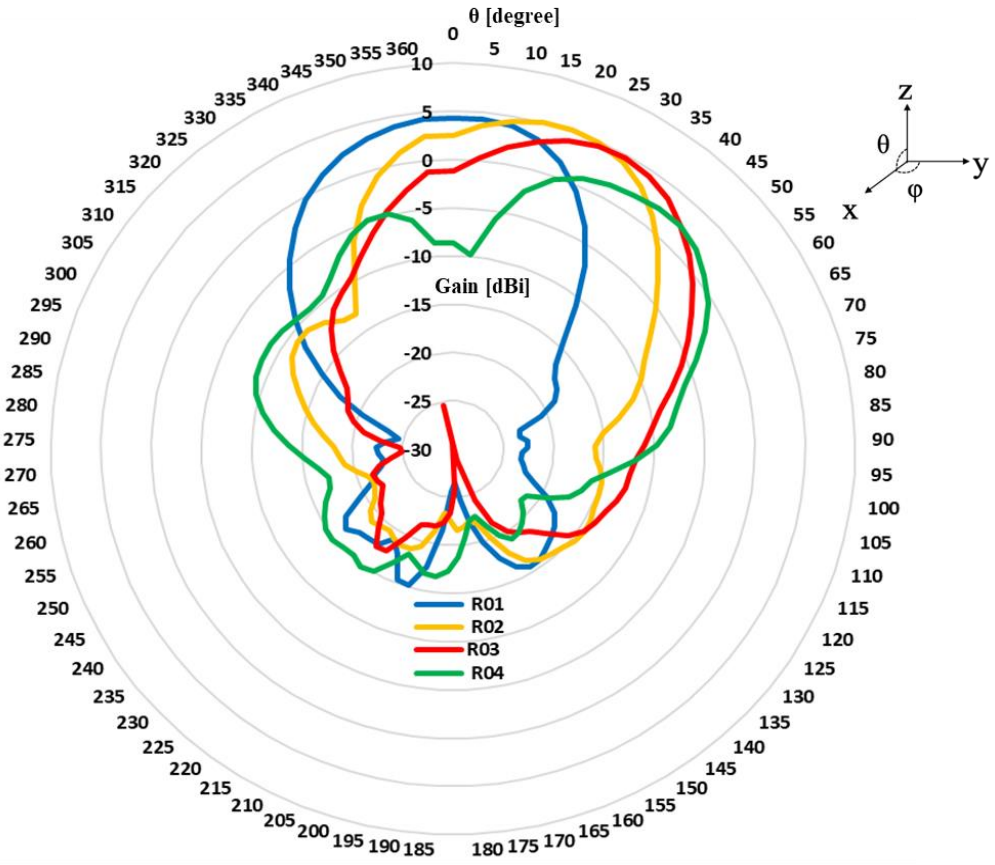

Fig. 3.9. Radiation patterns of the planar patch array antennas on the shoe in the xz plane at 2.4 GHz BLE band

This can be observed especially for Routes 1 and 2 where the difference of resonance frequencies between the planar and the curved structures reached more than 0.1 GHz. Compared to Routes 1 and 2, the influence of the curved structure on S_{11} seems smaller. However, the basic S_{11} performance of the array antenna with curved structure follows the performance of the planar structure and meets the BLE requirement.

Table 3.2. Summary of the array antenna radiation performances for the planar structure

Route	Gain [dBi]	Main direction	Half power beam width
1	6.3	10°	39.6°
2	5.7	20°	36.6°
3	4.7	30°	38.7°
4	2.2	50°	31.4°

Fig. 3.9 and Fig. 3.10 shows the radiation patterns when the planar and curved patch array antennas are mounted on the shoe respectively. The radiation patterns are in the xz plane. The main beam direction is changed by combining ON and OFF of the two switches in each route to adjust the excitation phases. This allows to sweep the main beam direction of the antenna and expand the signal coverage area. Table 3.2 summarizes the simulation results of the array antenna radiation performances. The maximum beam direction has been found to be 50^0 with a half-power beam width of 31.4^0 when using Route 4.

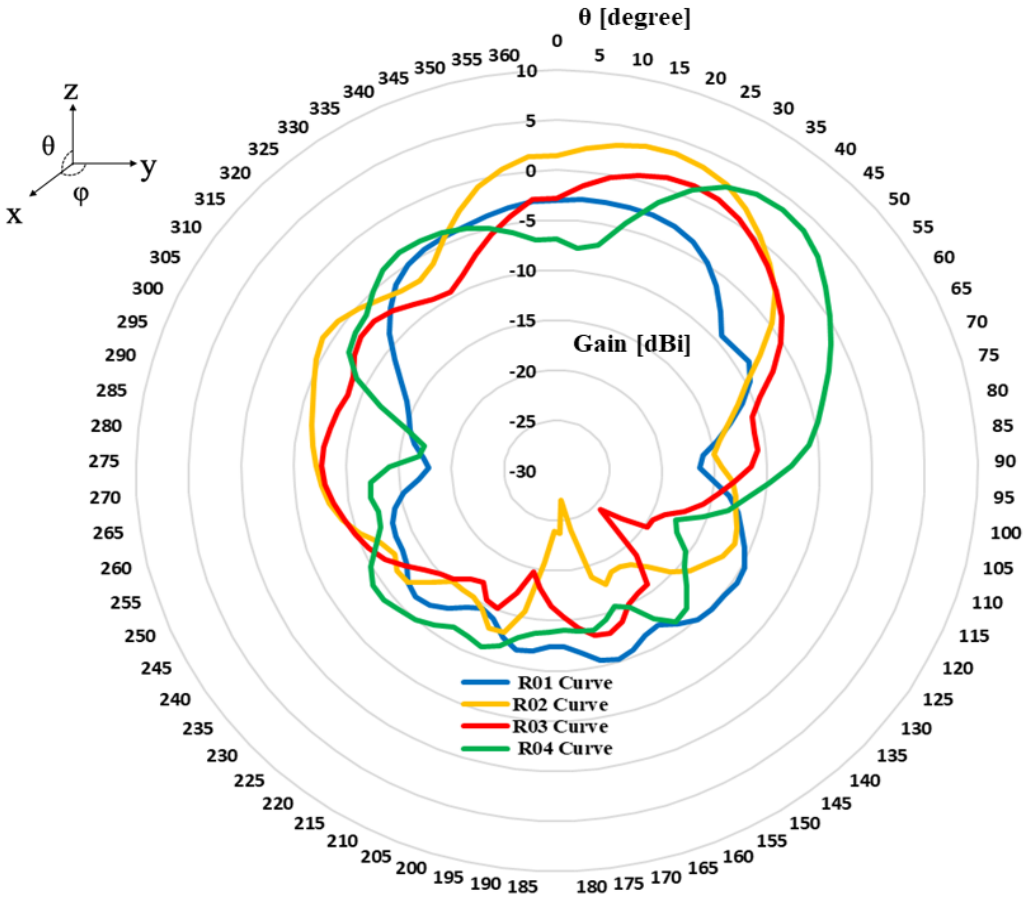

Fig. 3.10. Radiation patterns of the curved patch array antennas on the shoe in the xz plane at 2.4 GHz BLE band

It has a strong diagonal directivity towards the front of the toes, and is suitable for long distance transmission. Assuming that the communication distance between the BLE beacon and a smart phone user is 20 m, the coverage width of the main beam is 5.6 m, which is equivalent to the normal road width, so that the BLE signal can be effectively received by the smart phone user coming from the opposite side. In view of that the structure of Route 4 exhibits a reasonable main beam direction and beam width for identifying the position of elderly wanderers, a prototype patch array antenna was manufactured for the BLE beacon mounted on the shoe.

3.2.3 Measurement Results

The prototype array antenna was manufactured using Route 4 planar structure. However, since the planar structure is wider than the foot width, it is difficult to actually use. The curved structure can be adapted to the width of the foot, but it suffers from limitations of manufacture technology. Considering that the performance of the two structures is similar, the planar structure was adopted in this experimental verification. Fig. 3.11(a) shows the manufactured antenna, and Fig. 3.11(b) shows measured S11 using a network analyzer for comparison with simulated one.

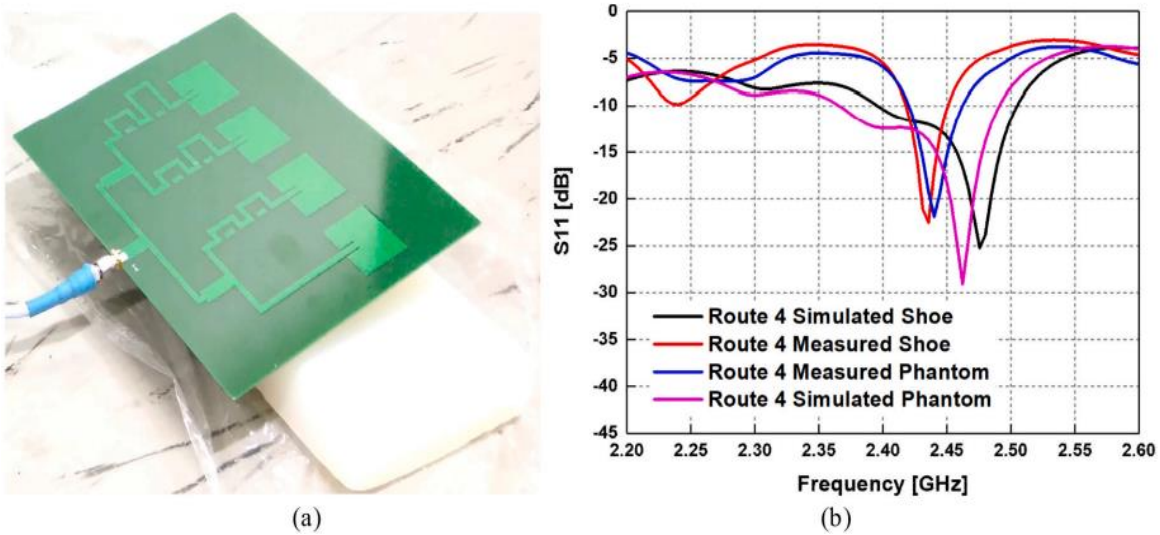

Fig. 3.11. (a) Manufactured patch array antenna on a phantom. (b) Simulated and measured S11 performances on shoe or gel phantom

For the measurement, a bio-equivalent gel phantom was made in the shape of a simplified foot, and the prototype antenna was mounted on its surface at a distance of 1 cm, taking into account the shoe's thickness. The biological-equivalent solid gel phantom was 25 cm ×10 cm × 2 cm, made of glycerin, deionized water, sodium benzoate, agar, and so on, and its dielectric properties were adjusted to have relative permittivity of 45 and conductivity of 2.5 S/m at 2.4 GHz, nearly 2/3 times the muscle's values at 2.4 GHz. The recipe for making it can be found in [80]. In addition, the prototype antenna was also directly mounted on a human foot with shoe or the gel phantom for S_{11} measurement. Fig. 3.11(b) shows the simulated S_{11} and measured S_{11} performances.

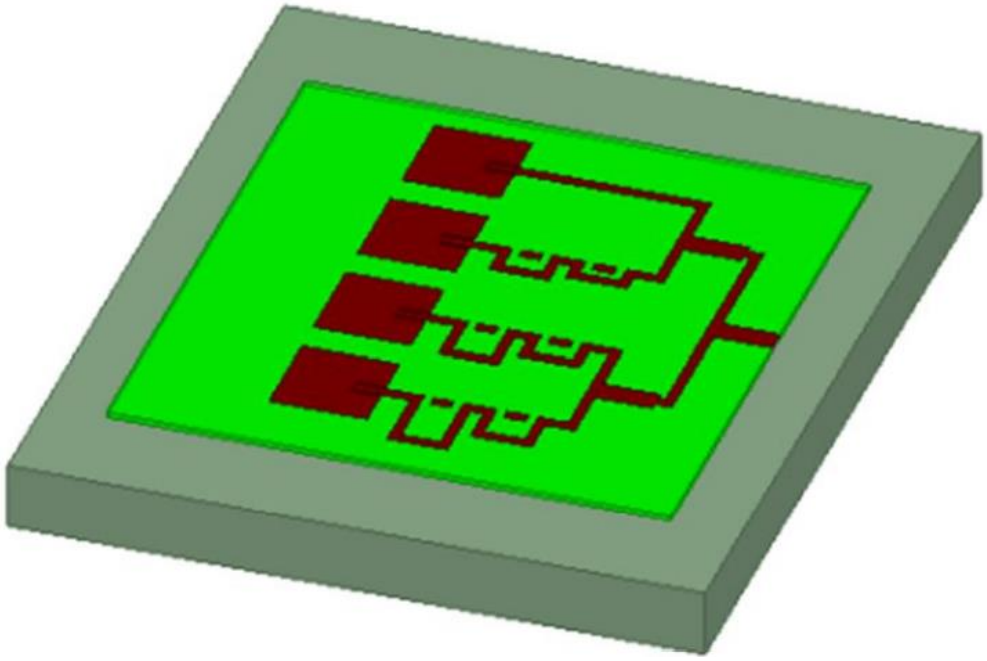

Fig. 3.12. Simulation environment with phantom

Fig. 3.12 shows the simulation environment with phantom. The results on shoe and on phantom show agreement for both measurement and simulation, but a difference between measurement and simulation exists. Compared to the simulated one, the -10 dB bandwidth of the measured S_{11} is narrower. This may be due to design and manufacturing accuracy of the array antenna. The influence of using the phantom instead of the actual foot does not seem to be very significant. The deviation between simulation and measurement may also be attributed to surface roughness of Cu structures. Allowing a bandwidth, at -6 dB minimum matching, the manufactured prototype antenna shows that its S_{11} is basically in the BLE band and can be used for BLE beacons.

3.3 Dielectric Lens Loaded Receiving Antenna Design

BLE beacon signals are expected to be received not only by smart phone users but also by receivers mounted on utility poles installed on the side walk. The utility poles are popular especially in Asia countries. We therefore also designed a directional array antenna used on the utility poles, which was required to have a diagonal downward directivity. The receiving antenna on the utility poles was design as a patch type 2 × 2 array antenna with a dielectric lens to form directivity, as shown in Fig. 3.13.

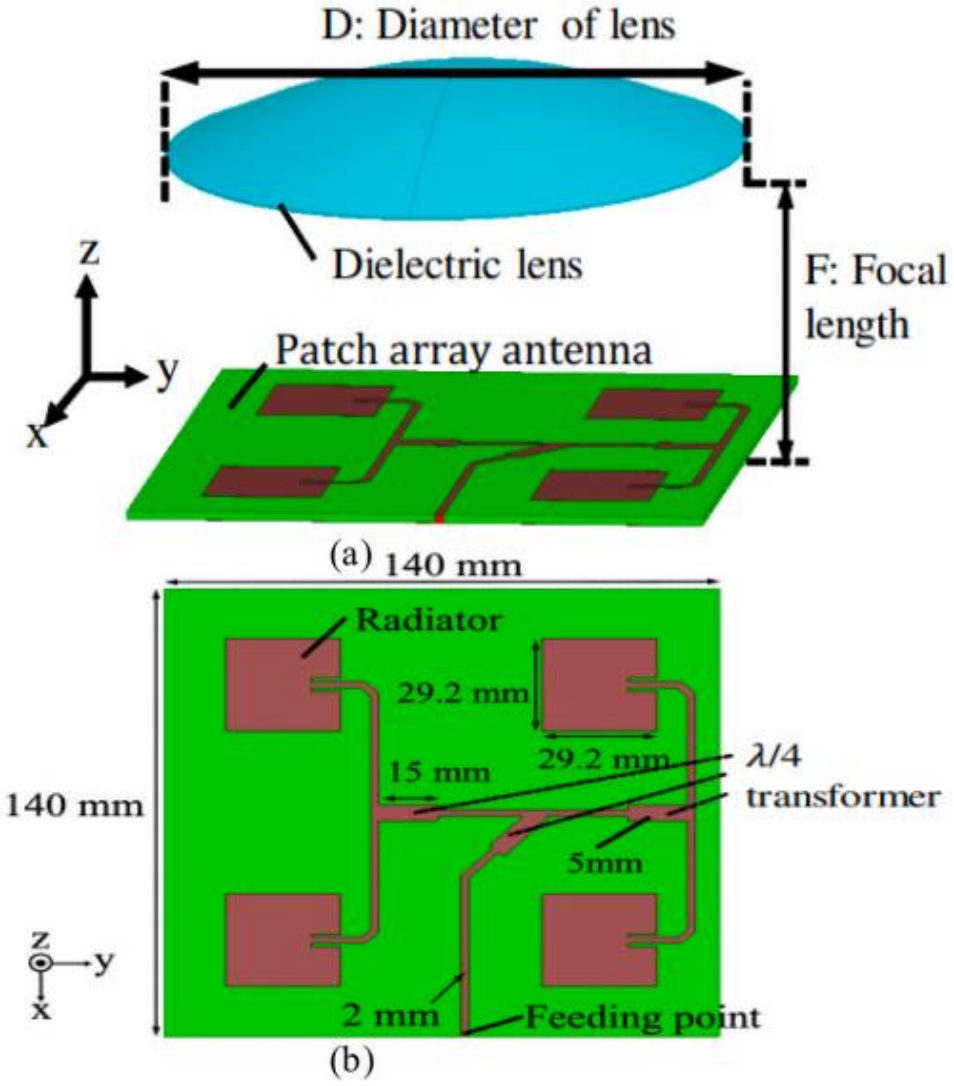

Fig. 3.13. Receiving antenna structure. (a) Side view. (b) Detail of array elements

The mounting area of antenna elements was within 14 cm × 14 cm. The spacing between the antenna elements was set at 80 mm based on the consideration that there is a trade-off between the half-power angle and the side lobe when the element spacing is changed. Impedance matching was performed by loading a λ/4 transformer at the branch point so that the input impedance *Zin* becomes 50 Ω for antenna feeding. The feeding signal was supplied to each antenna element in the same phase and with the same amplitude, where the radiation in the front direction of the antenna is the strongest. Fig. 3.14 shows the numerically simulated S_{11} performance of the design antenna.

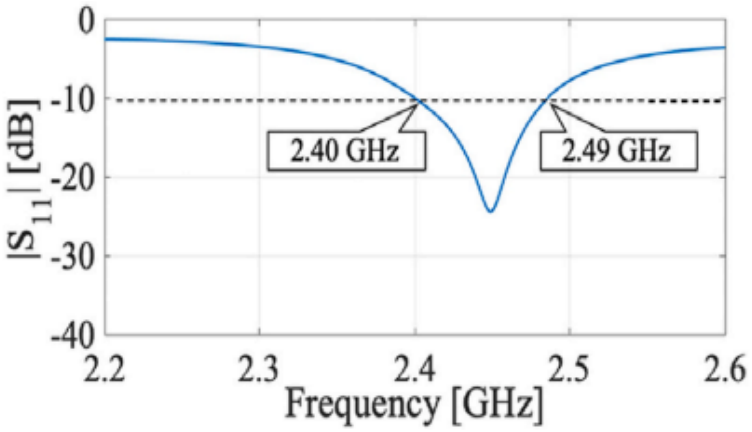

Fig. 3.14. S_{11} simulation result of the receiving antenna

The -10 dB band is from 2.4 GHz to 2.49 GHz, which meets the requirement of BLE beacons. In addition, the dielectric lens was designed to have a curved surface so that the spherical wave radiated from the antenna is converted into a plane wave [81]. Alumina with a relative permittivity of ε_r =9.4 and a relative permeability of μ_r = 1 was selected as the lens material in order to reduce the lens thickness. In order to determine appropriate *D* and *F*, in Fig. 3.13, the diameter *D* of the lens and the distance (focal length) *F* between the lens and the antenna were changed regularly, and the directivity pattern was evaluated from the viewpoint of half-power angle and side lobe. The lens diameter *D* was changed from 0 to 2λ and the focal length *F* was changed by λ/5 in the range of 0 to λ. The directionality in each x-z plane was obtained using numerical simulations. Fig. 3.15 shows the difference in half-power angle with and without lens, and the ratio of side lobe with and without lens. The ratio of side lobes is defined as the ratio of the side lobes to the side lobe without lens. From Fig. 3.15, the half-power angle was improved as the lens diameter increased, but no significant rule was observed in the side lobe. Therefore, as a

result of considering the half-power angle and side lobe, the best result was obtained when $D = 225$ mm $= 9\lambda/5$ and $F = 50$ mm $= 2\lambda/5$, at which time the half-power angle was 28.2°, and the ratio of the peak to side lobe was 10.7 dB.

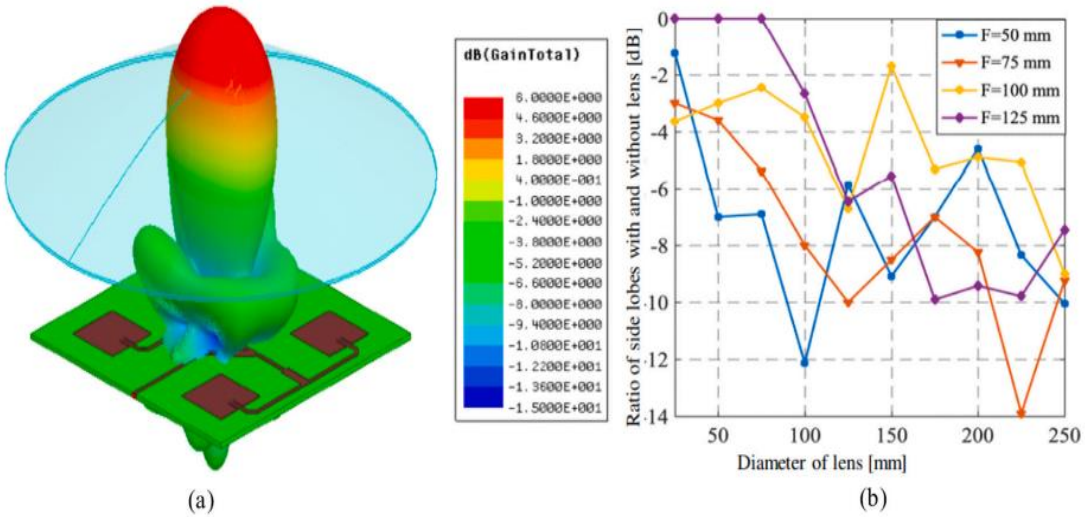

Fig. 3.15. (a) Directivity of receiving antenna with lens. (b) Ratio of side lobes

3.4 Evaluation of Transmission Performance and Position Identification

The transmission gain was first theoretically analyzed for the developed transmitting antennas. Figure 3.16 shows the transmission gain evaluation environment. The transmission gain G is the ratio of the transmission power P_t to the reception power P_r

$$G(\theta_0) = P_r / P_t = (\lambda/4\pi d)^2 G_t(\theta_0) G_r(|\theta_0 - \theta_r|) \tag{3.3}$$

where d is the distance between the transmitting and receiving antennas, l is the horizontal distance from the transmitting antenna to the receiving antenna, θ_0 is the direction angle of the transmitting and receiving antennas, θ_r is the main beam direction of the receiving antenna, G_t and G_r are the power gains of the transmitting and receiving antennas, and λ is the wavelength, The transmitting antenna was placed at the foot of the human body, and the receiving antenna was assumed at the utility pole height from the ground. It was assumed that there are no obstacles between or around the transmitting antenna and the receiving antenna.

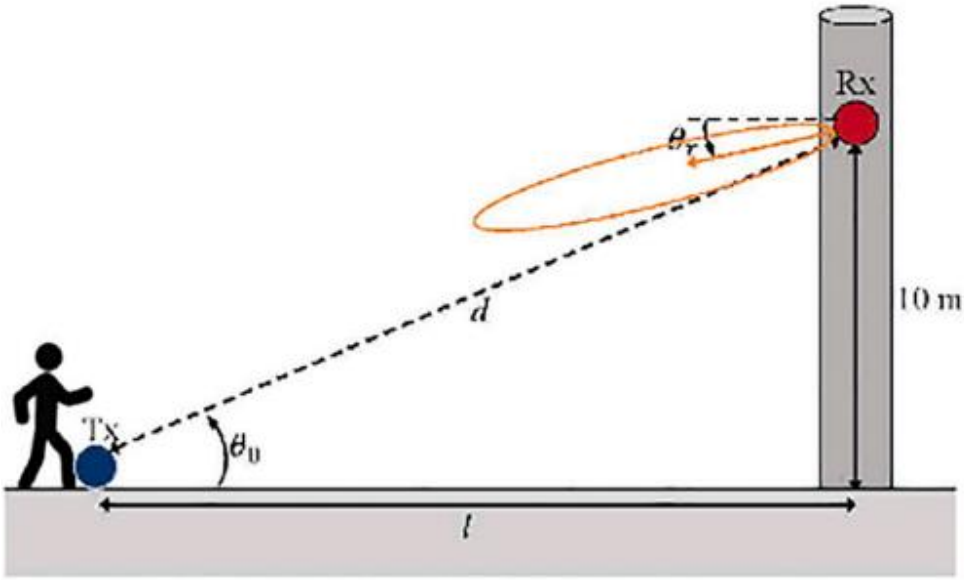

Fig. 3.16. Transmission gain evaluation environment

To calculate the transmission, gain G in each path using Eq. (3.3), the gain function of the designed directional array antenna was used as G_t and the gain function of another directional antenna designed for receiver mounted on the utility pole was used as Gr [79]. Fig. 3.17 shows the calculation results when the main beam direction of the receiving antenna is $\theta_r = 0^\circ$ and the horizontal distance l between the transmitting and receiving antennas was from 0 to 1000 m. When the horizontal distance between the transmitting and receiving antennas is smaller than a few meters, Route1 and Route 2 with strong directivity in the upward direction has larger transmission gain. However, as the distance increases, Route 4, which has strong directivity in the forward direction of the toes, has the best transmission gain. For example, if the horizontal distance between the transmitting and receiving antennas is 100 m, the transmission gain of Route 4 is 15 dB higher than that of Route 1. Therefore, Route 4 should be the most suitable for securing a reliable communication. Moreover, using the prototype antenna together with a signal generator as the BLE beacon, we measured possible communication distance in an urban environment. Fig. 3.18 shows a scene of measurement. The directional array antenna was mounted on the top of either the foot with shoe or the gel phantom, and transmitted the BLE signal with 4 dBm power at 2.4 GHz. IEEE defines three classes for Bluetooth output power. In addition, SAR (Specific Absorption Rate) is usually averaged either over the whole body, or over a small sample volume (typically 1 g or 10 g of tissue). The SAR

limit is 2 W/Kg or 2 mW/g averaged over the 10 g of tissue absorbing the most signal. So, the SAR value is 20mW or 13.01 dBm for 10g of tissue. The directional array antenna was mounted on the top of either the foot with shoe or the gel Phantom, and transmitted the BLE signal with 4 dBm power at 2.4 GHz. Therefore, we did not investigate simulation for SAR analysis. Because below 13.01 dBm power is safe for Human body.

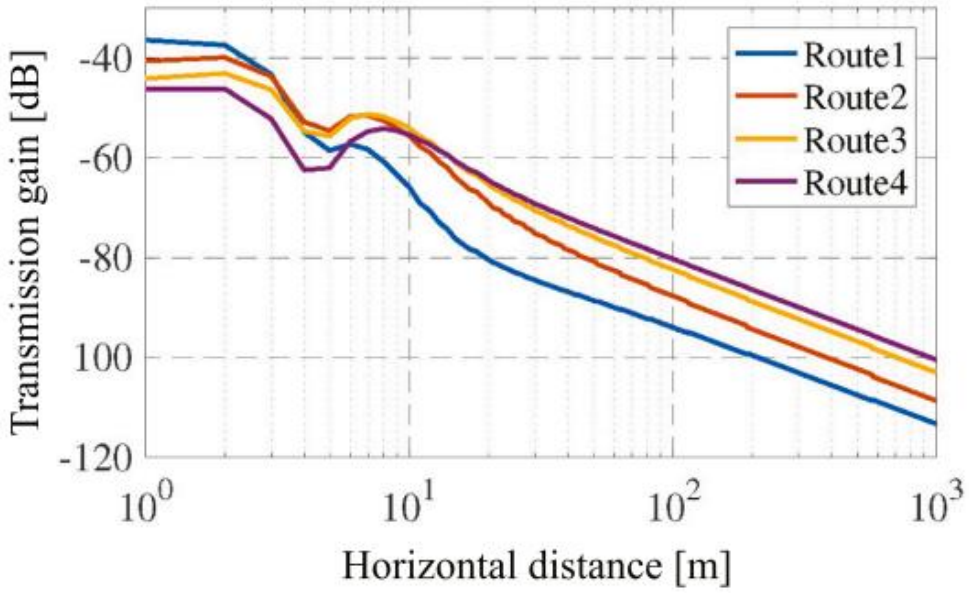

Fig. 3.17. Calculation results by considering the main beam direction and horizontal distance

We adopted class 2 which allows an output ranging from -6 dBm to +6 dBm. The receiving antenna was set at the height of the human chest and connected to a spectrum analyzer to measure the received power.

Fig. 3.18. Scene of measurement in a road of urban environment

The measurement was conducted in a road of urban environment. The receiving antenna was set to horizontal or vertical for measuring both polarization components. Fig. 3.19 shows the measured received power as a function of distance for the horizontal arrangement and vertical arrangement of the receiving antenna. The received power decreases as the distance increases, and the difference between the horizontal component and the vertical component are within 5 dB. This is because the patch array antenna radiates the signal diagonally upward. In addition, the difference in received power between when the antenna is mounted on the human foot and when it is mounted on the gel phantom does not exceed 3 dB. Since BLE receivers typically operate normally with received power in excess of at least -90 dBm, Fig. 3.19 suggests that the BLE beacons can transmit signals up to 20 m or more using the designed array antenna in an urban environment.

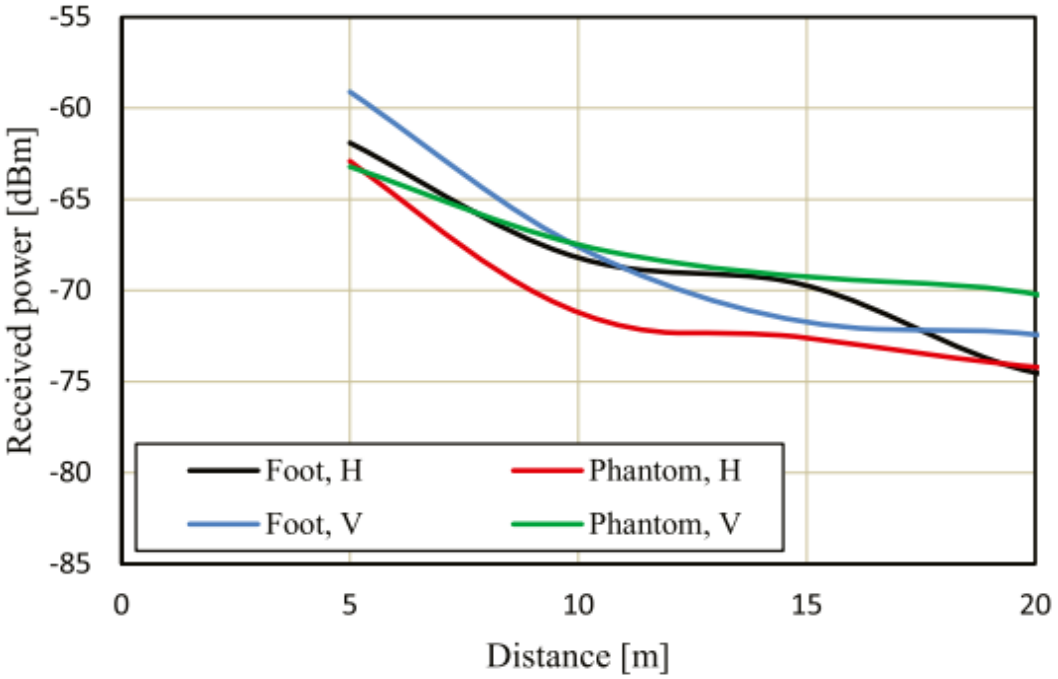

Fig. 3.19. Received power versus distance. H: horizontal component; V: vertical component

To verify the feasibility of the monitoring system of elderly wanderers shown in Fig. 3.1, we first conducted a received signal strength indicator (RSSI) measurement in an urban environment. Nine subjects carried a BLE beacon signal generator [82] and walked on different routes in the urban environment for three hours. The search area in the urban environment is shown in Fig. 3.20. The position labeled receivers in Fig. 3.20 were assumed to be the positions of the smart phone users or utility poles.

Fig. 3.20. An urban environment. The labels of receiver mean the smart phone user or utility pole positions

The nine subjects walked on different routes in the search area, and the received (RSSI) of the transmitted signal from their BLE beacons was measured by the receivers. Fig. 3.21 shows the measurement setup. We used half-wave dipole antenna as receiving antenna and commercial BLE module as the receiver. The subject walked along the sidewalk of roads, and the receiver was installed on the road side of the sidewalk. So, it is enough to cover a narrow angle for our purpose. The total number of the BLE signal was detected in the three hours is 19,798. Then the cumulative distribution of the RSSI was calculated. If the signal is detected by the receiver, the position of the wanderer can be identified. In such a way, we derived a relationship between the RSSI and the identification rate. It was found that the identification rate is about 40% at a RSSI of -85 dBm and 85% at a RSSI of -80 dBm.

Then, the RSSI of the directional array antenna and the RSSI of the BLE beacon signal generator were compared by measurement. The results show that the RSSI was improved by 5 dB by using the direction patch array antenna in the BLE beacon signal generator.

Incorporating this improvement into the above-described measurement result in the urban environment yields a cumulative distribution of RSSI, as shown in Fig. 3.22.

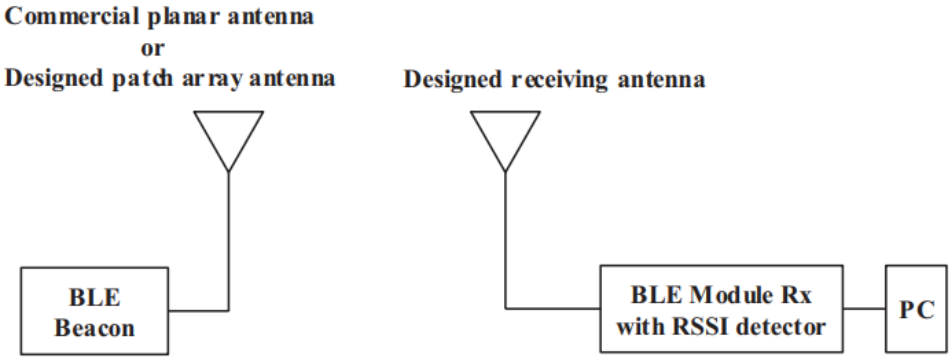

Fig. 3.21. RSSI measurement setup

According to Fig. 3.19, within a distance of 20 m, the received power is larger than -75 dBm for the developed directional array antenna. According to Fig. 3.22, this corresponds to an identification rate of nearly 100%. In other words, if a wanderer is within 20 m from a smart phone user or a utility pole, his/her position will be almost identified.

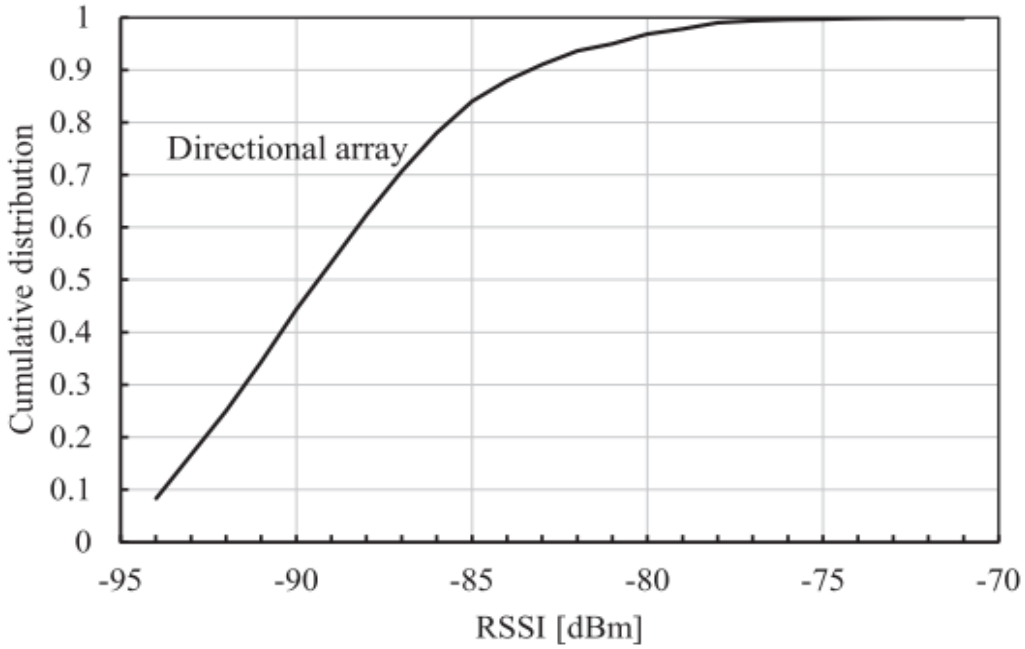

Fig. 3.22. Cumulative distribution of RSSI

3.5 Conclusion and Discussion

A directional patch array antenna with planar or curved structure has been designed for BLE beacons mounted on the foot/shoe for using in an elderly wanderer position monitoring system. The antenna performances have been evaluated by simulation, and the main beam direction has been found to sweep from 10^0 to 50^0 by combining ON and OFF of two switches in the feeding routes to adjust the excitation phases. The S11 performance and distance dependence of the designed antenna have been verified and derived by measurement for a manufactured prototype antenna. Moreover, a directional patch array antenna with dielectric lens has also be designed to receive beacon signals by mounting it on a utility pole. According to a feasibility experiment result of elderly wanderer position identification in an urban environment, the designed directional antenna can provide an almost 100% position identification rate if a wanderer is within 20 m from a smart phone user or a utility pole, which denotes the usefulness of the proposed monitoring system of elderly wanderers.

Chapter 4

Energy Harvesting for Powering Shoe-mounted Sensor

4.1 Overview

Wearables signify a vital part in our daily life. We use it for tracking our exercise performance as well as for medical monitoring. Currently, this technology mostly depends on batteries as a power supply. This is a drawback for a continuous measurement system. Depending on the location of the user or the placement of the battery, recharging or exchanging can be difficult. To ensure an independent system, energy harvesting from human motion could be a great alternative. Regardless of the energy harvester (EH) system, all of them contain the same structural components:

- ✓ Energy transducer
- ✓ Rectifier and storage capacitor
- ✓ Voltage regulator
- ✓ Optional energy storage unit
- ✓ Electronic load

In this case, the transducer consists of lead zirconate titanate (PZT) or a polyvinylidene fluoride (PVDF). It uses the piezoelectric effect, which generates electric energy by applying mechanical stress on the piezoelectric element. The output power itself is AC. Therefore, a rectification is needed to provide a DC power supply. The voltage regulator is used to adapt the voltage level to match the requirements of the device. The energy storage unit is optional, e.g., the device can be operated continuously or discontinuously. In this study, there is a shoe-mounted beacons for location identification which comprises a piezo or an array of piezo elements for powering shoe-mounted beacon. Each piezo element of the array is used simultaneously for energy harvesting.

We thereby can satisfy two needs:

- ✓ We get more energy thanks to the array – so far only shoes with one piezo element in the heel have been demonstrated.
- ✓ we can get a localization resolved pressure map called “pedobarometric map”. We can sense the pressure distribution at the feet. We can also do gait analysis based on this sensor array.

In the shoe, we would also place a cellular IoT modem, esp. 4G NB-IoT. This will give the shoe access to WAN, the internet, the cloud. Sensor Data can be passed to a central health record. We know this statement “to wear is to share”. Adidas passes sports data into social media platform called Runtastic [91]. From what we heard from Adidas, localization/GPS for alarming is key – so cellular connectivity is a must. Adidas does not want shoes to be charged from mains. They should be energy autonomous. This means the energy needed for communication must be totally harvested. It may mean that a sensor report can only be send every 10 minutes into the internet. This looks pretty similar to smart metering (water/gas meters). We see that the shoe must have two wireless interfaces. A WAN interface based on cellular 4G NB-IoT and a BAN may be based on HBC. At the shoe we may also combine mechanical harvesting and solar harvesting. There are piezo elements that can act as photovoltaic. It is also possible to get multimodal, combining mechanical and solar harvesting, which can make harvesting more reliable as energy is crucial in this use case. Other nodes in the BAN like a smart jacket could also host solar piezo e.g., at the shoulders and power BAC from it.

4.2 Energy harvesting by piezo

Piezoelectric material is a kind of material with non-centrosymmetric crystal structure that can generate displacement between anions and cations, thus producing surface charge when exposed to dimension change caused by stress. Among various kinds of piezoelectric materials, piezoelectric ceramic is a class of man-made polycrystalline piezoelectric materials composed of multiple ferroelectric particles that can be poled by external electric field to exhibit piezoelectricity.

The piezo electric effect in ferroelectric can be used to convert mechanical energy to electrical energy and vice versa. All ferroelectric materials are piezo electric. They can generate electrical current in respond to any change in temperature. Piezoelectric

materials can act as an energy harvester where electrical energy can be created from heat and required electrical circuit. Piezo electric material exhibits in the large varieties of application such as sensors, actuators, resonators. It can be used in biomedical implantable or wearable devices. Typical example of piezo material: PZT, PVDF and NKN etc. PZT, or lead zirconate titanate (Pb [Zr(x)Ti(1-x)] O3), is one of the world's most widely used piezoelectric ceramic materials. When fired, PZT has a perovskite crystal structure, each unit of which consists of a small tetravalent metal ion in a lattice of large divalent metal ions lead zirconium titanate exhibits greater sensitivity and has a higher operating temperature. Piezoelectric ceramics are chosen for applications because of their physical strength, chemically inertness and their relatively low manufacturing cost. PZT ceramic is the most used piezoelectric ceramic because it has an even greater sensitivity and higher operating temperature than other piezo ceramics. However, PZT is not good environment friendly due to a Restriction of Hazardous Substances (RoHS). Polyvinylidene fluoride or polyvinylidene difluoride (PVDF) is a highly non-reactive thermoplastic fluoropolymer produced by the polymerization of vinylidene difluoride. In the biomedical sciences, PVDF is used in immunoblotting as an artificial membrane, on which proteins are transferred using electricity. PVDF transducers have the advantage of being dynamically more suitable for modal testing than semiconductor piezoresistive transducers and more compliant for structural integration than piezoceramic transducers. For those reasons, the use of PVDF active sensors is a keystone for the development of future structural-health monitoring methods, due to their low cost and compliance.

The term **energy harvesting** is widely used when electricity is produced from sources such an ambient temperature, vibrations, mechanical stress, or air flows. Since there are no electronic circuits whose power requirement is on the order of mill watts, even though its energy yield is relatively low, energy harvesting with piezo material is a great of interest in situations where electricity cannot be supplied via power cables and one wants to avoid batteries and maintenance effort is required. It is possible to receive and energetically use the energy from radio waves via arrays of antenna or powering antenna by combining a piezo material. As a result, it is termed that piezoelectric crystals are also ideal for energy harvesting. They generate an electric voltage when force is applied in the form of pressure or vibrations, i.e., they use the kinetic energy available in their environment as shown in Fig.4.1.

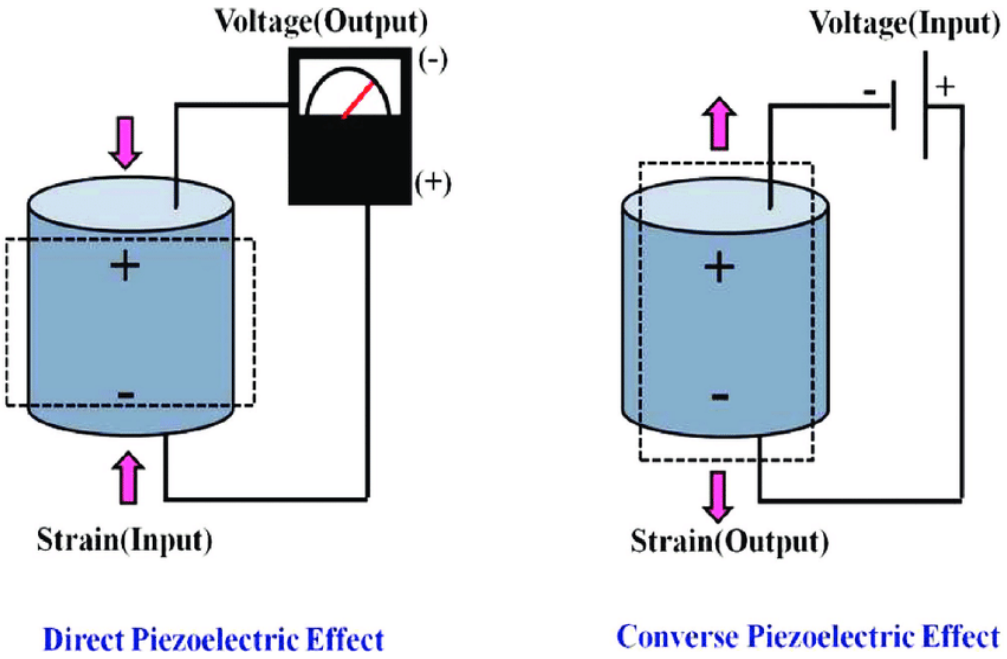

Fig. 4.1. Direct piezoelectric effect- Electromechanical Conversion

In studies, like Han et al. [83]-[85], a transducer was only used to convert the pressure of the heel strike, which provided over 2 mW of regulated power at 4.5 V as shown in Fig.4.2. Each shoe has a different task minimizing the required power supply. The left shoe is equipped with sensing hardware (e.g., accelerometer, pulse sensor, temperature sensor) to collect data while walking. The right shoe turns as transceiver to communicate with the user's smartphone via Bluetooth. The shoes itself communicate by ambient backscatter, thereby further reducing the power consumption. While in sleep mode the processor consumes 0.9 μA. As a result, the EH generates about 1-2 mW per step, which allows the system to establish a communication every 5-9 seconds.

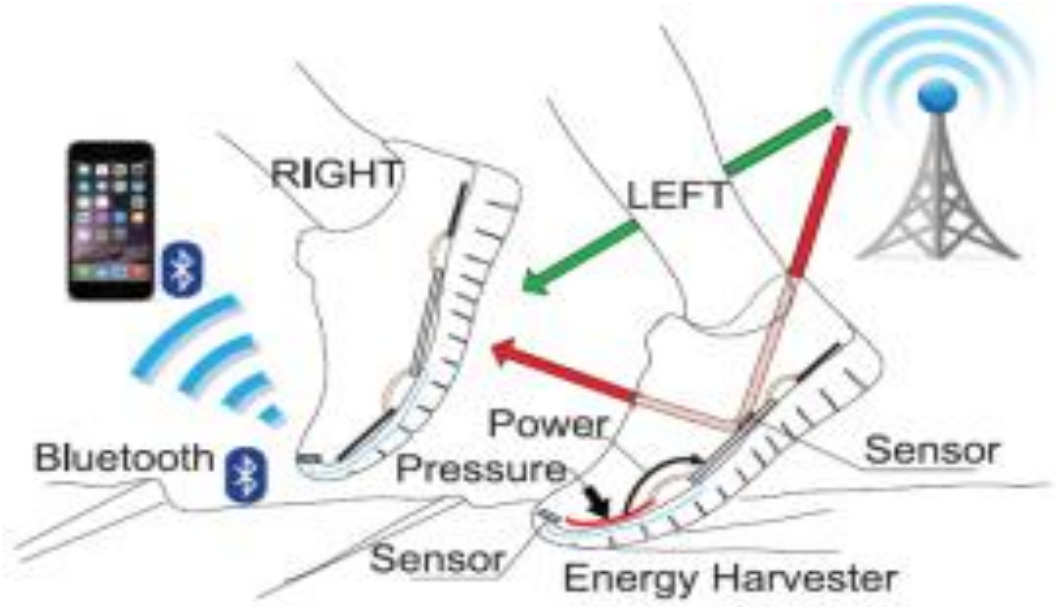

Fig. 4.2. System overview of energy harvesting in shoes

4.2.1 Measurement of pressure produced voltage by NKN

There have been different approaches to harvest the vibration energy by human motion efficiently. Particularly PZT and PVDF became very popular because of their high piezoelectric performance. Both materials are frequently used depending on the application of the EH system. In this case, NKN-(Na,K)NbO_3 piezo material has been used and investigated the performance pertinent for powering shoe mounted BLE beacon . For the voltage measurement, a NKN piezo sheet was made in the rectangular shape and placed under the shoe sole warned by a human. The piezo sheet composed of -(Na,K)NbO_3 polymer matrix and piezo electric particles. An Ag electrode was formed on the facing surfaces of the poled samples and a silicon rubber-tape was attached on that Ag electrode as shown in Fig.4.3. The thickness and area of polyimide sheet was 116 μm and 31.7 mm × 27.9 mm =8.84 cm^2 respectively. The electrode was considered as Ag paste and its area was 23.4 mm × 20.8 mm =4.87 cm^2. The piezoelectric constant was d_{33}~3 pC/N. Considering these dimensions and properties, the NKN material was adopted under shoe for the measurement of pressure produced voltage. Fig. 4.4(a) shows the prepared NKN sample, and Figure 4.4(b) shows a scene of measurement.

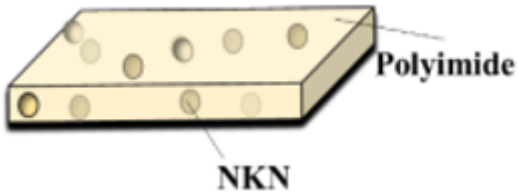

(a)

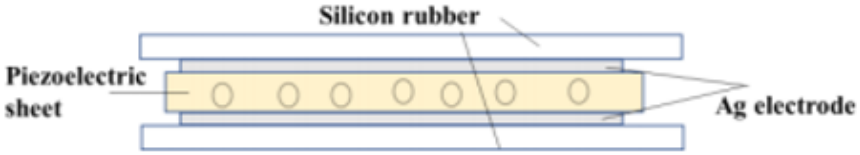

(b)

Fig. 4.3. Piezo structure. (a) 3D view. (b) Side view

IEEE defines an output ranging from 1.6 to 2.7 volt for Bluetooth operation. The NKN piezo sheet was mounted under the surface of the human foot with shoe and connected to an oscilloscope via some connectors to measure the pressure produced voltage. The NKN sheet was set to heel or toe for measuring at both sides. When the human walk by wearing this NKN sheet mounted shoe, some charges are generated which act as voltage on the electrode of the NKN piezo element due to the force applied with tension or pressure. For observing the phenomena of voltage generation, we performed the above mentioned experimental setup by using the oscilloscope. From the oscilloscope, we got time domain waveform. In practice, FFT (Fast Fourier transform) was applied from time domain data to frequency domain in order to extract the frequency response. After FFT analysis, we found voltage versus frequency spectrum. Fig. 4.5 and Fig. 4.6 shows the time waveform and frequency spectrum of the measured AC voltage respectively when the NKN piezo sheet was placed at heel side. Fig. 4.7 and Fig. 4.8 shows the time waveform and frequency spectrum of the measured AC voltage respectively when the NKN piezo sheet was placed at toe side. The maximum produced AC voltage from one NKN piezo sheet was found to be around 2.3 V as shown in time domain waveform. Usually, a man can give 2 steps per second. Therefore, frequency spectrum has been analyzed at 2 Hz. The maximum voltage was found to be 11 mV and 16 mV at 2 Hz in terms of heel and toe side respectively.

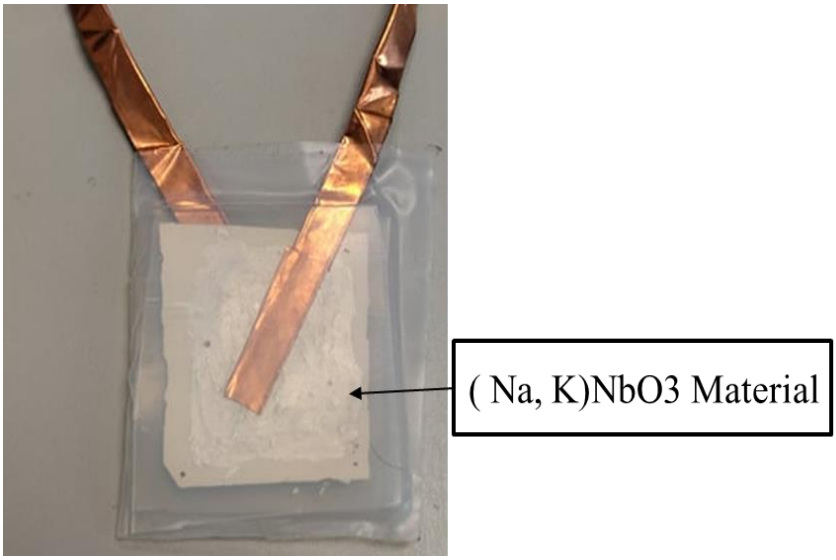

(a)

(b)

Fig. 4.4. Measurement setup. (a) NKN sample. (b) Scene of measurement

Piezo voltage generation from mounted shoe varies from man to man i.e it depends on weight, applied pressure and movement etc. We conducted this experiment to check the ability of the voltage measurement by piezo, by two different persons who carried their respective weight 58 kg and 67 kg. They applied dynamic pressure during walking and piezo sheet was able to generate voltage. If the person walks who carried 58 kg, the voltage is produced as to be around 1 V. If the person walks who carried 67 kg, the voltage is produced as to be around 2.3 V. So, it is possible to generate 2.7 V voltage if any person walks who can carry more than 67 kg and it is enough to operate Bluetooth for our purpose.

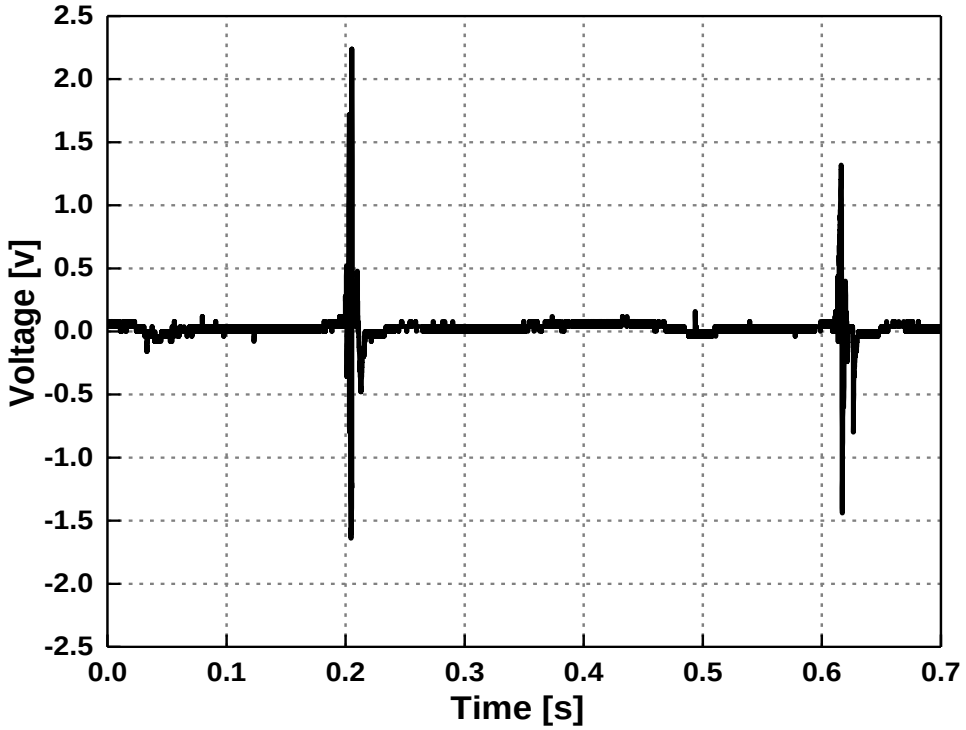

Fig. 4.5. Time waveform of measured AC voltage at heel side

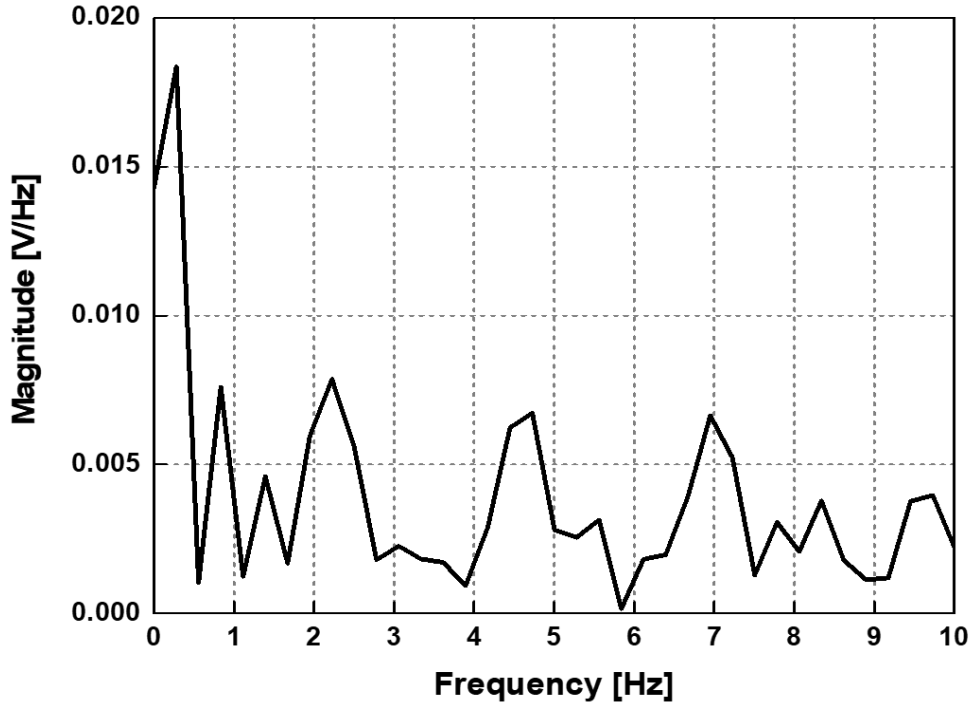

Fig. 4.6. Frequency spectrum of measured AC voltage at heel side

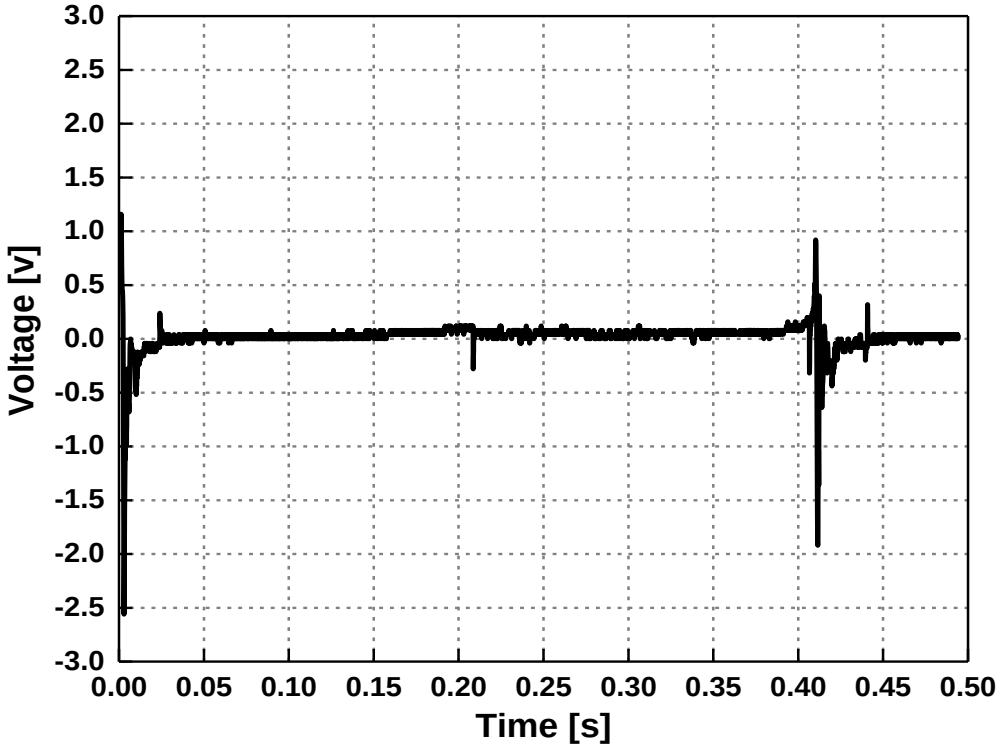

Fig. 4.7. Time waveform of measured AC voltage at toe side

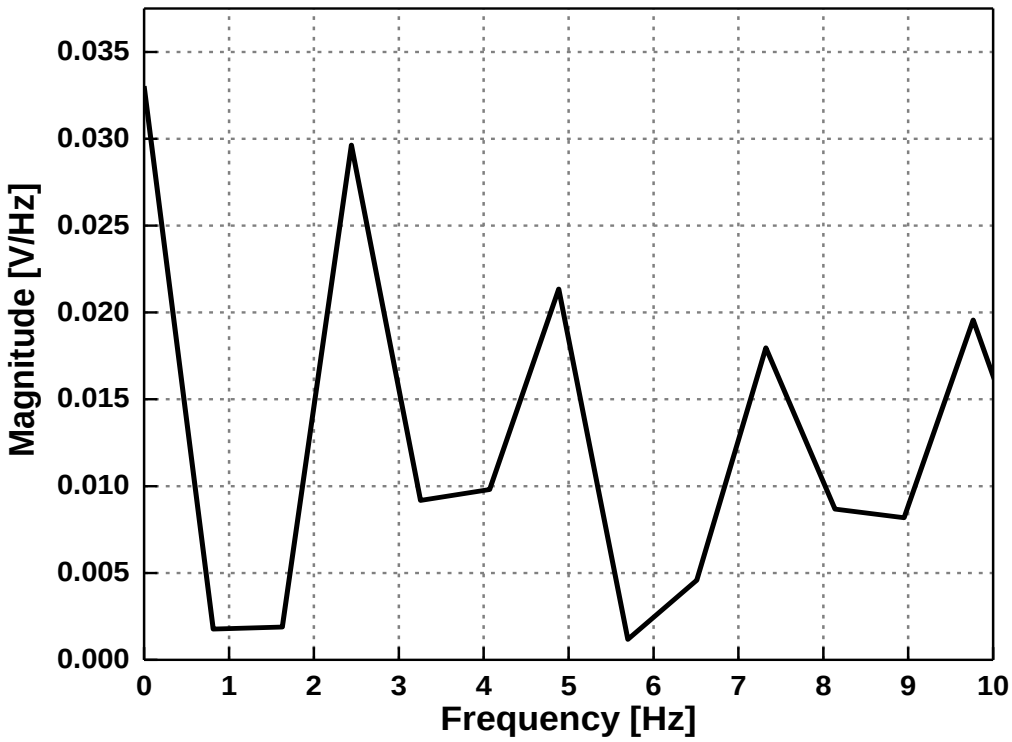

Fig. 4.8. Frequency spectrum of measured AC voltage at toe side

4.2.2 Measurement of pressure produced voltage by BCTZ

For measuring the voltage by BCTZ, the samples and the dimension are almost the same as NKN sample, but materials are different. The piezoelectric particle is (Ba, Ca) (Ti, Zr) O_3 that is Barium Titanate (BaTiO3) based material. The polymer material is Polyvinylidene fluoride (PVDF). In this case, (Ba, Ca) (Ti, Zr) O_3 piezo material has been used and investigated the performance pertinent for powering shoe mounted BLE beacon. For the voltage measurement, two BCTZ piezo sheets were made in the rectangular shape and placed under the shoe sole warned by a human. An Ag electrode was also formed on the facing surfaces of the poled samples and a silicon rubber-tape was attached on that Ag electrode. Two BCTZ piezo sheets were adopted under shoe at a time for the measurement of pressure produced voltage. Fig. 4.9 shows a scene of measurement by these piezo sheets.

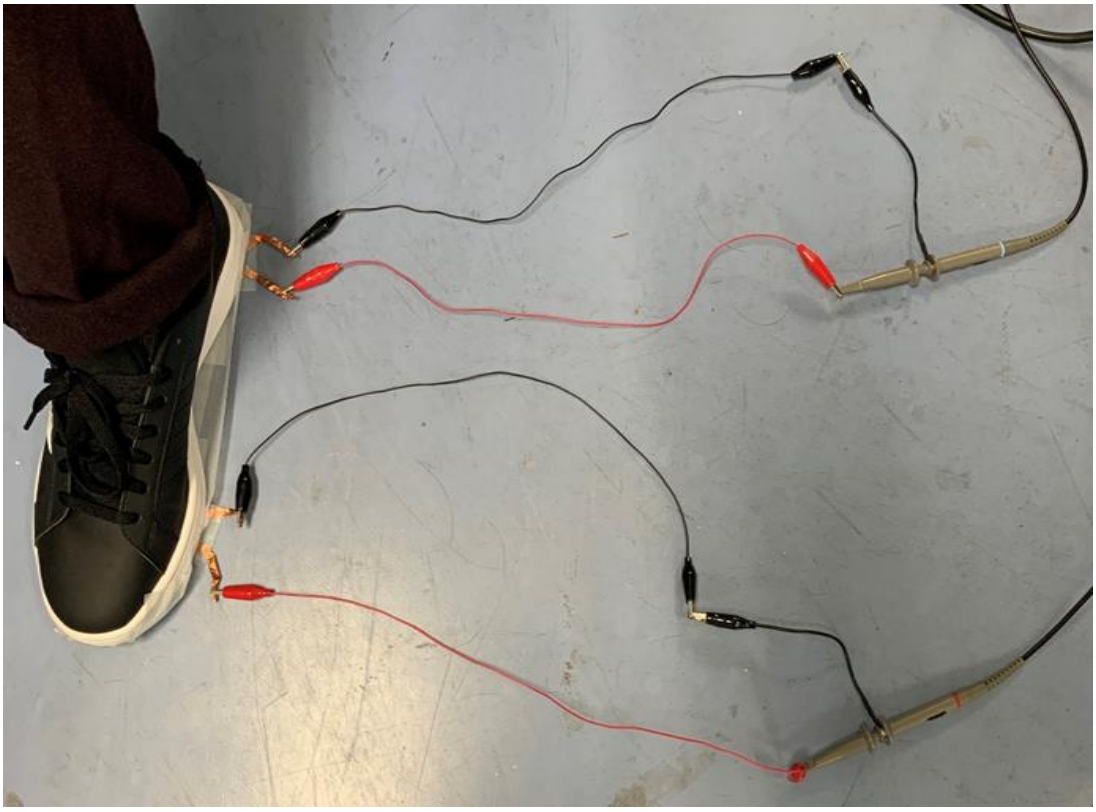

Fig. 4.9. Measurement setup by two BCTZ sheets

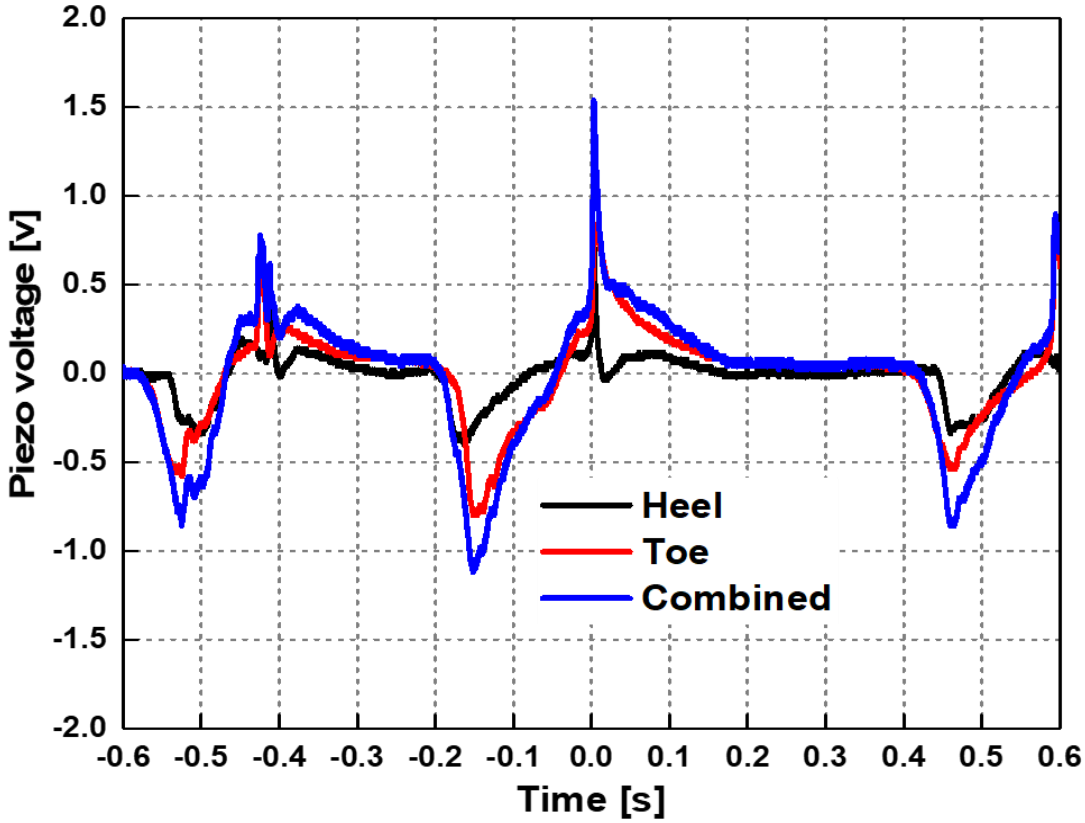

Fig. 4.10. Time waveform of measured ac voltage from BCTZ

The BCTZ piezo sheet was mounted under the surface of the human foot with shoe and connected to an oscilloscope via some connectors to measure the pressure produced voltage. In the shoe-mounted voltage measurement, we therefore used two BCTZ piezo sheets together with the oscilloscope and connected them into the shoe. Although the BCTZ was connected into the shoe, it did not directly touch the oscilloscope probe. There were some cables between them. It was connected to a digital oscilloscope using a ferrite-covered coaxial cable. This avoided direct coupling between cables and achieved good isolation and protection the probe of oscilloscope. In this way, the BCTZ sheet was set to heel and toe for measuring at both sides together. When the human walk by wearing this BCTZ sheet mounted shoe, some charges are generated which act as voltage on the electrode of the BCTZ piezo element due to the force applied with tension or pressure. For observing the phenomena of voltage generation, we performed the above mentioned experimental setup by using the oscilloscope. From the oscilloscope, we got time domain waveform. In addition, FFT (Fast Fourier transform) was applied from time domain data to frequency domain in order to extract the frequency response. After FFT analysis, we

found voltage versus frequency spectrum. Fig. 4.10 and Fig. 4.11 shows the time waveform and frequency spectrum of the combined measured AC voltage respectively when the one BCTZ piezo sheet was placed at heel side and another at toe side. The maximum produced AC voltage from two piezo sheets was found to be around more than 1.5 V as shown in Fig. 4.10.

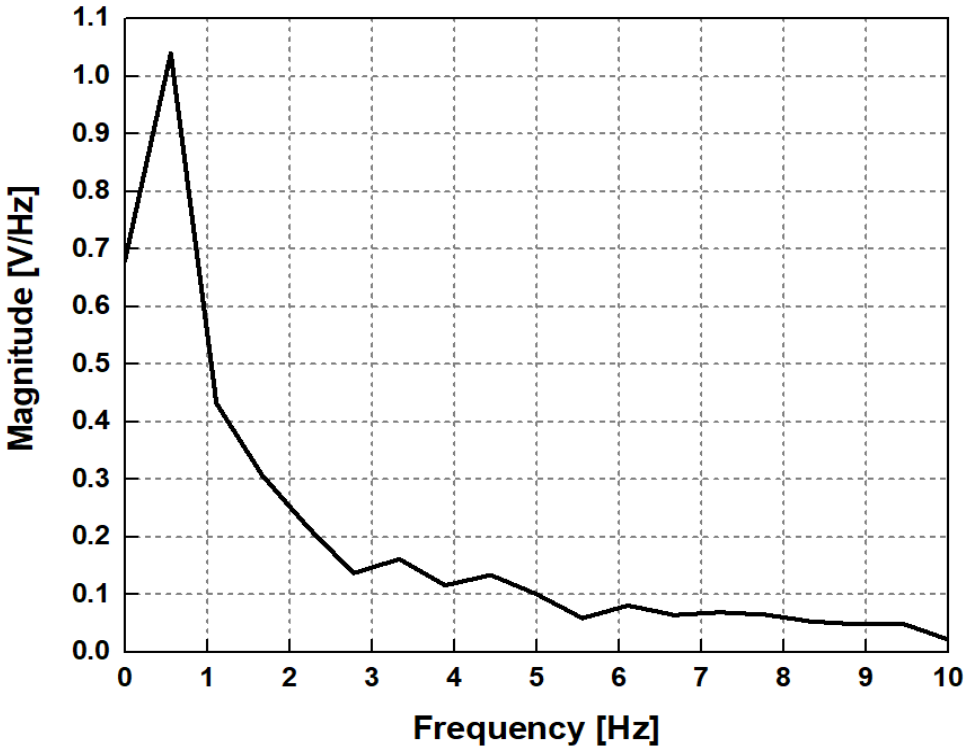

Fig. 4.11. Frequency spectrum of measured ac voltage from BCTZ

Moreover, the measured data values were also processed using MATLAB/ Origin Software to observe CCRF (cross co-relation function) to measure time delay between two obtained waveforms which has been shown in Fig.4.12. The voltage was found to be 72 mV at 2 Hz as shown in Fig. 4.11. The time delay between two waveforms in Fig. 4.10 is very small and it looks around 4ms which has been investigated by CCRF technique in Fig. 4.12.

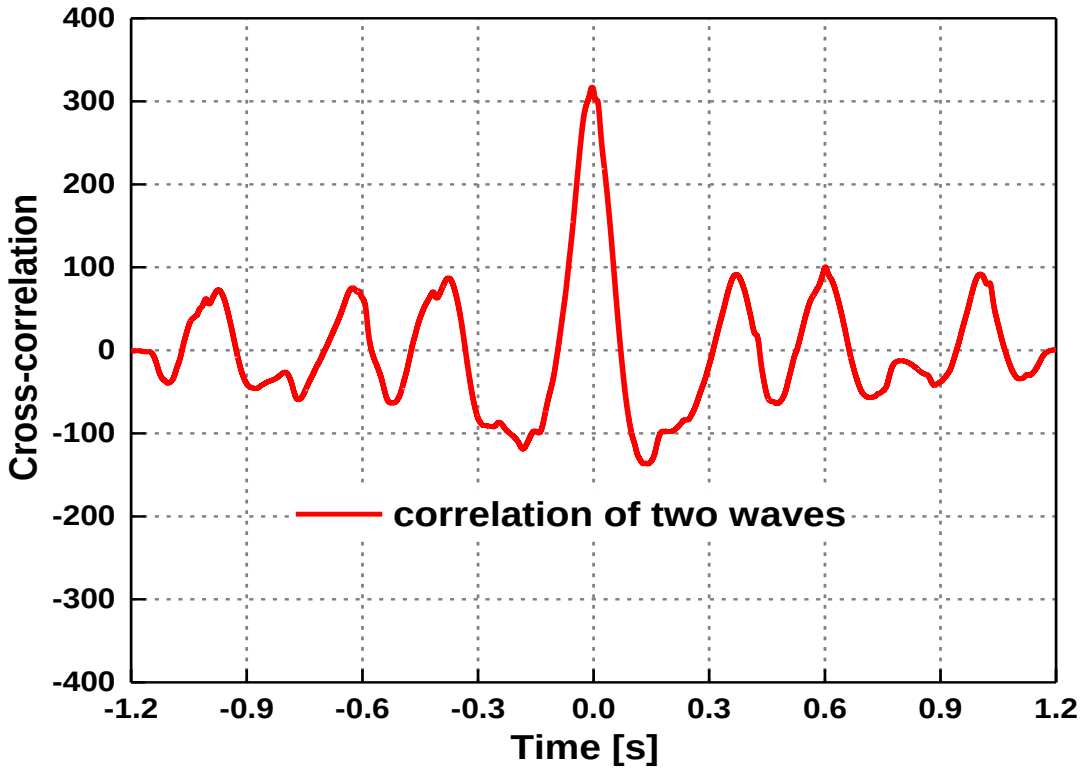

Fig. 4.12. CCRF between two waveforms in fig.4.10 for measuring time delay

4.2.3 Comparison of measurement performance between NKN and BCTZ

We have measured voltage of our two different types of piezo materials under the same conditions, and tabulated the maximum output voltages V_{out} across those materials as shown in Table 4.1. As can be seen in Fig. 4.5 and 4.10, for pressure produced voltage the best type of piezo is the NKN piezo, which has a maximum produced AC voltage of around 2.3 V. To obtain 2.7 V produced voltage, the NKN might have a higher performance and better results than the other type. In terms of reaching the requirement voltage generation to BLE beacon, NKN and BCTZ type piezo are the leaders, both of them having voltage generation beyond a 1.6 V voltage. It is clear that up to a 2.7 V voltage, the NKN will have the best performance, while above a 2.3 V output voltage. Since there is a significant difference in terms of voltage generation between NKN and BCTZ piezo samples, we decided to use the NKN piezo to operate the BLE beacon with the harvester. Even though a one NKN piezo has higher performance results than two BCTZ sheets based on the experimental measurement obtained results.

Therefore, BCTZ sample is not preferred, because it needs more sheets to meet our desired operation.

Table 4.1. Summary of the experimental results for energy harvesting

Piezo Name	Maximum output voltage
NKN	2.3 V
BCTZ	1.6 V

BCTZ means having extra piezo components, greater complexity, and larger device size, which is very concerned in wearable systems. Considering the performance results NKN seems the best option to achieve highly efficient operation in harvesters

4.3 Rectifier Circuit for AC-DC conversion

Rectification is a process used to convert alternating current (AC), which periodically reverses direction, to direct current (DC), which flows in only one direction. The reason we need rectification in BLE beacon is that most low-power electronic devices use only a low DC voltage to operate. Therefore, the AC voltage obtained from harvesters needs to be rectified, converted into a usable DC voltage. Rectifier circuits are the most common diode applications in getting DC power supplies from AC power generators.

4.3.1 Si Diode based rectifier

As mentioned before an EH-system with piezoelectric elements as a transducer needs a rectifier to generate a DC power output. For this demand, we used freeware package LTspice, which implements a SPICE simulator of electronic circuits. LTspice provided both a schematic capture and waveform for each circuit. Circuit simulations based on the experimental measurement results, have been realized and plotted. The output DC voltage and efficiency calculation reports, have been obtained from the simulation software, which is produced by semiconductor manufacturer Linear Technology (LTC). During all simulation tests, the input signal amplitude values were used as measurement data values from piezoelectric material.

The diode bridge rectifier has been the most-used type for many years, and is well-known. It consists of four silicon diodes in a bridge configuration. A 100μF capacitor is

connected in parallel to further smoothing the voltage ripple. The circuit schematic is shown in Fig.4.13. For measurement data values as input amplitude, the Vin and Vout waveforms are shown in Fig.4.14, with the forward voltage drop. After that, voltage efficiency is calculated by as follows

$$\eta_V = \frac{V_{out}}{V_{in}} * 100\% \tag{4.1}$$

where Vout is the amplitude of the DC output signal and Vin is the amplitude of the AC input signal. At the maximum applied input amplitude of Vin=2.3 V, the output voltage amplitude is found to be as 595 mV, voltage efficiency is 41.74%.

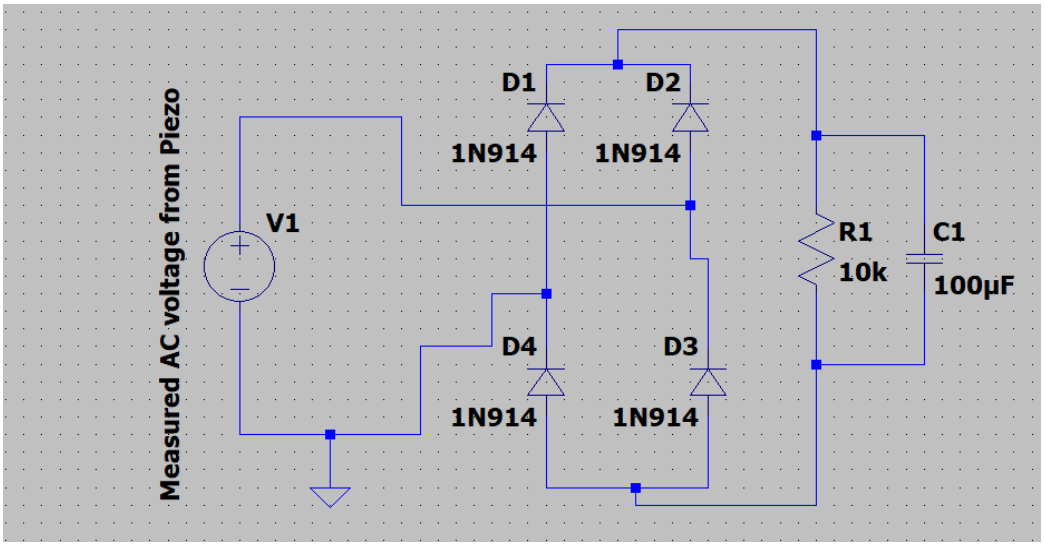

Fig. 4.13. Full-wave Si diode based rectifier

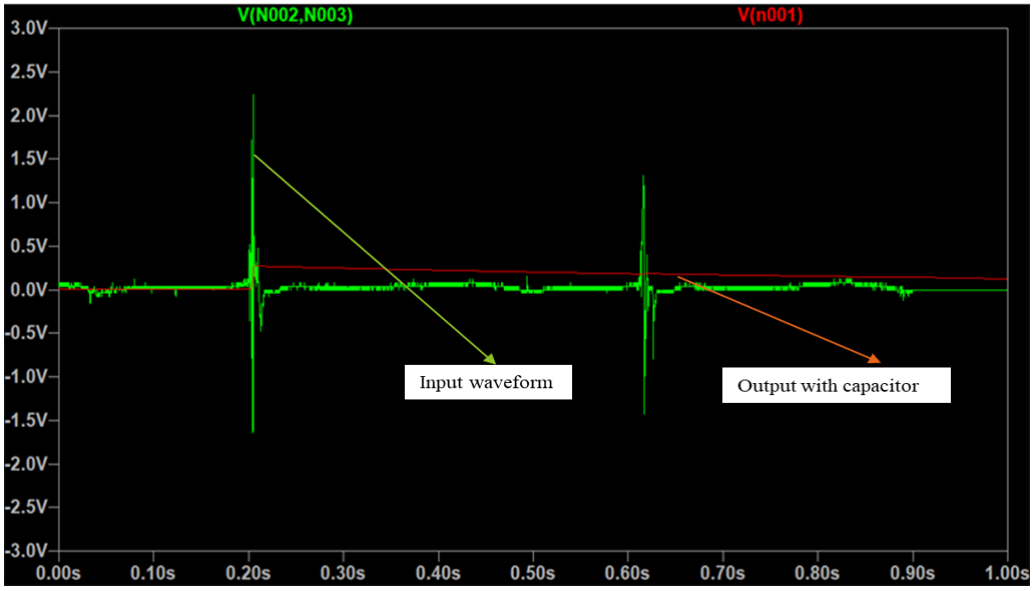

Fig. 4.14. Vin and Vout signals of full-wave diode bridge rectifier

4.3.2 Schottky Diode based rectifier

The full-wave Schottky diode bridge rectifier is another type, which uses Schottky diodes, which have a lower forward voltage drop compared to silicon diodes. The circuit schematic is shown in Fig.4.15. For each cycle, only two diodes conduct the current; during the positive half cycle of the AC input, D2 and D4 are forward biased and conduct the current, while D1 and D3 are reverse biased and not conducting. However, during the negative half-cycle of the AC supply voltage, D1 and D3 are forward-biased and conduct the current, while D2 and D4 are reverse-biased and not conducting. For each case the direction of the current is the same, so we have unidirectional current flow, which is DC voltage. For measurement data values as input amplitude, the Vin and Vout waveforms are shown in Fig.4.16, with the forward voltage drop. At the maximum applied input amplitude of Vin=2.3 V, the output voltage amplitude is found to be as 1.4 V, voltage efficiency is 60.89%.

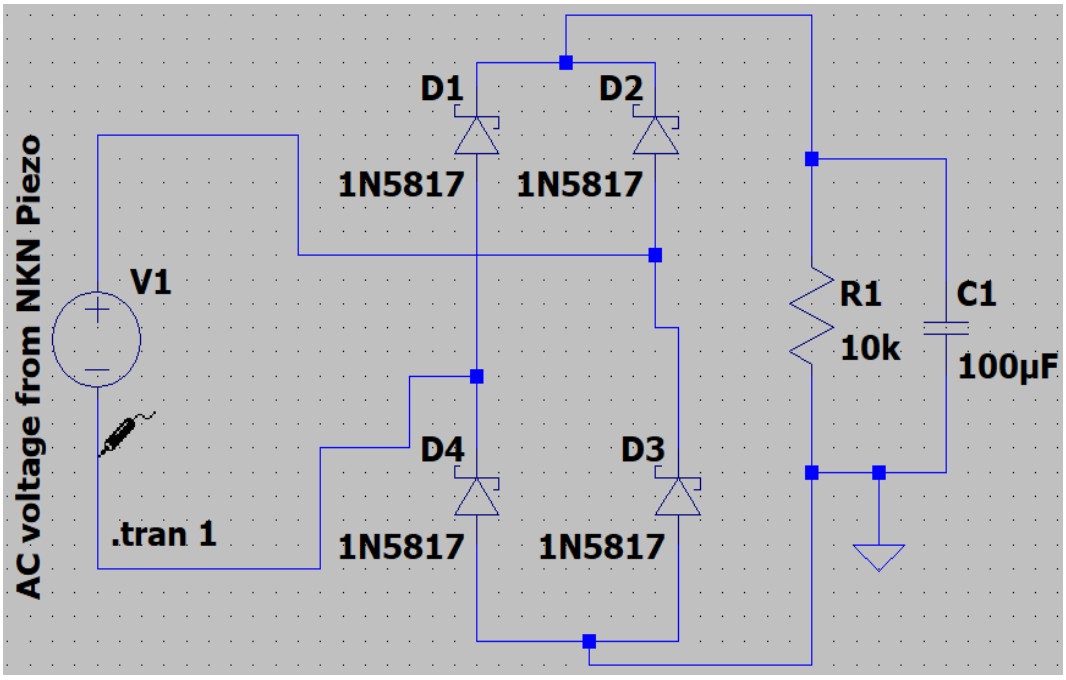

Fig. 4.15. Full-wave Schottky diode based rectifier

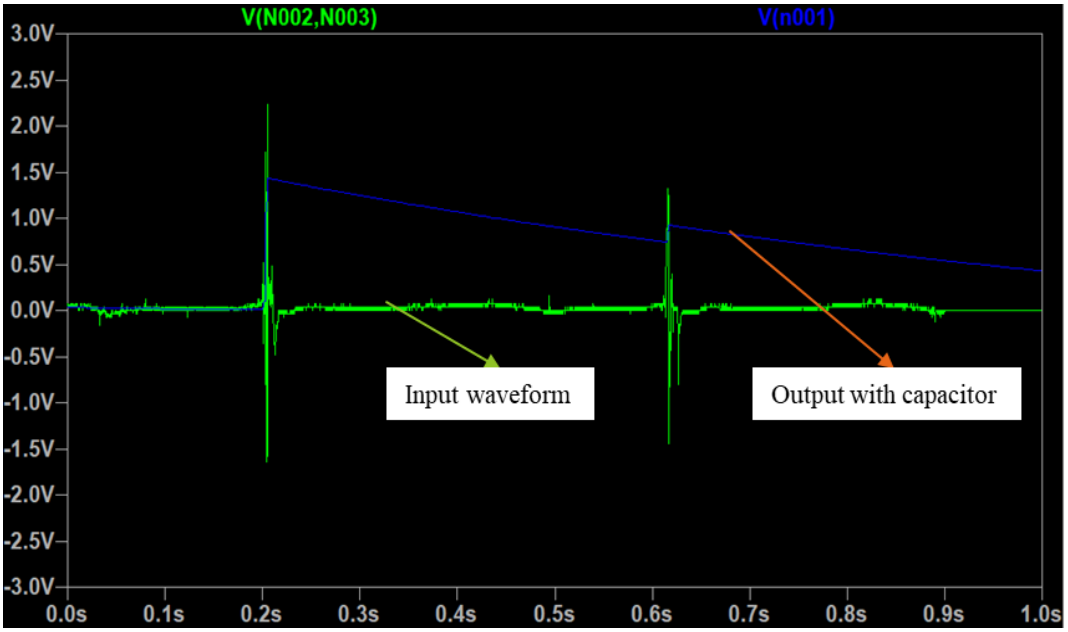

Fig. 4.16. Vin and Vout signals of full wave Schottky diode-based bridge rectifier

4.3.3 Full wave passive MOSFET

Junction-based diodes are not the best choice for energy harvesters, which have low-voltage output, because of their forward voltage drop. To eliminate forward voltage, drop, many different circuit topologies have been studied [86], [87]. Recently, integrated circuits fabricated with CMOS technology have been used to minimize voltage drop as much as possible [87], [88]. Diodes are usually replaced with MOSFETs fabricated with CMOS technology in a diode-tied configuration. Although Schottky diodes have a lower forward voltage drop, they have more ripples, and higher reverse leakage current when they are reverse biased. In addition to having high reverse leakage current, their fabrication costs are also high, as they are not compatible with CMOS technology [88]. The new type of full-wave rectifier which uses four MOSFETs in a bridge configuration [87]; two P-type and two N-type MOSFETs. MOSFETs act as a switch with a small on-resistance when they are fully turned on. To turn the MOSFETs on, there is a threshold voltage that which must be applied to the gate of the MOSFET, which determines the minimum voltage requirement to start operation of a MOSFET. In practice, a capacitor is used in the circuit to act as a filter to reduce ripple voltage. To make sure the DC output terminals of the rectifier so that the polarities match, I connected the 100µF and 500µF

capacitor properly across the output terminal to check the influence of smoothness or filter the ripple present in the rectified DC. The circuit schematics are shown at 100µF and 500µF in Fig. 4.17 and Fig.4.19 respectively.

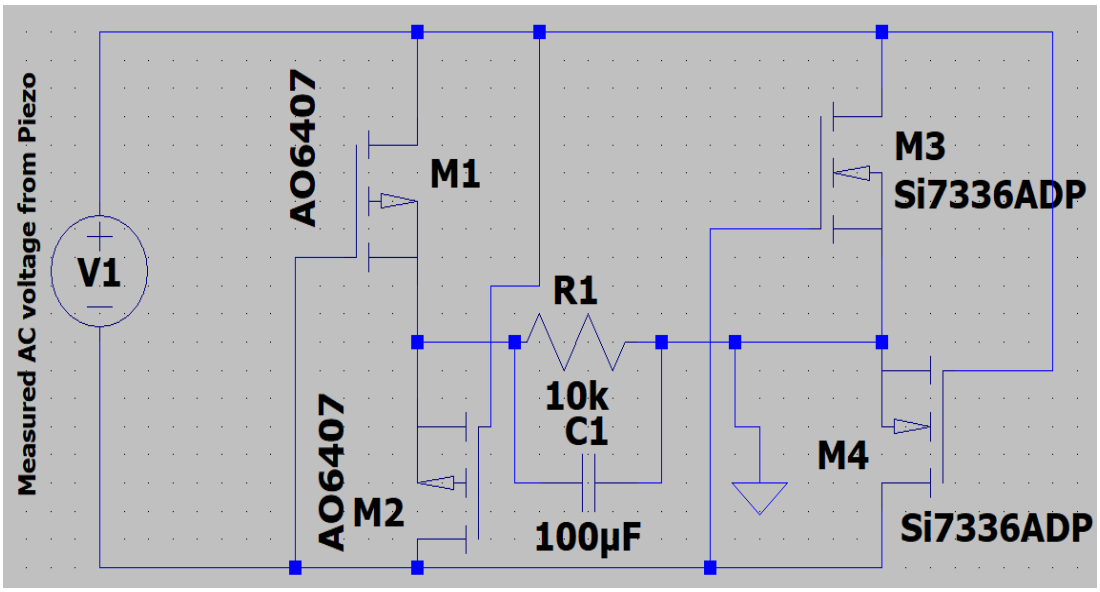

Fig. 4.17. Full-wave passive MOSFET bridge rectifier, C=100µF

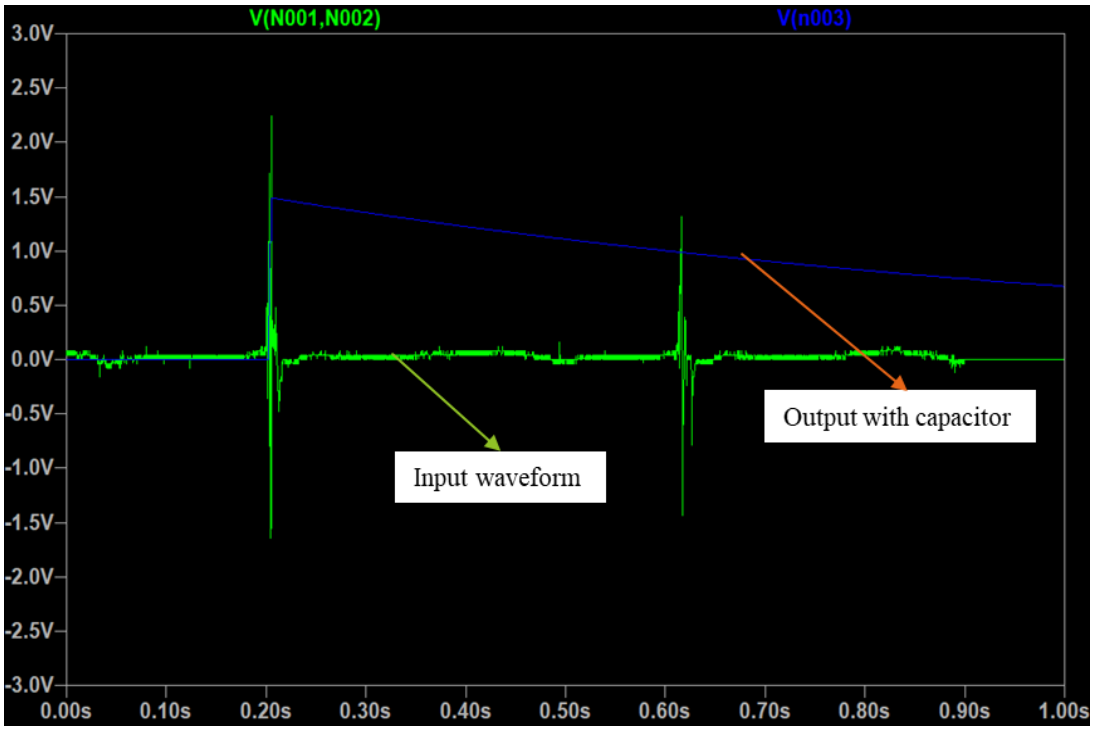

Fig. 4.18. Vin and Vout signals of full-wave passive MOSFET bridge rectifier, C=100µF

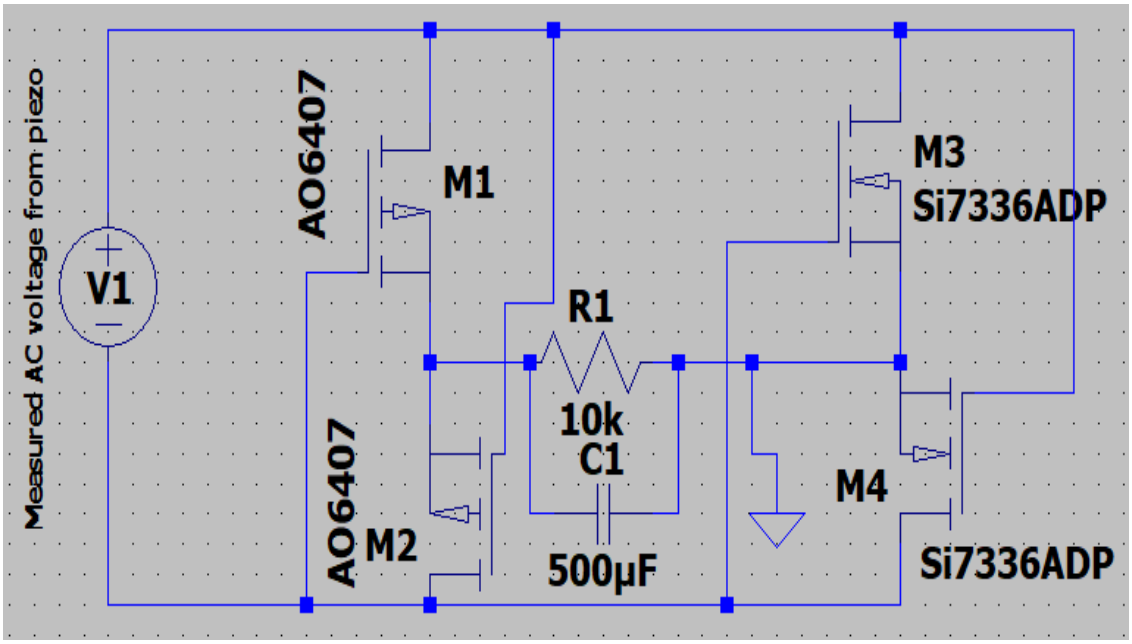

Fig. 4.19. Full-wave passive MOSFET bridge rectifier, C=500µF

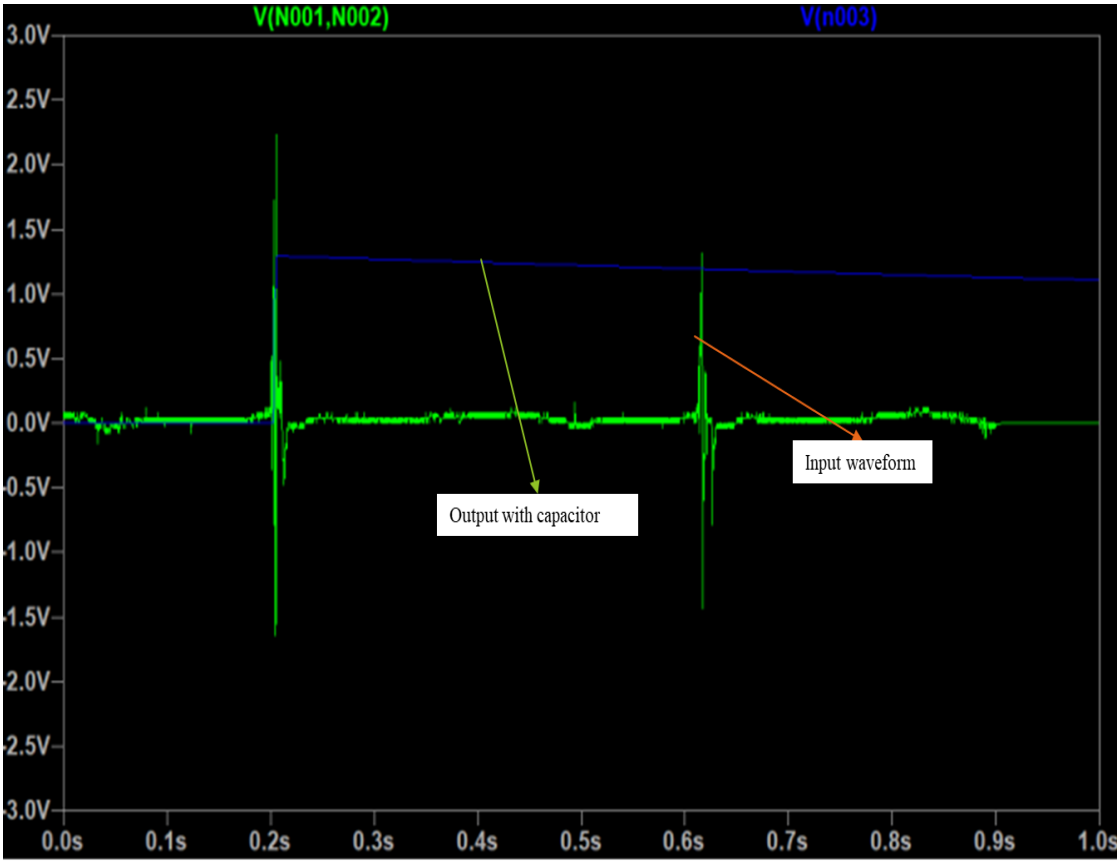

Fig. 4.20. Vin and Vout signals of full-wave passive MOSFET bridge rectifier, C=500µF

For measurement data values as input amplitude, the Vin and Vout waveforms at 100μF and 500μF are shown in Fig.4.18 and Fig.4.20 respectively, with the minimum forward voltage drop. It is observed than a smoother DC voltage can be attained with the 500μF capacitor filter between 500μF capacitor and 100μF capacitor filter. At the maximum applied input amplitude of Vin=2.3 V, the output voltage amplitude is found to be as 1.5V, voltage efficiency is 65.22%.

4.3.4 Performance comparison of different circuits

We have simulated our different types of full-wave bridge rectifier under the same conditions and observed the output voltages for rectification. Table 4.2 summarizes the performances of different rectifiers. Even though a full-wave rectifier offers a higher power efficiency, smaller output ripples, and greater breakdown voltage compared to half-wave rectifiers, their most serious drawback in the case of micro-power generators is a significant forward voltage drop when the device is conducting in the forward direction, and leakage current when the diode is reverse biased. In particular, the forward voltage drops results in undesirable voltage and power losses and reduces the total system efficiency. As can be seen in the evaluated results for voltage efficiency the best type of rectifier is the passive MOSFET full-wave bridge rectifier, which has a maximum voltage efficiency of around 65.22%.

Table 4.2. Comparison of voltage efficiency for different rectifiers

Rectifier	Voltage efficiency
Si diode	41.74%
Schottky diode	60.89%
MOSFET	65.22%

4.4 Conclusion and Discussion

We presented the fundamentals of energy harvesting. The two NKN and BCTZ of piezo material for powering shoe-mounted sensor were also discussed in this chapter. Power conditioning in vibration-based energy harvesters was introduced, and the pressure produced voltage measurement by shoe-mounted foot was discussed. For making independent monitoring system, the energy harvesting phenomena has been analyzed for powering a shoe-mounted sensor using the piezo material with a real human foot pressure. The results for voltage generation have been obtained. When the NKN sheet is used, the maximum output AC voltage is found to be 2.3 V. When the BCTZ sheet is used, the maximum output AC voltage is found to be 1.6 V. The NKN and BCTZ have revealed that the BCTZ material dominate energy harvesting in this research. Based on the concepts of AC-DC conversion, different types of rectifiers were reviewed, alongside studying their rectified signal calculations, voltage efficiency have been analyzed. The Full-wave passive MOSFET bridge rectifier shows the better performance of 66% efficiency. Assuming that the communication distance between the BLE beacon and a smart phone user is 20 m, the coverage width of the main beam is 5.6 m, which is equivalent to the normal road width, so that the BLE signal can be effectively received by the smart phone user coming from the opposite side. In view of this point, a BLE beacon can send a signal for notifying the location, and therefore 1.6 V to 2.7 V DC output voltage to maintain the required power supply for identifying the position of elderly wanderers.

In future, At the shoe we may also combine mechanical harvesting and solar harvesting where piezo elements can act as photovoltaic. It might be multimodal, combining mechanical and solar harvesting, which can make harvesting more reliable as energy source for self-powering BLE beacon for wanderer location identification. In addition, a smart jacket could also be another future idea for the remedy of the dementia affected people.

Chapter 5

Summary

As the aging society problem draws great attention, the sensing technology and monitoring scheme of bio potential signals has advanced tremendously over the years. The bio potential signals include electromyogram (EMG), electrocardiogram (ECG), electroencephalogram (EEG), electrooculogram (EOG) and many others. They are widely employed in medical and healthcare applications. For example, the body area network (BAN) with wearable sensing technologies can collect these signals as vital data for health-state monitoring, which is considered as an emerging solution to soaring healthcare costs and shortages of medical resources. The potential of bio signals is still to be exploited when sensing technologies advance further. In addition to medical treatment and healthcare, they could also be considered as an irreplaceable interface between human body and devices. In this study, a core idea runs through all our works: On body to In-body technology, On-body to OFF-body technology to prevent the vulnerabilities of aged people or patient and combination of energy harvesting technique to operate this technology independently. Contents of the thesis is as follows.

In Chapter 1, we introduced about issues for the elderly, On-body to In-body transmission, On-body to Off-body transmission and contents of the thesis.

In Chapter 2, we discussed the necessity of channel modeling as a vital step in designing transceivers for wireless implant communication systems due to the extremely challenging environment of the human body. The in-to-on body path loss and group delay were first analyzed using an electric dipole and a current loop in the 10-60 MHz human body communication band. A path loss model was derived using finite difference time domain (FDTD) simulation and an anatomical human body model. As a result, it was found that the path loss increases with distance in an exponent of 5.6 for dipole and 3.9 for loop, and the group delay variation is within 1 ns for both dipole and loop which suggests a flat phase response. Moreover, the electric and magnetic field distributions revealed that the magnetic field components dominate in-body signal transmission in this frequency band. Based on

the analysis results of the implant channel, the link budget was analyzed. An experiment on a prototype transceiver was also performed to validate the path loss model and bit error rate (BER) performance. The experimentally derived path loss exponent was between the electric dipole path loss exponent and the current loop path loss exponent, and the BER measurement showed the feasibility of 20 Mbps implant communication up to a body depth of at least 15 cm.

In Chapter 3, a novel monitoring system was discussed using BLE beacon to detect wanderer location identification. The monitoring system with Bluetooth low energy (BLE) beacons is promising for position identification of elderly wanderers. BLE beacons can be mounted in shoes for convenience, and a shoe-mounted directional antenna is expected to efficiently radiate the beacon signals to the data server of the monitoring system. In this paper, a directional array antenna with planar or curved structure was designed on the shoe surface for this purpose. The antenna was designed to sweep diagonally upward from 10◦ to 50◦, and the simulated and measured S11 performances revealed reasonable agreement. The antenna was assumed to be used in an urban environment, and a directional patch array antenna with dielectric lens was also designed to receive beacon signals by mounting it on utility poles. According to a feasibility experiment result of elderly wanderer position identification, the designed directional antenna can provide an almost 100% position identification rate if a wanderer is within 20 m from a smart phone user.

In Chapter 4, we proposed the aspects of piezoelectric materials as energy harvester system for powering our designed shoe-mounted sensor. We provided a state-of-the-art of pressure produced voltage about energy harvesting system, which use NKN and BCTZ piezo materials to explain the mechanism for wearables. Implementation of our approach was conducted by placing the piezo materials of shoe sole. Experiments are performed to verify its effectiveness. The maximum produced AC voltage from one piezo sheet was found to be around 2.3 V as shown in time domain waveform. Furthermore, we highlighted the advantages of using a full-wave passive rectifier over the conventional full-wave bridge rectifier for AC-DC conversion. Together with multiple piezo sheets and, using passive rectifier, a desirable output power can be accomplished to operate BLE mounted sensor.

Final conclusion is that this thesis book considers wireless transmission from In-body to On-body and On-body to Off-body for healthcare purpose in an aging society. The mechanism of wireless transmission is explained, in particular from the standpoint of healthcare data collection and localization by considering elderly issues. Communicational requirements for the key scenarios of the healthcare are introduced and discussed. Both IB2OB and OB2OB wireless networks are considered. Both network approaches have unique advantages, but no single network is best suitable for all the scenarios of the human body communication. Therefore, we characterized of 10-60 MHz band On-body to In-body transmission as the key backbone network of healthcare issues for the wireless body area network. Such network is discussed and its suitability to relevant scenarios is discussed. Moreover, we have developed a monitoring system with Bluetooth low energy (BLE) beacons position identification of elderly wanderers at 2.4 GHz band On-body to In-body transmission as the another key pillar network of healthcare issues for the wireless body area network. Using the developed system, we have succeeded for the first time over the world in estimating an almost 100% position identification rate if a wanderer is within 20 m from a smart phone user. It might be promising for position identification of elderly wanderers. But depending on the location of the user or the placement of the battery, recharging or exchanging can be difficult. To operate independently, the vital device of this system, we conducted experimental measurement to develop an energy harvesting by piezo from human motion as a great alternative that no one in the world has achieved. The solution exploits the advantages of both network approaches and is a future-proof solution for advanced healthcare in the years to come. Future work include more precise characterization of the requirements of the environments, as well as implementing and evaluating the performance of a reconfigurable hybrid network particularly suitable for healthcare scenario.

References

[1] UN World Population Prospect 2021.

[2] P. Bonato, “Wearable sensors and systems - from enabling technology to clinical applications,” IEEE Eng. Med. Biol. Mag., vol. 29, no. 3, pp. 25–36, 2010.

[3] K. Hung, Y.T. Zhang, B. Tai, “Wearable Medical Devices for Tele-Home Healthcare”, In Proceeding of 26th Annual International Conference of the IEEE Engineering in Medicine and Biology Society (IEMBS ’04), San Francisco, CA, USA, 1–5 pp. 5384–5387, September 2004.

[4] D.J. Margolis, J. Knauss, W. Bilker, M.; Baumgarten, “Medical conditions as risk factors for pressure ulcers in an outpatient setting”, Age Ageing, 32, 259–264, 2003.

[5] S. Dong, et al., “Doppler Cardiogram: A Remote Detection of Human Heart Activities,” IEEE Transactions on Microwave Theory and Techniques vol. 68, no. 3, 1132–1141, 2020.

[6] E. Cardillo, A. Caddemi, “Radar range-breathing separation for the automatic detection of humans in cluttered environments,” IEEE Sensor Journal, 1–1, 2020.

[7] E. Cardillo, A. Caddemi, “A. A review on biomedical MIMO radars for vital sign detection and human localization,” Electronics, vol. 9, 1497, 2020.

[8] S. Schellenberger, K. Shi, F. Michler, F. Lurz, R. Weigel, A. Koelpin, “Continuous In-Bed Monitoring of Vital Signs Using a Multi Radar Setup for Freely Moving Patients,” Sensors, vol. 20, 5827, 2020.

[9] F. Michler, et al., “A Radar-Based Vital Sign Sensing System for In-Bed Monitoring in Clinical Applications,” 2020 German Microwave Conference (GeMiC), Cottbus, Germany, pp. 188–191, 2020.

[10] C. Covaci, A. Gontean, “Piezoelectric Energy Harvesting Solutions: A Review”,

Sensors, 20, 3512, 2020.

[11] H. Landaluce, L. Arjona, A. Perallos, F. Falcone, I. Angulo, F.A. Muralter, “A Review of IoT Sensing Applications and Challenges Using RFID and Wireless Sensor Networks”, Sensors 20, 2495, 2020.

[12] B. Maamer, A. Boughamoura, A.M.F. El-Bab, L.A. Francis, F.A. Tounsi, “A review on design improvements and techniques for mechanical energy harvesting using piezoelectric and electromagnetic schemes”, Energy Convers. Manag. 199, 111973, 2019.

[13] M. Rodgers, “Dynamic biomechanics of the normal foot and ankle during walking and running”, Phys. Ther. 68, 1822–1830, 1988.

[14] M. Zhou, M. Al-Furjan, B. Wang, “Modeling and Efficiency Analysis of a Piezoelectric Energy Harvester Based on the Flow Induced Vibration of a Piezoelectric Composite Pipe”, Sensors 18, 4277, 2018.

[15] C. Vankecke et al., “Multisource and battery-free energy harvesting architecture for aeronautics applications,” IEEE Trans. Power Electron, vol. 30, no. 6, pp. 3215–3227, June 2015.

[16] S. Adami et al., “A flexible 2.45-GHz power harvesting wristband with net system output from −24.3 dBm of RF power,” IEEE Trans. Microw. Theory Techn., vol. 66, no. 1, pp. 380–395, Jan. 2018.

[17] SPIES, Peter; POLLAK, Markus; MATEU, Loreto (Hg.). Handbook of energy harvesting power supplies and applications. CRC Press, 2015.

[18] B.H. Li, K.Y. Yazdandoost, and B. Zhen, “Wireless Body Area Network”, River Publishers, Aalborg. 2010.

[19] T.G. Zimmerman, “Personal area networks: near-field intra body communications”, IBM System Journal, 35 (3&4), 609-6017, 1996.

[20] M.R. Yuce, G. Alici, T.D. Than, "Wireless Endoscopy". *Wiley Encyclopedia of*

Electrical and Electronics Engineering. pp. 1–25(2014).

[21] M. Bhattarai, P. Bansal, Y. Khan "Longest duration of retention of video capsule: A case report and literature review", *World Journal of Gastrointestinal Endoscopy*. **5** (7):3525 (July 2013).

[22] https://wlab.web.nitech.ac.jp/english/research.html

[23] M. Prince, A. Comas-Herrera, M. Knapp, M. Guerchet, and M. Karagiannidou, "World Alzheimer report 2016: improving healthcare for people living with dementia: coverage, quality and costs now and in the future," 2016.

[24] A. Association et al., "2017 alzheimer's disease facts and figures," Alzheimer's & Dementia, vol. 13, no. 4, pp. 325–373, 2017.

[25] R. G. Logsdon, L. Teri, S. M. McCurry, L. E. Gibbons, W. A. Kukull, and E. B. Larson, "Wandering: a significant problem among community residing individuals with alzheimer's disease," The Journals of Gerontology Series B: Psychological Sciences and Social Sciences, vol. 53, no. 5, pp. P294–P299, 1998.

[26] D. L. Algase, D. H. Moore, C. Vandeweerd, and D. Gavin-Dreschnack, "Mapping the maze of terms and definitions in dementia-related wandering," Aging & mental health, vol. 11, no. 6, pp. 686–698, 2007.

[27] J. Corey-Bloom, D. Galasko, "Adjunctive therapy in patients with alzheimer's disease," Drugs & aging, vol. 7, no. 2, pp. 79–87, 1995.

[28] Q. Lin, D. Zhang, X. Huang, H. Ni, and X. Zhou, "Detecting wandering behavior based on gps traces for elders with dementia," in Control Automation Robotics & Vision (ICARCV), 12th International Conference on. IEEE, pp. 672–677, 2012.

[29] P.S. Hall, Y. Hao, Y.I. Nechayev, A. Alomainy, C.C. Constantinou, C.G. Parini, M.R. Kamruddin, T.Z. Salim, D.T.M. Hee, R. Dubrovka, A. Wadally, W. Song, Serra, P. Nepa, M. Gallo, M. Bozzetti, "Antennas and Propagation for On-Body Communication Systems", IEEE Antennas and Propagation Magazine, 49, 41-58(2007).

[30] Y.I. Nechayev, P.S. Hall, Z.H. Hu, “Characterization of Narrowband Communication Channels on the Human Body at 2.45 GHz”, IET Microwaves Antennas and Propagation, 4, 722-732(2010).

[31] B. Sanz-Izquierdo, F. Huang, J.C. Batchelor, “Dual-Band Wearable Button Antenna”, Electronics Letters, 42, 3-4(2006).

[32] A. Alomainy, Y. Hao, F. Pasveer, “Numerical and Experimental Evaluation of a Compact Sensor Antenna for HealthCare Devices”, IEEE Transactions on Medical Circuits and Systems, 1, 242-249 (2007).

[33] A. Alomainy, Y. Hao, A. Owadally, C.G, Parini, P.S., Hall, C.C. Constantinou, “Statistical Analysis and Performance Evaluation for On-Body Radio Propagation with Microstrip Patch Antennas”, IEEE Transactions on Antenna and Propagation, 55, 245-248(2007).

[34] A. Alomainy, Y. Hao, D.M. Davenport, “Parametric Study of Wearable Antennas Varying Distances from the Body and Different On-Body Positions”, Proceedings of the IET Seminar on Antennas and Propagation for Body Centric Wireless Communications, London, 84-89, 24-24 April 2007.

[35] G.A. Conway, W.G. Scanlon, “Antennas for over Body-Surface Communication at 2.45 GHz”, IEEE Transactions on Antennas and Propagation, 57, 844-855 (2009).

[36] J. Wang and Q. Wang, Body area Communications, Wiley-IEEE, 2013.

[37] IEEE Std 802.15.6-2012, “IEEE standard for local and metropolitan area network–Part 15.6: Wireless body area networks,” Feb, 2012.

[38] M. R. Yuce and T. Dissanayake, “Easy-to-swallow wireless telemetry,” IEEE Microwave Magazine., vol. 13, no. 1, pp. 90-101, Sep. 2012.

[39] P. Bose, A. Khaleghi, S. Mahmood, B. Mohammad, J. Bergsland, and I. Balasingham, “Evaluation of data telemetry for future leadless cardiac pacemaker,” IEEE Access, vol. 7, pp.157933-157945, Oct. 2019.

[40] J. Shi, D. Anzai, J. Wang, “Channel modeling and performance analysis of diversity reception for implant UWB wireless link,” IEICE Trans. Commun., vol. E95-B, no. 10, pp. 3197-3205, Oct. 2012.

[41] D. Anzai, K. Katsu, R. Chavez-Santiago, Q. Wang, D. Plettemeier, J. Wang and I. Balasingham, “Experimental evaluation of implant UWB-IR transmission with living animal for body area networks,” IEEE Trans. Microwave Theory Tech., vol.62, no.1, pp.183-192, Jan. 2014.

[42] Y. Shimizu, D. Anzai, R. Chavez-Santiago, P. A. Floor, I. Balasingham, and J. Wang, “Performance evaluation of an ultra-wideband transmit diversity in a living animal experiment,” IEEE Trans. on Microw. Theory Techn., vol. 65, no. 7, pp. 2596-2606, July 2017

[43] J. Wang, K. Nomura, H. Narita, F. Ito, D. Anzai, J. Bergs and, and I. Balasingham, “Development and in vivo performance evaluation of 10-60-MHz band impulse-radio-based transceiver for deep implantation having 10 Mb/s,” IEEE Trans. Microw. Theory Techn., vol.66, no.9, pp. 4252-4260, Sept. 2018.

[44] J. Wang, J. Liu, K. Suguri, and D. Anzai, “An in-body impulse radio transceiver with implant antenna miniaturization at 30 MHz,” IEEE Microw. Wireless Compon. Lett., vol. 25, no. 7, pp. 484-486, Jul. 2015.

[45] J. Wang, “Wide band human body communication technology for wearable and implantable robot control,” IEICE Trans. Commun., vol. E103-B, no. 6, June 2020.

[46] T. Nagaoka, S. Watanabe, K. Saurai, E. Kunieda, S. Watanabe, M. Taki, and Y. Yamanaka, “Development of realistic high-resolution whole-body voxel models of Japanese adult males and females of average height and weight, and application of models to radio-frequency electromagneticfield dosimetry,” Phys. Med. Bio., vol.49, pp.1-15, 2004.

[47] C. Gabriel, “Compilation of the dielectric properties of body tissues at RF and microwave frequencies,” Brooks Air Force Tech. Rep. AL/OE-TR-1996-0037, 1996.

[48] H. Akaike, “Information theory as an extension of the maximum likelihood principle,” Proc. 2nd Inter. Symp. on Information Theory, pp. 610-624, 1992.

[49] Y. Peng, K. Saito, and K. Ito, “Antenna design for impulse radio-based wireless capsule endoscope communication systems,” IEEE Trans. Antennas and Propagation, vol. 66, no. 10, pp. 5031-5042, Oct. 2018.

[50] P. A. Humblet, and M. Azizoglu, “On the bit error rate of light wave systems with optical amplifiers,” J. Lightw. Technol., vol. 9, no. 11, pp. 1576-1582, 1991.

[51] J. G. Proakis and M. Salehi, Digital communications, McGraw-Hill, 2008.

[52] The Radio Use Website, 2015, Online Available: http://www.tele.soumu.go.jp/j/ref/material/rule/ (in Japanese).

[53] K. Nomura, D. Anzai, and J. Wang, “Experimental evaluation of 30 MHz band implant communication using automatic equalization technique,” IET Microw. Antennas Propag., vol.12, no.13, pp. 2089-2093, Sept. 2018.

[54] UN, Department of Economic and Social Affairs, Population Dvision, World Population Ageing 2019 ST/ESA/SER. A/430, United Nations, New york, 2019.

[55] Aging in Japan | ILC-Japan, www.ilcjapan.org. Retrieved 2017-03-21., 2021.

[56] M. Khalil, C.E. Teunissen, M. Otto, F. Piehl, M.P. Sormani, Gattringer, “Neurofilaments as biomarkers in neurological disorders”, Nat Rev Neurol. 14 (10) 577–589 (2018).

[57] C. Bridel, W.N. van Wieringen, H. Zetterberg, B.M. Tijms, C.E. Teunissen, J. C. Alvarez-Cermeno, “Diagnostic value of cerebrospinal fluid neurofilament light protein in neurology”, JAMA Neurol. 76 (9) 1035–1048 (2019).

[58] G. Palermo, S. Mazzucchi, A. Della Vecchia, G. Siciliano, U. Bonuccelli, C. Azuar, “Different clinical contexts of use of blood neurofilament light chain protein in the spectrum of neurodegenerative diseases”, Mol Neurobiol. 57 (11) 4667–4691 (2020).

[59] G.U. Hoglinger, G. Respondek, M. Stamelou, C. Kurz, K.A. Josephs, A.E. Lang, “Clinical diagnosis of progressive supranuclear palsy: the movement disorder society criteria”, Mov Disord, 32 (6), 853–864, 2017 (https://doi.org/10.1002/ mds.26987).

[60] E.A.J. Willemse, I.S. van Maurik, B.M. Tijms, F.H. Bouwman, A. Franke, I. Hubeek, “Diagnostic performance of Elecsys immunoassays for cerebrospinal fluid Alzheimer’s disease biomarkers in a nonacademic, multicenter memory clinic cohort: the ABIDE project, Alzheimers Dement (Amsterdam, Netherlands)”, Elsevier 10, 563–5, 2018.

[61] F. de Wolf, M. Ghanbari, S. Licher, K. McRae-McKee, L. Gras, G.J. Weverling, Plasma tau, “neurofilament light chain and amyloid- levels and risk of dementia; a population-based cohort study, Brain”, 143 (4), 1220–1232, 2020.

[62] Dementia, WWW.WHO.int. Retrieved 7 November 2020., 2021.

[63] G. Livingston, J. Huntley, A. Sommerlad, “Dementia prevention, intervention, and care: 2020 report of the Lancet Commission”, Lancet. 396 (10248), 413–446, 2020 (doi:10.1016/S0140-6736(20)30367-August).

[64] IEEE 802.15.1-2002, IEEE Standard for Telecommunications and Information Exchange Between Systems - LAN/MAN - Specific Requirements - Part 15: Wireless Medium Access Control (MAC) and Physical Layer (PHY) Specifications for Wireless Personal Area Networks (WPANs), 2002.

[65] J. Wang, Q. Wang, Body Area Communications, Wiley-IEEE, Singapore, 2013. ISBN 978-111-818-848-4.

[66] A. Iwata, J. Wang, S. Shiramatsu, M. Suto, G. Mauricio, N. Magatsuma, “Monitoring plus-watching system using improved BLE beacon and LPWA communication”, Meas. Control 58 (2) 109–114, Feb 2019 Feb.

[67] Y. Shimizu, S. Hiyama, D. Anzai, M. Kugler, A. Iwata, J. Wang, “Design and performance evaluation of wearable BLE antenna for a localization system of aged wanderer”, in: Proc. IEEE BHI 2017, Orlando, USA, Feb 2017.

[68] A. Romani, R.P. Paganelli, M. Tartagni, “Fast and reliable modeling of piezoelectric transducers for energy harvesting applications”, Procedia Eng. 25, 1345–1348, 2011.

[69] Y.-Y. Chen, D. Vasic, F. Costa, W.-J. Wu, C.-K. Lee, “A self-powered switching circuit for piezoelectric energy harvesting with velocity control”, Eur. Phys. J. Appl. Phys. 57, 1–7, 30903, 2012.

[70] S. Bamberg, A.Y. Benbasat, D.M. Scarborough, D.E. Krebs, J.A. Paradiso, “Gait analysis using a shoe-integrated wireless sensor system”, IEEE Trans. Inf. Technol. Biomed. 12, 413–423, 2008.

[71] L. Shu, T. Hua, Y. Wang, Q. Li, D. Feng, X. Tao, “In-shoe plantar pressure measurement and analysis system based on fabric pressure sensing array”, IEEE Trans. Inf. Technol. Biomed. 14, 767–775, 2009.

[72] V. Karam, P.H.R. Popplewell, A. Shamim, J. Rogers, C.A. Plett, “A 6.3GHz BFSK transmitter with on-chip antenna for self-powered medical sensor applications”, in: Proceeding of IEEE Radio Frequency Integrated Circuits (RFIC) Symposium, Honolulu, HI, USA, 3-5 June, pp. 101–104, 2007.

[73] L. Lavery, S. Vela, J. Fleishli, D. Armstrong, D. Lavery, “Reducing plantar pressure in the neuropathic foot”, Diabetes Care 20, 1706–2171, 1997.

[74] M. Mueller, “Application of plantar pressure assessment in footwear and insert design”, J. Orthop Sports Phys. 29, 747–755, 1999.

[75] S. Praet, J. Louwerens, “The influence of shoe design on plantar pressures in neuropathic feet”, Diabetes Care 26, 441–445, 2003.

[76] championchip, http://www.championchip.com.my/home/., 2021.

[77] M.I. Haque, K. Yoshibayashi, J. Wang, G. Fischer, J. Kirchner, “Directive antenna design at 2.4GHz on foot surface for wanderer location identification”, in: 2020 International Symposium on Antennas and Propagation (ISAP), pp. 635–636, 2021 (https://doi.org/10.23919/ISAP47053.2021.9391396).

[78] W.L. Stutzman, G.A. Thiele, Antenna Theory and Design, Third edition, Wiley, 2012.

[79] K. Yoshibayashi, D. Anzai, J. Wang, “A directional array antenna with dielectric lens at 2.4GHz band”, in: Proc. 2019 Joint EMC Sapporo & APEMC Symposium, Sapporo, Japan, June 3-7, 2019.

[80] K. Ito, H. Kawai, K. Saito, “State of the art and future prospects of biological tissue equivalent phantoms”, Trans. IEICE B85 (5) 582–596 (2002 May).

[81] J.J. Lee, Antenna Handbook, vol. 2, Van Nostrand Reinhold, NewYork, 1993.

[82] alpsalpine,https://tech.alpsalpine.com/prod/e/html/communication/bluetooth/ugmz2a/ugmz2a1.html., 2021.

[83] H. Ding, K. Ville, “Micro structured polymer for shoe power generation”, In: Solid-State Sensors, Actuators and Microsystems Conference, 2009. TRANSDUCERS 2009. International. IEEE, S. 1393-1396, 2009.

[84] S. Nathan, A. Joseph, “Energy scavenging with shoe-mounted piezo electrics”, IEEE micro, Jg., Nr. 3, S. 30-42, 2001.

[85] Z. Jingjing, Y. Zheng, “A shoe-embedded piezoelectric energy harvester for wearable sensors”, Sensors, Jg., Nr. 7, S. 12497-12510, 2014.

[86] M. Yilmaz, E. M. Abdel-Rahman, S. Park, K. Elrayes, M. Yavuz, M. A. E. Mahmoud, M. S. M. Soliman, and R. A. Elshatshat, “Testing of a passive full-wave MOSFET rectifier” Proceeding of the 24th CANCAM Saskatoon, Saskatchewan, Canada, June 2013.

[87] C. Peters, O. Kessling, F. Henrici, M. Ortmanns, and Y. Manoli, “CMOS integrated highly efficient full wave rectifier,” Proc. IEEE Int. Symp. Circuits syst., pp. 2415-2418, 2007.

[88] S. Hashemi, M. Sawan, and Y. Savaria, “A novel low drop CMOS rectifier for RF-

powered devices: Experimental results," Microelectron. J, Volume 40, pp. 1547-1554, 2009.

[89] M. I. Haque, J. Wang, D. Anzai, "Path Loss and Group Delay Analysis at 10-60 MHz Human Body Communication Band", IEICE Technical Report, EMCJ2019-78,13th Dec 2019.

[90] Q. Liu, K. G. Mkongwa, C. Zhang, "Performance issues in wireless body area networks for the healthcare application: a survey and future prospects", SN Applied Sciences (2021) 3:155 | https://doi.org/10.1007/s42452-020-04058-2.

[91] https://www.runtastic.com/de/

[92] C. Jagger, "Trends in life expectancy and healthy life expectancy", Foresight, Gov of Sci. pp 1–29, 2015. Retrieved from https:// assets.publishing.service.gov.uk/government/uploads/system/uploads/attachment_data/464275/gs-15-13-future-agein g-trends-life-expectancy-er12.pdf

[93] O. Letwin, S. Harper, M. Walport, "Future of an ageing population", Oxford Inst Popul Ageing, p. 1–124, 2016. Retrieved from https://www.ageing.ox.ac.uk/fles/Future_of_Ageing_Repor t.pdf

[94] H.A Salam, B.M Khan, "Use of wireless system in healthcare for developing countries", 2016, Digit Commun Netw. https://doi. org/10.1016/j.dcan.2015.11.001

Acknowledgements

In the name of Almighty ALLAH, The Most Gracious and The Most Merciful. I would like to explicit my profound thankfulness and recognition to ALLAH for granting me the blessings to do this research. With the help and permission of ALLAH, I achieved many things, including this thesis. Indeed, without the relief of ALLAH, nothing is carried out. Many most profound blessings for Prophet Mohammed (Peace be upon him) because he guides us for ALLAH. We ask ALLAH to help us to follow his message and get forgiveness in the hereafter.

I would like to express my deep respect to my advisor, Prof. Dr. Jianqing Wang. For more than three years, he continuously supports me in promoting inflectional research in a focused way. It was a real pleasure for me to have such a motivated and authentic person as an advisor. He makes me more confident by telling me that it is my work, and I have to lead everything in my own thesis. His office door was open, and I will never forget the hours of deductive discussion we had throughout three years. Special deep thanks to Prof. Dr. Yutaka Ishibashi for his efforts and valuable suggestions to come to Japan.

I would also like to express my gratitude to the other members in our laboratory and my family for their support and warm encouragement. Besides, I would like to thank Associate Prof. Dr. Anzai, Prof. Dr. Kikuma, Prof. Dr. Hirata, Prof. Dr. Saito and Prof. Dr. Georg for their comments. The authors would like to thank Prof. Dr. Kakimoto and Mr. Yamamoto of Nagoya Institute of Technology for providing the NKN and BCTZ piezo materials. Special thanks to Prof. Dr. Georg Fischer, Dr. Jens Kirchner, and Friedrich-Alexander University of Erlangen-Nuremberg for their support during my stay in Erlangen. This study was supported in part by the JSPS Japanese-German Graduate Externship (Grant No. 2019/R1). The authors also gratefully acknowledge financial support for this work by the Deutsche for schungsgemeinschaft under GRK2495/A. There is someone who still lionized my victories and heartened me through hard times, someone whose encouragement, love, and sacrifice were everlasting. Thank you, my all-family members, from the basement of my heart. I would like to thank my parents, brothers, and sister for all their unconditional love and support during the long years of my learning.

Publication lists

5.1 Journal Papers

[1] **M. I. Haque**, R. Yamada, J. Shi, J. Wang, D. Anzai, "Channel Characteristics and Link Budget Analysis for 10-60 MHz Band Implant Communication", IEICE Transactions on Communications, Vol. E 104-B, No.4, pp.410-418, Apr. 2021 (doi: 10.1587/transcom.2020EBP3075).

[2] **M. I. Haque**, K. Yoshibayashi, J. Wang, G. Fischer, J. Kirchner, "Design and Evaluation of Directional Antenna for Shoe-mounted Sensor for Position Identification of Elderly Wanderer", Sensing and Bio-Sensing Research, Elsevier, Volume 34, December 2021, 100451 (doi: 10.1016/j.sbsr.2021.100451).

5.2 International Conference Papers

[1] **M. I. Haque**, K. Yoshibayashi, J. Wang, G. Fischer, J. Kirchner, "Directive Antenna Design at 2.4 GHz on Foot Surface for Wanderer Location Identification", 2020 International Symposium on Antennas and Propagation (ISAP), January 25-28, 2021, Osaka, Japan, pp. 635-636. (doi: 10.23919/ISAP47053.2021.9391396).

5.3 Oral Presentations

[1] **M. I. Haque**, J. Wang, D. Anzai, "Path Loss and Group Delay Analysis at 10-60 MHz Human Body Communication Band", IEICE Technical Report, EMCJ2019-78,13th Dec 2019.

[2] **M. I. Haque**, K. Yoshibayashi, J. Wang, D. Anzai, "Performance Investigation of Directive Antenna at 2.4 GHz on Foot for Wanderer Location", IEICE General Conference, B-4-32, March 2021.